GEOLOGICAL SURVEY OF CANADA
PAPER 91-11

SEDIMENTOLOGY OF AN ARCTIC BASIN: ITIRBILUNG FIORD, BAFFIN ISLAND, NORTHWEST TERRITORIES

James P.M. Syvitski and Frances J. Hein

1991

Energy, Mines and Resources Canada Énergie, Mines et Ressources Canada

Canada

THE ENERGY OF OUR RESOURCES

THE POWER OF OUR IDEAS

GEOLOGICAL SURVEY OF CANADA
PAPER 91-11

SEDIMENTOLOGY OF AN ARCTIC BASIN: ITIRBILUNG FIORD, BAFFIN ISLAND, NORTHWEST TERRITORIES

James P.M. Syvitski and Frances J. Hein

1991

92-01866/

©Minister of Supply and Services Canada 1991

Available in Canada through
authorized bookstore agents and other bookstores
or by mail from

Canada Communication Group — Publishing
Ottawa, Canada K1A 0S9

and from

Geological Survey of Canada offices:

601 Booth Street
Ottawa, Canada K1A 0E8

3303-33rd Street N.W.,
Calgary, Alberta T2L 2A7

A deposit copy of this publication is also available for reference
in public libraries across Canada

Cat. No. M44-91/11E
ISBN 0-660-14197-3

Price subject to change without notice

Critical readers

J.T. Andrews
G. Vilks
D. Forbes

Authors' addresses

James P. M. Syvitski
Geological Survey of Canada
Bedford Institute of Oceanography
Box 1006, Dartmouth, Nova Scotia
B2Y 4A2

Frances J. Hein
Dept. of Geology and Geophysics
The University of Calgary
Calgary, Alberta
T2N 1N4

Original manuscript received: 1990-11-15
Final version approved for publication: 1991-02-08

CONTENTS

1 Abstract/Résumé

3 Summary/Sommaire

6 Introduction
7 Acknowledgments

8 Environmental setting
8 Geologic framework
8 Climate
9 Climate and discharge
12 Wind

12 Sediment inputs
12 Glaciofluvial inputs
13 Glacial inputs
16 Aeolian inputs
17 Marine inputs

18 Basin characteristics
18 Acoustic basement characteristics
18 Present seafloor morphology
19 Synoptic oceanography
23 Suspended particulate matter

23 Sedimentary environments
23 Delta
26 Prodelta
31 Sidewall environment
32 Basin
33 Sills and the outer sill complex

34 Facies analysis
34 Data base and facies definition
37 Regional acoustic units
43 Sedimentary facies
53 Textural data summary
55 Correlation between litho- and seismo-stratigraphy

55 Summary models
55 Horizontal and vertical distribution of facies
58 Balancing sediment inputs and basin fill

62 Conclusions

64 References

Figures

7 1. Loation of Itirbilung Fiord on the NE coast of Baffin Island, N.W.T.
7 2. Drainage basins, ice fields and glaciers, and areas of Quaternary sediment cover or exposed Precambrian bedrock surrounding Itirbilung Fiord
9 3. The major drainage basins and a synthetic discharge curve for the main fiord-valley river
10 4. Wind data from the head of Itirbilung Fiord collected in 1983 and 1985
10 5. The pattern of ice retreat and sediment deposition of two side-entry glaciers situated on the northern margin and at the head of Itirbilung Fiord

11	6.	Salinity, temperature, suspended sediment concentration and clay fraction within SPM for Itirbilung Fiord in September of 1982
12	7.	Salinity, temperature, suspended sediment concentration and per cent clay within SPM Itirbilung Fiord in September of 1983
13	8.	Bathymetry and acoustic basement of Itirbilung Fiord with overlain ship track lines of seismic surveys
14	9.	Submarine channels cut into the seafloor of Itirbilung Fiord with position of sediment cores
15	10.	Bathymetry of the fiordhead prodelta showing location of hydrographic lines weather station and oceanographic moorings
16	11.	Echosounder profiles from the fiordhead prodelta (cf. Fig. 10 for positions)
17	12.	The prodelta environment of Itirbilung Fiord showing channels and listric fault scarps
18	13.	Salinity and temperature profiles inside and outside Itirbilung fiord
19	14.	Oceanographic and associated wind data for August of 1983
20	15.	Oceanographic and associated wind data for July and August of 1985
21	16.	Complexity of turbidity current events
22	17.	The river plume flowing down Itirbilung Fiord
24	18.	Location of onshore and offshore grabs and cores, Itirbilung Fiord, collected between 1982 and 1987
26	19.	Airphotos (July, 1958 and August, 1948) showing side-entry glaciers that feed directly into the Itirbilung sandur
28	20.	Photographs of sedimentological features on the Itirbilung delta, including the delta front, main fluvial channel, wind blown sand accumulation, gravel sand waves deposited during a jøkolhlaup event, ice-cored Little Ice Age moraine, and raised glacial marine deposits
30	21.	Sidescan sonagram of the foresets of the Itirbilung prodelta environment
30	22.	Sidescan sonagram of the front of the Itirbilung delta showing partly buried slide faces
31	23.	Acoustic profile of the seafloor parallel to the foresets of the Itirbilung prodelta
31	24.	Relation between channel area and the number of channels with distance from the Itirbilung delta front
32	25.	Submersible photographs of the Itirbilung prodelta environment
33	26.	Sidescan sonographs of the fiord walls near the head of Itirbilung Fiord
34	27.	Sidescan imagery across the fiord, showing older glaciomarine sediment retrogressively cut by slides
35	28.	Sidescan imagery of a bedrock wall and a debris mantled slope partially covered by a slump deposit
36	29.	Submersible photographs of the sidewall margins and sill crest
37	30.	Sidescan imagery of the outer sill bounding Itirbilung Fiord
38	31.	Sidescan imagery of the outer approaches to Itirbilung Fiord
40	32.	Correlation chart of core lithology within basins 1 and 2
42	33.	Correlation chart of core lithology within basins 3 and 4
43	34.	Seismo-stratigraphic interpretation of airgun profiles.
44	35.	Airgun reflection seismic record from fix 11 to 25
44	36.	Huntec profile of a paleo ice marginal position and subsequent slump generated after retreat of the terminus
45	37.	Seismic interpretation of a sidewall-generated slump with associated debris flow deposits
45	38.	Interpretation of a slide complex from the margin of a Itirbilung basin
46	39.	Huntec profile of the prodelta region of Itirbilung Fiord
47	40.	X-radiographic print of Facies A pebbly-sandy-mud
48	41.	Photographs of split cores, showing Facies A, B, C, D, E, and F
49	42.	Grain size-frequency curves for Facies A pebbly sandy mud
49	43.	Grain size-frequency curves for Facies B bioturbated mud
49	44.	Grain size-frequency curves for Facies C wispy laminated sand and mud
50	45.	X-radiographic prints of Facies D laminated sand and mud, and Facies G, crossbedded sand

50 46. Sedimentary peel of Facies D laminated sand and mud and sediment trap data
51 47. Photographs and textural analyses of Facies E graded-stratified gravel
51 48. Photographs of Facies F sands with representative grain size-frequency distribution
52 49. Photographs of Facies F sands with a large silty mud intraclast, with representative grain size-frequency distribution curves
52 50. Photographs of Facies G, crossbedded sands, with representative grain size-frequency distribution curves
53 51. Moment measures for all samples analyzed from Itirbilung cores.
54 52. Per cent silt and clay versus sand for cores dominated by Facies D and Facies F
55 53. Measured sand content of cores and the sand content estimate from facies distribution
56 54. Major seismic reflectors of Huntec deep-tow profiles over three core sites
57 55. Down-fiord variation in facies percentages
58 56. Downcore variation in mean grain size for various Itirbilung cores
59 57. Itirbilung Fiord piston core logs showing predominantly Facies D, laminated sands and muds with some interbeds of Facies F, pebbly sand and sand
60 58. Representative Itirbilung Fiord piston core logs showing predominantly thin Facies F, Facies C, and Facies B with thick Facies F
61 59. Paleogeographic reconstruction of basin 1 during a period of high sediment input, with glaciers, active fiordhead delta progradation and slumping of delta front sand and mud
62 60. Paleogeographic reconstruction of basin 2 during a period of high sediment input, with glaciers, active side-entry delta progradation and slumping of delta front sand and mud

Tables

8 1. SAFE investigations at Itirbilung Fiord
9 2. Climate data relative to the calculation of discharge for the Itirbilung drainage basin area based on 30 year averages of Canadian climate normals
9 3. The components of glacio-fluvial discharge
10 4. Sediment flux data for the Itirbilung Fiord hinterland
11 5. Geomorphological statistics of Itirbilung Fiord in comparison with other Baffin Island fiord morphologies
25 6. Sample information for grab and core samples, Itirbilung Fiord
27 7. Textural parameters for submarine grab samples collected in Itirbilung Fiord
39 8. Facies percentages for core samples collected in Itirbilung Fiord
42 9. Textural characteristics of facies for core samples collected in Itirbilung Fiord
56 10. Measured or predicted sand content of Itirbilung cores

SEDIMENTOLOGY OF AN ARCTIC BASIN: ITIRBILUNG FIORD, BAFFIN ISLAND, NORTHWEST TERRITORIES

Abstract

Itirbilung Fiord was investigated using geophysical, oceanographic and sediment surveys in 1982, 1983, 1985, and 1987. Itirbilung typifies a deep arctic basin that experiences episodic sedimentation events, cycled principally by nival and glacier melt with punctuations by mass-sediment failures. Aeolian transport of sediment into the fiord basin may also be large, possibly four times the sediment volume transported by the Itirbilung River. A Quaternary fill of greater than 150 m is located in two of the four basins. Paleohydraulic calculations suggest that for the period 8400 to 6000 years BP, Itirbilung fiord received up to five times the present rate of fluvial delivery, reflecting the ablation of the Late Foxe Ice Sheet. Between 6000 and 150 years BP, a time of Neoglacial ice storage, sediment yield was much lower.

Fiord circulation is related to meltwater (from both rivers and melting sea ice) during the summer, wind-generated drift during the late summer and fall, deep water exchanges during the fall, isohaline-generated circulation of winter, and tidal currents which operate over the entire year. Up-fiord winds initiate downwelling at the fiordhead and an internal seiche the period of which is equal to the diurnal tide. Down-fiord winds caused the dissipation of these internal tides.

Itirbilung River delta, one of the largest sandurs on Baffin Island, is largely conditioned by Little Ice Age events. A catastrophic jøkolhlaup about 100 years ago removed much of the raised marine deposits that once covered the sandur, armoured the sandur surface with gravel waves and large boulders, and initiated a massive failure of the delta front. Little Ice Age deposits are very thin over most of the fiord, however, and are of significance only near the head of the fiord. Sixty per cent of the fluvial load is moved offshore by sediment gravity flows that travel along numerous submarine channels. These channels decrease in number and size down-fiord. Nine medium-strength gravity flow events ($<0.36\ m \bullet s^{-1}$), lasting between 1 and 5 hours, were measured in one submarine channel. Two types of flows were observed: (1) powerful single events which may represent coarse-grained delta front failure, and (2) weaker multi-event flows which may result from retrogressive failure of the prodelta muds.

The rate of sediment accumulation decreases down the fiord, punctuated by side-entry fan deltas that further contribute large volumes of sediment. Basin deposits are largely ponded between the fiord walls, although two of the sills are mantled by hemipelagic deposits. Five seismo-stratigraphic units are identified and may represent a single phase of ice sheet advance and retreat, i.e. the Late Foxe glaciation. The upper three seismic units contain seven sedimentary facies that show little correlation between basins: pebbly-sandy-mud, from the melt of debris-laden ice; burrowed/mottled mud, reflecting the bioturbation of hemipelagic deposits; wispy laminated/mottled mud, from low velocity turbidity currents and/or meltout of aeolian sand covering sea ice cover; laminated sand and mud, from the hypopycnal discharge of river plumes; coarse sand/gravel, and pebbly sand and sand, reflecting very rapid deposition from high concentration, viscous sediment-gravity flows, either as turbidity currents or as sandy debris flows; and the extremely rare crossbedded sands, that may relate to the reworking of turbidity current deposited sands by reverse flow mechanisms.

Résumé

Des études géophysiques, océanographiques et sédimentaires ont été menées dans le fjord Itirbilung en 1982, en 1983, en 1985 et en 1987. Ce fjord est typique d'un bassin arctique profond où il se produit des événements sédimentaires périodiques dont les cycles sont fonction principalement de la fonte nivale et de la fonte glaciaire avec parfois des ruptures de masses de sédiments. Le volume de sédiments éoliens transportés dans le bassin du fjord pourrait aussi être important, possiblement jusqu'à quatre fois le volume de sédiments transportés par la rivière Itirbilung. Deux des quatre bassins sont comblés de remblais quaternaires dont l'épaisseur dépasse 150 m. Les calculs paléohydrauliques portent à croire que pendant l'intervalle de 8 400 à 6 000 ans avant aujourd'hui, le fjord Itirbilung a reçu jusqu'à cinq fois plus de sédiments fluviatiles qu'aujourd'hui, ce qui reflète l'ablation de la nappe glaciaire du Foxe tardif. L'intervalle de 6 000 à 150 ans a été marqué par l'accumulation de la glace néoglaciaire, et la production de sédiments y a été moins importante.

La circulation des eaux dans le fjord est associée aux eaux de fonte (provenant de la fusion des glaces de cours d'eau et de mer) l'été, à l'effet des vents à la fin de l'été et en automne, aux échanges d'eau en profondeur l'automne, à l'effet des variations isohalines l'hiver et aux courants de marée tout au long de l'année. Les vents qui soufflent vers l'amont du fjord provoquent la plongée des eaux au fond du fjord ainsi qu'un seiche interne dont la période est égale à la marée diurne. Les vents qui soufflent vers l'aval du fjord dissipent ces marées internes.

Le delta de la rivière Itirbilung, un des plus grands sandurs de l'île de Baffin, est en grande partie le produit d'événements survenus au cours du Petit âge glaciaire. Un jökulhaup catastrophique a jadis inondé le sandur, formant à sa surface une cuirasse de vagues de gravier et de grands blocs et provoquant une rupture massive du front du delta. Cependant, les dépôts du Petit âge glaciaire sont très minces dans la plus grande partie du fjord sauf à son extrémité aval, où ils sont importants. Soixante pour cent de la charge fluviatile sont transportés au large de la côte par des écoulements gravitaires de sédiments qui empruntent de nombreux chenaux sous-marins. Le nombre et la grandeur de ces chenaux diminuent vers l'aval du fjord. Dans un de ces chenaux, on a mesuré neuf écoulements gravitaires d'importance moyenne (<0,36 • m/s), qui ont duré de 1 à 5 heures. On y a observé deux types d'écoulements : (1) des événements simples, puissants, qui pourraient représenter la rupture d'un front de delta à grain grossier, et (2) des écoulements multiples moins puissants qui pourraient être produits par suite de la rupture rétrogressive des boues prodeltaïques.

Le taux d'accumulation de sédiments diminue vers l'amont du fjord; cependant, des cônes de déjection latérale sont des apports importants de matériaux. Les dépôts de bassin sont largement retenus entre les parois du fjord, bien que deux des seuils soient tapissés de sédiments hémipélagiques. Cinq unités sismo-stratigraphiques y sont reconnues et pourraient représenter une phase unique d'avancée et de retrait de la nappe glaciaire, soit la glaciation du Foxe tardif. Les trois unités sismiques supérieures contiennent sept faciès sédimentaires, dont la corrélation d'un bassin à l'autre est faible : une boue sablo-caillouteuse, déposée par la fonte de la glace chargée de débris; une boue tachetée, criblée de terriers, qui reflète la bioturbation de sédiments hémipélagiques; une boue tachetée, finement laminée, déposée par des courants de turbidité à faible vitesse ou composée de sable éolien qui couvrait la glace de mer et qui s'est accumulé suivant la fusion de cette glace; du sable et de la boue laminés provenant de l'influx hypopycnal de panaches fluviatiles; du sable/gravier grossier, du sable caillouteux et du sable accumulés très rapidement à partir d'écoulements gravitaires visqueux, à forte concentration de sédiments, soit des courants de turbidité, soit des coulées de débris sableux; et des sables à stratification oblique, faciès extrêmement rare qui pourrait être associé au remaniement, par des écoulements inverses, de sables déposés par des courants de turbidité.

SUMMARY

1. *Fluvial discharge:* Itirbilung Fiord experiences episodic sedimentation events under arctic conditions -- the annual discharge cycle is extremely short, of less than three months duration. Approximately half of the discharge of river water into the fiord is from snow melt in the early summer. Late summer flows occur as short duration events that relate equally to periods of rainfall and warm sunny days affecting the melt of hinterland ice sheets. A simple climate-glaciological model is used to simulate the discharge of rivers. Sediment yield predictions vary between 9 and 91 $t \bullet km^{-2} \bullet a^{-1}$, of which 92% of the estimated annual flux of fluvial sediment (about 1.4×10^5 $t \bullet a^{-1}$) enters near the head of the fiord.

2. *Glacial input:* At present there are no tidewater glaciers along Itirbilung Fiord, although in the early 1950s four tidewater glaciers existed. These glaciers reached their maximum tidewater position during the Little Ice Age. Thus for at least 100 years, the fiord received direct input of glacial sediment to its basin. Based on the volume of their ice proximal deposits, these glaciers annually contributed up to one order-of-magnitude more sediment than is presently delivered to the fiord by river discharge. Paleohydraulic calculations suggest that for the period 8400 to 6000 years BP, Itirbilung fiord received five times the present rate of fluvial sediment delivery, reflecting the ablation of the Late Foxe Ice Sheet. For the period 6,000 and 150 years BP, a time of Neoglacial ice storage, the sediment delivery rate is thought to have been reduced to half the present level of sediment delivery.

3. *Aeolian transport:* Winds are a constant feature of Itirbilung Fiord, occasionally in excess of 145 km h^{-1}. Large events, lasting five days, indicate the presence of large weather systems over Baffin Island and Baffin Bay. Shorter duration events reflect a local katabatic influence. We estimate that critical winds for the movement of sediment in the down-fiord direction occur 20% of the time and affect 30% of the sandur surface. However, ultimate threshold conditions for full sediment mobility occur only 1% of the year. The annual transport of aeolian sediment into the fiord basin is predicted to be 3.6×10^5 $t \bullet a^{-1}$, approximately three times the estimate of suspended sediment transport by the Itirbilung River.

4. *Marine input:* The total autochthonous component within Itirbilung Fiord sediments is about 3.5% by weight, dominated by the siliceous tests of pelagic diatoms that accumulate in basinal muds.

5. *Oceanography:* Three oceanographic seasons have been described. Currents are largely driven by meltwater discharge (from both rivers and melting sea ice) during the summer, wind-generated drift during the late summer and fall, deep-water exchanges during the fall, isohaline-generated circulation of winter, and tidal currents which operate over the entire year. There is some evidence that resuspension of sill sediment is

SOMMAIRE

1. *Débit fluviatile* : Le fjord Itirbilung subit des phénomènes sédimentaires épisodiques dans des conditions arctiques; on note que le cycle de décharge annuel est extrêmement court, soit moins de trois mois. Environ la moitié de l'eau qui se déverse dans le fjord provient de la fonte nivale au début de l'été. Les écoulements qui se produisent à la fin de l'été sont des phénomènes brefs qui s'associent tant à des périodes de pluie qu'à des journées chaudes et ensoleillées qui par conséquent entraînent la fonte des nappes glaciaires de l'arrière-pays. Un modèle climato-glaciologique simple permet de simuler le débit des cours d'eau. Les prévisions quant aux apports de sédiments varient de 9 à 91 t/km/a, dont 92 % de la charge annuelle estimative de sédiments fluviatiles (environ $1,4 \times 10^5$ t/a) sont déversés près de l'extrémité amont du fjord.

2. *Apport glaciaire* : Il n'existe actuellement aucun glacier de marée le long du fjord Itirbilung, bien qu'au début des années 1950, il y en avait quatre. Ces glaciers ont atteint leur limite maximale d'avancée au cours du Petit âge glaciaire. Par conséquent, le bassin du fjord a reçu des apports directs de sédiments glaciaires pendant au moins 100 ans. À en juger par le volume de leurs sédiments proglaciaires, ces glaciers ont contribué annuellement à une quantité de sédiments qui pouvait dépasser le volume contribué actuellement par les cours d'eau. Les calculs paléohydrauliques portent à croire que pendant l'intervalle de 8 400 à 6 000 ans avant aujourd'hui, le fjord Itirbilung a reçu cinq fois plus de sédiments fluviatiles qu'aujourd'hui, ce qui reflète l'ablation de la nappe glaciaire du Foxe tardif. L'intervalle de 6 000 à 150 ans a été marqué par l'accumulation de la glace néoglaciaire, et les apports de sédiments n'étaient vraisemblablement que 50 % de ceux d'aujourd'hui.

3. *Transport éolien* : Les vents soufflent constamment dans le fjord Itirbilung et leur vitesse dépasse parfois 145 km/h. Des événements importants, qui durent cinq jours, indiquent la présence de vastes systèmes météorologiques au-dessus de l'île de Baffin et de la baie de Baffin. Des événements de plus courte durée reflètent une influence catabatique locale. Nous estimons que des vents suffisamment forts pour déplacer des sédiments vers l'aval du fjord se produisent 20 % du temps et touchent à 30 % de la surface du sandur. Cependant, le seuil requis pour permettre le déplacement de toute la gamme de sédiments ne se réalise que pendant 1 % de l'année. Le volume de sédiments éoliens transportés jusque dans le bassin du fjord est estimé à $3,6 \times 10^5$ t/a, soit environ trois fois le volume estimé des matériaux en suspension transportés par la rivière Itirbilung.

4. *Apport marin* : La composante autochtone totale des sédiments du fjord Itirbilung est environ 3,5 % par poids; elle comprend principalement des coques siliceuses de diatomées pélagiques qui s'accumulent dans les boues du bassin.

5. *Océanographie* : Trois saisons océanographiques ont été décrites dans la région. Les courants sont actionnés largement par le déversement des eaux de fonte (provenant de la fusion des glaces de cours d'eau et de mer) l'été, par les vents à la fin de l'été et en automne, par des échanges d'eau en profondeur l'automne, par des variations isohalines l'hiver et par des courants de marée tout au long de l'année. Certains indices portent à croire que la remise en suspension des sédiments du

associated with the influx of shelf water. Up-fiord winds initiate downwelling at the fiordhead. Particularly strong winds initiate an internal seiche the period of which is equal to the diurnal tide. Down-fiord winds cause a dissipation of these internal tides. Although seabottom currents are usually weak, 9 gravity flow events (up to 0.36 $m \cdot s^{-1}$) were measured in a submarine channel over a five week period. Each event lasted 1 to 5 hours.

6. *Offshore bathymetry:* Four bedrock-controlled sills separate Itirbilung Fiord into basins, of which two contain ≥150 m of Quaternary fill. The seafloor is dissected by a number of submarine channels that decrease down-fiord both in number and size. These channels may be straight and U-shaped, broad and meandering, or braided. Most of the channels carry sediment in the seaward direction, however channels originating on sill 3 carry sediment up-fiord.

7. *Turbidity currents:* Two types of sediment gravity flows were observed: (1) powerful single events which appear to represent coarse-grained delta-front chute failures, and (2) weaker multi-event flows which may result from retrogressive slide failures of the prodelta muds. Sediment traps moored within a submarine channel collected turbidite sands interlayered with hemipelagic muds. A turbidity current was observed using a manned submersible, and experimentation with the submersible arm digging into the steep wall of a submarine channel enabled us to generate turbidity currents easily.

8. *Sandur:* Itirbilung sandur is one of the largest on Baffin Island, largely conditioned by Little Ice Age events. Three prominent side-entry glaciers have contributed large volumes of push moraines and stagnation deposits which presently supply fluvial and aeolian sediment. The sandur deposits principally reflect the aggradation and progradation of a bedload-dominated braided river system. The effects of aeolian transport are ubiquitous. The action of waves, a consequence of autumn winds, is confined to the aerially limited tidal flats.

9. *Little Ice Age jøkolhlaup:* A catastrophic jøkolhlaup, about 100 years ago, removed much of the raised marine deposits that once covered the Itirbilung River sandur. The upper sandur surface was left armoured with gravel waves and large boulders. We suspect a 10 m thick ponded slide mass (20 million m^3), located between 7 and 9 km offshore, relates to the jøkolhlaup event and its massive transport of sediment offshore.

10. *Itirbilung prodelta:* The Itirbilung River prodelta annually receives about 5×10^5 tonnes of sediment: 75% through aeolian transport, 25% as fluvial load. Sixty-one per cent of the fluvial bedload is used in

seuil est associée à l'arrivée d'eau de la plate-forme. Les vents qui soufflent vers l'amont du fjord provoquent la poussée des eaux au fond du fjord. Des vents particulièrement forts produisent un seiche interne dont la période est égale à la marée diurne. Des vents qui soufflent vers l'aval du fjord dissipent ces marées internes. Bien que les courants de fond soient généralement faibles, on a mesuré neuf écoulements gravitaires (pouvant atteindre 0,36 m/s) dans un chenal sous-marin sur une période de cinq semaines. Chaque événement a duré de 1 à 5 heures.

6. *Bathymétrie extracôtière* : Quatre seuils lithodépendants séparent le fjord Itirbilung en bassins, deux de ces seuils contiennent plus de 150 m de remblais quaternaires. Des chenaux sous-marins sillonnent le fond marin; leur nombre et leur grandeur diminuent vers l'amont du fjord. Ils peuvent être droits et en U, larges et sinueux, ou anastomosés. La plupart d'entre eux transportent des sédiments vers la mer; or, les chenaux qui naissent sur le seuil 3 transportent des sédiments vers l'amont du fjord.

7. *Courants de turbidité* : On a observé deux types d'écoulements gravitaires de sédiments : (1) des événements simples, puissants, qui semblent représenter des ruptures d'un front de delta à grain grossier, et (2) des écoulements multiples moins puissants qui pourraient être produits par suite de la rupture rétrogressive des boues prodeltaïques. Des collecteurs de sédiments amarrés dans un chenal sous-marin ont recueilli des sables turbiditiques interstratifiés de boues hémipélagiques. Un courant de turbidité a été observé à partir d'un submersible habité, et des courants de turbidité ont été provoqués sans difficulté en creusant la paroi abrupte d'un chenal sous-marin à l'aide du bras du submersible.

8. *Sandur* : Le sandur d'Itirbilung est un des plus grands sandurs de l'île de Baffin; il est en grande partie le produit d'événements survenus au cours du Petit âge glaciaire. Trois grands glaciers latéraux ont contribué à l'apport de volumes considérables de dépôts de moraines de poussée et de sédiments de stagnation qui servent actuellement de sources pour les sédiments fluviatiles et éoliens. Les dépôts du sandur reflètent principalement l'aggradation et la progradation d'un réseau de cours d'eau anastomosés où prédominait la charge de fond. Les effets du transport éolien se ressentent partout. L'action des vagues, conséquence des vents d'automne, se fait sentir uniquement sur les estrans à superficie limitée.

9. *Débâcle glaciaire du Petit âge glaciaire* : Une débâcle glaciaire catastrophique qui s'est produite il y a environ 100 ans a enlevé une grande partie des sédiments marins soulevés qui tapissaient jadis le sandur de la rivière Itirbilung. Elle a formé à la surface du sandur une cuirasse de vagues de gravier et de grands blocs. Nous croyons qu'une masse de sédiments glissés (20 millions de m^3) de 10 m d'épaisseur, qui se situe entre 7 et 9 km au large de la côte, est associée à la débâcle glaciaire et à son transport vers le large de volumes considérables de sédiments.

10. *Prodelta de la rivière Itirbilung* : Le prodelta de la rivière Itirbilung reçoit annuellement environ 5×10^5 tonnes de sédiments; 75 % de ce volume proviennent du transport éolien et 25 %, du transport fluviatile. Soixante et un pour cent de la

the annual delta front progradation rate of 2.6 $m \cdot a^{-1}$. The remaining sediment is moved offshore in the form of slumping and turbidity currents along chutes and channels that cover the seafloor. The channels are of low sinuosity, their floors covered in sand. Other features related to semicontinuous slope failure include listric fault scarps often broken by crevasses and conjugate fractures. A deep-seated growth fault may control these retrogressive slide scarps.

11. *Basin deposits:* Sediments are largely ponded between the fiord walls, although two of the sills are mantled by hemipelagic deposits. Using various lines of evidence, the rate of sedimentation decreases down the fiord. This pattern is punctuated by side-entry fan deltas that have often failed prograding onto the steep margins of the fiord, further contributing large volumes of sediment to the basin floors.

12. *Acoustic Units:* Five seismo-stratigraphic units are interpreted as primarily representing a single phase of ice sheet advance and retreat. Units include: (1) ice contact sediment subdivided into a depositional facies and an ice loaded facies, (2) rapidly deposited ice proximal sediment under the influence of submarine glaciofluvial discharge partly syndepositional with unit 1, (3) ice distal accumulation of glaciomarine sediment from the hemipelagic deposition under turbid surface plumes, (4) paraglacial deposits associated with the rapid growth of deltas from the terrestrially-based ice cap and during a period of rapidly falling sea level, and (5) Neoglacial deposits when sea level was more or less stable and sedimentation considerably reduced. Little Ice Age deposits are very thin over most of the fiord and are only of significance in the inner of the four basins. The texture of the most recent sediments within basins 1 and 2, are considerably finer-grained than older sediments and may reflect the decrease in sedimentation following the initial phase of ablation of the Little Ice Age. In basins 3 and 4, where sedimentation rates are much lower, the coarser and more surficial sediments may reflect the sedimentation regime of unit 4. The older and more deeply buried sediments which are finer-grained may reflect the ice-distal sediments of unit 3. Through mass balance calculations we surmise that units 2 through 5 have deposited since the advance and ablation of the Late Foxe ice dome. Unit 1 may or may not represent sediment deposits that predate this event.

13. *Lithologic facies:* Seven sedimentary facies have been identified within cores collected from deposits of units 4 and 5 and possibly unit 3. Facies A, pebbly-sandy-mud, comprises less than 7% of the sediment volume and relates to the meltout of material from debris-laden ice of local origin. Its contribution increases dramatically down-fiord, probably a reflection of decreasing rates of sedimentation. Facies B, burrowed/mottled mud, dominates the sediment column accounting for just under half of the sampled volume,

charge de fond s'accumulent dans le delta, ce qui permet au front deltaïque de prograder à un rythme annuel de 2,6 m/a. Les autres sédiments sont transportés vers le large par des décrochements et des courants de turbidité qui empruntent les chenaux qui sillonnent le fond marin. Les chenaux sont faiblement sinueux et leurs fonds sont couverts de sable. D'autres détails associés à la rupture semi-continue des talus sont des escarpements de faille listrique que coupent souvent des crevasses et des fractures conjuguées. Une faille synsédimentaire profonde pourrait contrôler ces escarpements de glissement rétrogressif.

11. *Dépôts de bassin* : Les sédiments sont largement retenus entre les parois du fjord, bien que deux des seuils soient tapissés de sédiments hémipélagiques. Divers indices montrent que le taux de sédimentation diminue vers l'aval du fjord. Ce motif est interrompu par des cônes de déjection latéraux qui se sont souvent effondrés, progradant ainsi sur les marges abruptes du fjord et contribuant à l'apport de volumes considérables de sédiments aux fonds des bassins.

12. *Unités acoustiques* : Cinq unités sismo-stratigraphiques sont interprétées comme représentant principalement une phase unique d'avancée et de retrait de la nappe glaciaire. Les unités comprennent : (1) des sédiments de contact glaciaire qui comportent un faciès sédimentaire et un faciès glaciaire; (2) des sédiments proglaciaires qui se sont accumulés rapidement sous l'influence de déversements fluvioglaciaires sous-marins produits en partie en même temps que l'unité 1; (3) une accumulation distale de sédiments glaciomarins qui résulte du dépôt de sédiments hémipélagiques sous des panaches superficiels turbides; (4) des dépôts périglaciaires associés à la croissance rapide de deltas à partir de la calotte glaciaire terrestre, au cours d'une période de baisse rapide du niveau marin; et (5) des sédiments néoglaciaires accumulés lorsque le niveau marin était relativement stable et la sédimentation beaucoup moins importante. Les sédiments du Petit âge glaciaire sont très minces dans la plus grande partie du fjord; ils ne sont importants que dans le bassin le plus intérieur des quatre bassins. Dans les bassins 1 et 2, les sédiments les plus récents sont beaucoup plus fins que les sédiments plus anciens et pourraient refléter la réduction de la sédimentation suivant la phase initiale d'ablation au cours du Petit âge glaciaire. Dans les bassins 3 et 4, où les taux de sédimentation sont beaucoup plus faibles, les sédiments plus grossiers et plus près de la surface pourraient refléter le régime sédimentaire de l'unité 4. Les sédiments plus anciens et plus profondément enfouis, qui sont également plus fins, pourraient représenter les sédiments distaux de l'unité 3. Les calculs du bilan massique portent à croire que les unités 2 à 5 ont été déposées depuis l'avancée et l'ablation du dôme de glace du Foxe tardif. Les sédiments de l'unité 1 pourraient être antérieurs à cet événement.

13. *Faciès lithologiques* : Sept faciès sédimentaires sont reconnus dans les carottes provenant des unités 4 et 5 et possiblement de l'unité 3. Le faciès A, une boue sablo-caillouteuse, représente moins de 7 % du volume de sédiments et se compose de matériaux accumulés par suite de la fonte de la glace locale chargée de débris. Son volume diminue considérablement vers l'aval du fjord, vraisemblablement en raison d'une réduction des taux de sédimentation. Le faciès B, une boue tachetée, criblée de terriers, prédomine dans la colonne sédimentaire et constitue juste un peu moins de 50 % du volume

and implies that locally the rate of biological mixing exceeds the rate of sedimentation. The distribution of facies B reflect locations under the distal influence of river plumes. Facies C, wispy laminated/mottled mud, accounts for less than 4% of the sampled volume and may relate to suspension fallout punctuated by small volume, low velocity turbidity currents. An alternate explanation may have the thin sand lenses related to the meltout of aeolian sand initially transported onto the sea ice cover of winter. Facies D, laminated sand and mud, accounts for 21% of the sediment volume and relates to the high sedimentation fallout of sand and mud from hypopycnal discharge of river plumes. The shifting of the modal grain size reflects the changes in the level of discharge and thus the particle size of the suspended load. Facies E, coarse sand/gravel, is an extremely rare facies possibly an end-member of facies F. Facies F, pebbly sand and sand, accounts for 24% of the cored sediment volume and represents very rapid deposition from high concentration, viscous sediment-gravity flows, either as turbidity currents or as sandy debris flows. Facies F sands are typically interlayered with Facies B basinal muds. Facies G, crossbedded sands, is also an extremely rare facies (<1% by volume) that may relate to the reworking of turbidity current deposited sands by reverse flow mechanisms.

des échantillons; il indique que, localement, le taux de mélange biologique dépasse le taux de sédimentation. Sa distribution reflète des emplacements situés sous l'influence distale des panaches fluviatiles. Le faciès C, une boue tachetée, finement laminée, représente moins de 4 % du volume échantillonné; il pourrait provenir du dépôt de matériaux en suspension et, périodiquement, de courants de turbidité à faible vitesse et à faible volume. Par contre, il existe aussi une autre possibilité : les lentilles peu épaisses pourraient se composer de sable éolien qui couvrait la glace de mer et qui s'est accumulé suivant la fusion de cette glace. Le faciès D, composé de sable et de boue laminés, représente 21 % du volume de sédiments et est associé à l'accumulation de quantités considérables de sable et de boue provenant de l'influx hypopycnal de panaches fluviatiles. La variation de la granulométrie modale reflète les changements survenus dans le débit, et donc la granulométrie des matériaux en suspension. Le faciès E, un sable et du gravier grossier, est un faciès extrêmement rare qui pourrait être un terme extrême du faciès F. Le faciès F, composé de sable caillouteux et de sable, représente 24 % du volume de sédiments dans les carottes; il a été déposé très rapidement par des écoulements gravitaires visqueux, riches en sédiments, sous la forme soit de courants de turbidité, soit de coulées de débris sableux. Les sables du faciès F sont typiquement interstratifiés de boues de bassin du faciès B. Le faciès G, extrêmement rare lui aussi (moins de 1 % par volume), comprend des sables à stratification entrecroisée qui pourraient être un produit du remaniement, par des écoulements inverses, de sables déposés par des courants de turbidité.

INTRODUCTION

Fiords are deep, high-latitude estuaries which have been, or are presently being, modified by land-based ice. They are both an interface and a buffer between glaciated continents and the oceans. Most fiords act as sediment traps, containing a comparatively high-resolution sedimentary record that reflects both terrestrial and marine processes. Arctic fiords are subject to periglacial processes on land and influenced by the presence of sea ice through at least part of the year (Syvitski, 1986). Their specific characteristics are dependent on the relative influence of tides, wind, river discharge and glaciers.

Prior to 1982, investigations into the marine geology of arctic fiords have been limited in their scope and accomplishments: complex logistical requirements and an inhospitable climate have made detailed studies difficult. These early studies have been reviewed by Gilbert (1983). In view of these shortcomings, the Geological Survey of Canada initiated a multidisciplinary and international project to investigate Canadian arctic fiords: Sedimentology of Arctic Fiords Experiment (SAFE). The scope and objectives of this project are reviewed by Syvitski and Schafer (1985). Of the ten fiords surveyed during the first SAFE expedition in 1982, Itirbilung Fiord was considered representative of one class of arctic fiords, and received more detailed study in 1983, 1985, and 1987, both through ship and helicopter-based operations.

Itirbilung Fiord, located on the east coast of Baffin Island, is about 400 km south of Pond Inlet and 800 km north of Iqaluit (Fig. 1). It typifies a marine coastal basin that receives much of its sediment from a large sandur complex at the head of the fiord. The fiord is 55 km long (to the position of the outer sill), with a mean width of 3 km, a maximum water depth of 450 m, a surface area of 162 km^2, and a total water volume of 41 km^3. The tidal prism is 89 x 10^6 m^3. The distance from the head of the fiord and depth of water at the four sills within the basin are respectively: sill 1, at 6.5 km, 170 m; sill 2, between 11 and 16 km, 325 m; sill 3, between 20 and 24 km, 310 m; sill 4 at the fiord mouth in 275 m water depth.

Itirbilung Fiord drains a hinterland area of 2184 km^2, 31.9% of which is covered in ice fields or glaciers and 1.6% is composed of lakes. Gilbert and MacLean (1983) note that lakes act as effective sediment traps for 61.1% of the drainage basin area and 42.5% of the ice fields. The peak elevation within the hinterland is 1680 m, on the drainage divide between Itirbilung and McBeth fiords (Fig. 2).

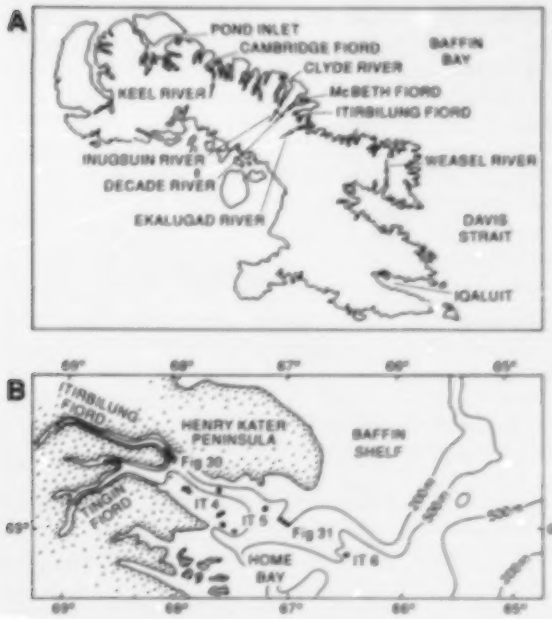

Figure 1. (A) Location of Itirbilung Fiord on the NE coast of Baffin Island, N.W.T. **(B)** Location of stations IT4, IT5, and IT6 and Figures 30 and 31.

The objective of this study is to investigate an arctic marine basin experiencing episodic sedimentation processes, using sedimentological and geophysical tools having very different levels of resolution. SAFE investigations on the Itirbilung site are summarised in Table 1. Details on the sampling logistics, equipment specifications, and methodologies employed can be found in Syvitski (1982), Syvitski and Blakeney (1983a,b), Asprey and Johnston (1984), Syvitski (1984a,b), Syvitski et al. (1985), and Syvitski and Praeg (1987). Andrews and Jennings (1987), Andrews (1990), and Andrews and Syvitski (in press) have reported on sediment magnetic characteristics, grain size and chronology of some of the piston cores described in more detail in our paper.

Acknowledgments

We thank everyone who helped in the collection and organization of a vast data set. This includes D. Praeg, D. Clattenburg, M. Reasoner, A. Wolberg, J.T. Andrews, A. Hay, C.T. Schafer, J. Stravers, G. Vilks, R. Trites, W. Petrie, G.S. Boulton and G. Benns. Our field support includes a hundred individuals that supported the SAFE project. They include the officers and crew of the C.S.S. Hudson, the M/V Pandora II, and Pisces IV, with special mention to the energy of K.W. Asprey, G.D. Hodge, K. Robertson, R. Belanger, G.V. Winters, R. Fitzgerald, K. Ellis, R. Murphy, J. Nielsen, A. Boyce, T. Atkinson, M. Gorveatt, and G. Bika. Our financial support came largely from the GSC projects 810042 (JPMS), 860026

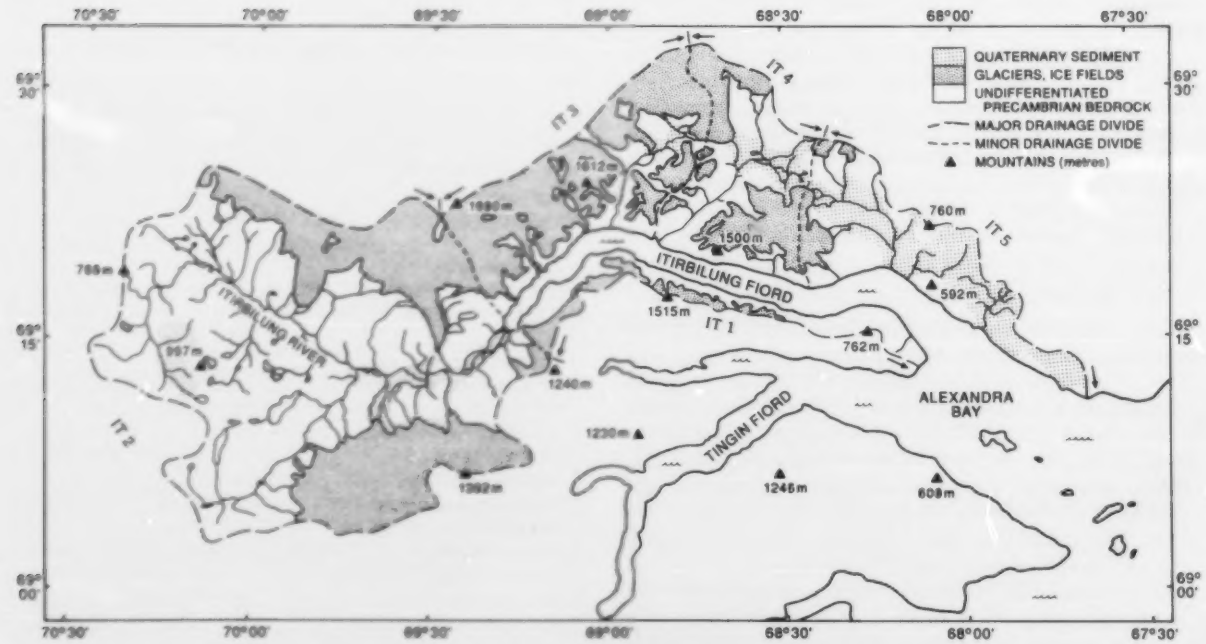

Figure 2. Drainage basins, including major rivers and lakes, surrounding Itirbilung Fiord. Shown are the major mountains (heights in m), the position of ice fields and glaciers, and areas of Quaternary sediment cover or exposed Precambrian bedrock.

(JPMS), and NSERC grants to FJH. Secondary support came from a 1982/83 University of Alberta President Grant (FJH), a 1983/84 and a 1985/86 DEMR Research Agreement (FJH), and a 1983/84 and a 1985/86 Boreal Institute for Northern Studies Grant (FJH). This paper represents Contribution No. 19 of the Sedimentology of Arctic Fiords Experiment (SAFE) project. Drs. John Andrews, Gustav Vilks, and Donald Forbes are thanked for their critical reviews.

ENVIRONMENTAL SETTING

Geologic framework

Except for two ship-track sounding lines collected by the C.C.G.S. d'Iberville in 1967 (Løken and Hodgson, 1971), no marine surveys of any kind had been previously conducted within Itirbilung Fiord. Land-based surveys were of a more regional nature, where site information from the Itirbilung Fiord hinterland contributed to a general understanding of Baffin Island geology.

Much of the marine portion of the fiord trough is surrounded by Archean layered granite-granodiorite-tonalite gneiss with locally abundant amphibolite lenses (Henderson, 1985). Near the head of the fiord, and further up the fiord valley, the rock type changes to Proterozoic schists and gneisses of the Foxe Fold Belt. The hinterland basin consists mostly of unvegetated bedrock or ice fields. Quaternary sediments are present only as discontinuous cover within the floors of the river valleys (Fig. 2).

The origin of the Itirbilung Fiord basin is poorly known. Dowdeswell and Andrews (1985) argue that the orientation and shape of the basin may relate initially to tectonic activity during the period of rifting (Cretaceous/early Tertiary) between West Greenland and Baffin Island. During this period, fluvial erosion actively downcut through the newly formed coastal mountains. Glacial action during the Quaternary modified these fluvial valleys, possibly overdeepening the troughs (e.g. Laine, 1980). The eastern margin of Baffin Island is considered to be one of Canada's most active seismic areas (cf. Syvitski, 1985). For instance in 1933, a Richter 7.3 earthquake shook the NE Baffin coast (Basham et al., 1977). The Itirbilung Fiord lies within the zone where horizontal ground accelerations may exceed 3 $m \cdot s^{-2}$.

The Quaternary framework of the Itirbilung area can be interpolated from observations just south of our study area (King, 1969; Andrews et al., 1970a,b), and from observations just east of our study area (Miller, 1985). Glaciation along the Baffin coast is considered to have commenced during the Early Pleistocene or even Pliocene (Syvitski and Piper, 1990). Based on seismo-acoustic records, glaciers are considered to have once reached the outer portion of the Baffin Shelf (MacLean, 1985). During the Early Foxe event (about 100 ka BP: Andrews and Miller, 1984), outlet glaciers were restricted to the fiords and troughs, leaving much of the low coastal forelands free of ice (Løken, 1966). No Middle Foxe glacial event (about 40 ka: Andrews and Miller, 1984) is yet recognized for the central Baffin region, and the Late Foxe glacial event (about 10 ka: Andrews and Miller, 1984) was even less extensive than that of the Early Foxe. The Neoglacial period began about 4 ka BP, as a result of moist winters and cool, dry summers. During this period cirque glaciers developed, reaching their maximum extent during the Little Ice Age (0.35 to 0.10 ka BP). These glaciers formed within the coastal mountains, flowing perpendicular to the margins of the fiord valleys. This is in contrast to the larger Pleistocene glaciers that had flowed along the fiord valleys from the central Baffin uplands. Over the past 50 to 100 years, the north-central Baffin region has experienced a warming trend. Glaciers are retreating rapidly, and tidewater glaciers of 40 years ago are presently subaerial (Syvitski, 1987a).

Sea level at the heads of the NE Baffin Island fiords, such as Itirbilung, has fallen exponentially over the last 8000 years BP, from a marine limit of 40 to 50 m above present levels (cf. Løken, 1965). However, much of the raised marine sediment along the Itirbilung River valley has been eroded through fluvial action since the onset of the Little Ice Age. There a large sandur has formed – described by Church (1972) as one experiencing active fluvial transport, possibly under the influence of jøkolhlaup (ice-dammed) discharges. Although sea level may still be falling at the fiordhead, the outer portion of the fiord (i.e. Cape Henry Kater: Figure 1b) is considered to be stable or experiencing a marine transgression (J. Stravers, pers. comm., 1987).

Climate

The present climate on Baffin Island is not well recorded. There are only 13 established weather stations to cover a land area exceeding 500 000 km^2. These stations are positioned mostly within coastal settlements and information on the landward side of the coastal mountains is almost nonexistent.

Table 1. SAFE investigations at Itirbilung Fiord

	1982	1983	1985	1987
Quaternary mapping	x	x		x
Lehigh gravity coring	x	x	x	
Grab sampling	x	x	x	
Piston coring	x	x		
Long-coring facility				x
Sediment trap moorings		x	x	
Current measurements		x	x	
CTD profiling	x	x	x	
Weather station observations		x	x	x
UMEL stereo bottom photography	x	x		
Klein side-scan sonar surveys	x	x	x	
BIO side-scan sonar surveys	x	x		
SPM water sampling	x	x	x	
Delta sampling/drilling	x	x	x	x
Submersible dives-unmanned (DART)		x		
Submersible dives-manned			x	
Attenuance profiling		x		
Boomer (HUNTEC DTS) seismics	x	x		x
Airgun reflection seismics	x			
Micro-macro benthos sampling	x	x	x	x
Bacteriology	x			
C.S.S. Hudson	x	x		x
M.V. Pandora II — Pisces IV			x	
P.C.S.P. helicopter support		x	x	x

None of the 13 weather stations lie within the Itirbilung drainage basin; the closest being Cape Hooper (125 km SE), Dewar Lakes (110 km SW), Longstaffe Bluff (230 km W), and Clyde River (120 km N). Climate within the Itirbilung drainage basin can be estimated using interpolations of data collected over a 30 year period (1951-1980) from the Baffin Island weather station grid (Table 2). In addition, Church (1972) collected weather data over a two year period for the Ekalugad drainage basin, approximately 50 km south of the Itirbilung drainage basin.

The Baffin Island climate can be considered "marine arctic". The summer is a period of relative calm, with the outer portions of the fiords being subject to fog and drizzle. During the autumn, frontal disturbances become more intense, and by late September the storms are most severe (Church, 1972). During winter, storms continue from the interplay of a major high pressure system overlying the western and central Canadian arctic, and the low pressure system over Baffin Bay and Davis Strait.

Climate and discharge

River discharge is important in the study of sedimentary processes within a fiord basin, as it plays a dominant role in the rate sediment is delivered to the fiord, affecting both the quantity and size of particles, or amount of bed load and suspended load transport. Discharge also affects the maintenance of the estuarine circulation within the water column, and the formation and break-up of sea ice.

There are few rivers in the Canadian arctic gauged by the Water Survey of Canada (only the Duval River near Pangnirtung, on Baffin Island). A few studies have collected river discharge data for short periods of time (Ekalugad Rivers in 1967-68: Church (1972); Inugsuin and Decade Rivers in 1965-67: Østrem et al., (1967), Stanely and Land (1968)). Based on topographic information and climate data, the freshwater input into Itirbilung may be estimated and a synthetic discharge curve produced using the following relationships (for details see Syvitski et al., 1984a):

(1) $Q_r = A \bullet S$

(2) $Q_n = (C \bullet W) + (G \bullet W)$

(3) $Q_i = g\,(W + (S \bullet a))$

(4) $Q_T = T \bullet t = Q_r + Q_n + Q_i$

where

Q_r is the summer rain runoff

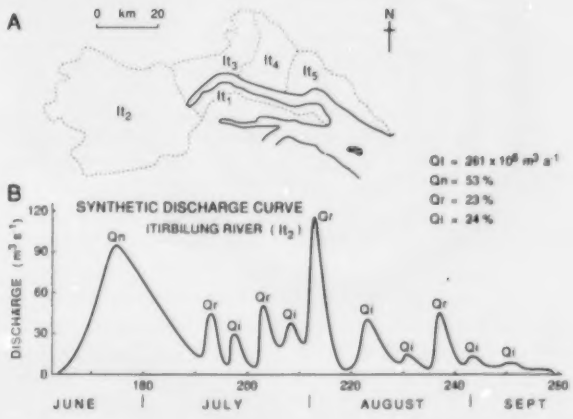

Figure 3. **(A)** The major drainage basins used in the climate-discharge modelling discussed in text. **(B)** A computed synthetic discharge curve for the main fiord-valley river (drainage basin It_2) with peaks labelled as to whether they are from nival melt (n), rain runoff (r), or glacier ablation (i).

Table 2. Climate data relative to the calculation of discharge for the Itirbilung drainage basin area based on 30-year averages of Canadian climate normals (from Atmospheric Environmental Services, Environment Canada: see Syvitski et al., 1984a for details). Shown below are the range in values from inland to the coast.

Nival Accumulation	(= Sept. 15 to June 15)	125 - 165 mm of water
Rainfall	(= June 15 to Sept. 15)	60 - 35 mm
Greatest rainfall in 24 hours		37 - 33 mm
Number of days of measurable rainfall	(July)	7.5 - 4
Standard deviation of precipitation	(July)	24 - 20 mm
Number of days of measurable rainfall	(August)	7 - 6
Standard deviation of precipitation	(August)	28 - 20 mm
Mean annual temperature		-12.5 to -10.5°C
Degree days above 10°C	(annual)	8 - 6

Table 3. The components of discharge as calculated using equations 1 through 4 (see text for details and definition of terms). Values of Q are ± 20%.

Basin (Fig. 3)	t (km^2)	g (km^2)	ELA (m)	SFL (m)	S (m)	W (m)	Q_n (m^3 x 10^6 a^{-1})	Q_r	Q_i	Q_t
It_1	128.2	30.4	700	1500	0.045	0.15	14.7	5.8	4.5	25.0
It_2	1344.8	376.2	850	1500	0.046	0.148	143.4	61.9	55.6	260.9
It_3	378.9	228.7	780	1500	0.046	0.15	22.2	17.4	33.9	73.5
It_4	275.3	74.7	725	1500	0.046	0.15	30.1	12.7	11.2	54.0
It_5	298.9	13.8	650	1500	0.045	0.148	40.7	13.0	2.1	55.8
Total							251	111	107	470
(%)							53%	23%	24%	

Q_n is the nival freshet

Q_i is the glacier melt runoff

Q_T is the total runoff

S is the summer precipitation (see Table 2)

W is the winter precipitation (see Table 2)

t is the total basin area

C is the total nonglaciated area

g is the total glaciated area above the ELA (a glaciers equilibrium position)

G is the total glaciated area below the ELA

B is the total glaciated area

a is the area above the SFL (average summer freezing level)

A is the area below the SFL

T = S + W

The first assumption with equations 1 through 4, is that precipitation falls evenly within a hinterland: elevation-caused variations in precipitation have not been corrected. The average summer freezing level (SFL) was estimated as being 200 m less than the maximum summer

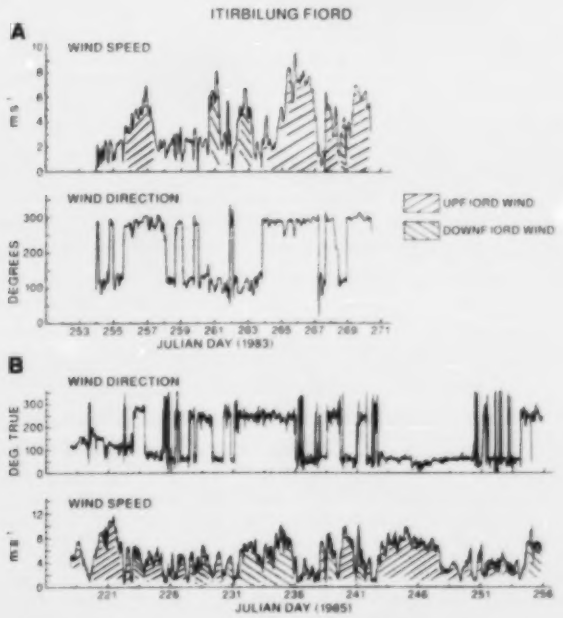

Figure 4. Wind data from the head of Itirbilung Fiord collected in 1983 (**A**) and 1985 (**B**). The station was positioned midvalley at 69° 14.0'N and 69° 16.0'W, 200 m from high tide line. Wind direction in true azimuth and wind speed is measured 2 m above the ground and 3 m above mean sea level. For instrument details and data processing techniques employed see Syvitski (1987b). See Figure 10 for station location.

Table 4. Sediment flux data for the Itirbilung Fiord hinterland

Basin (Fig. 3)	area (km^2)	equation	suspended load ($t \cdot a^{-1}$)	(‰)	total[1] sediment yield ($t \cdot km^{-2} \cdot a^{-1}$)
It_1	128.2	5a	560	0.8	9
It_2	1344.8	5a	60,800	84.5	91
It_3	378.9	5c	5,400	7.5	28
It_4	275.3	5a	2,600	3.6	19
It_5	288.9	5a	2,600	3.6	18
Total	2416.1		71,960		
	(km^2)		($t \cdot a^{-1}$)		

[1] total = suspended plus bedload and bedload = suspended load

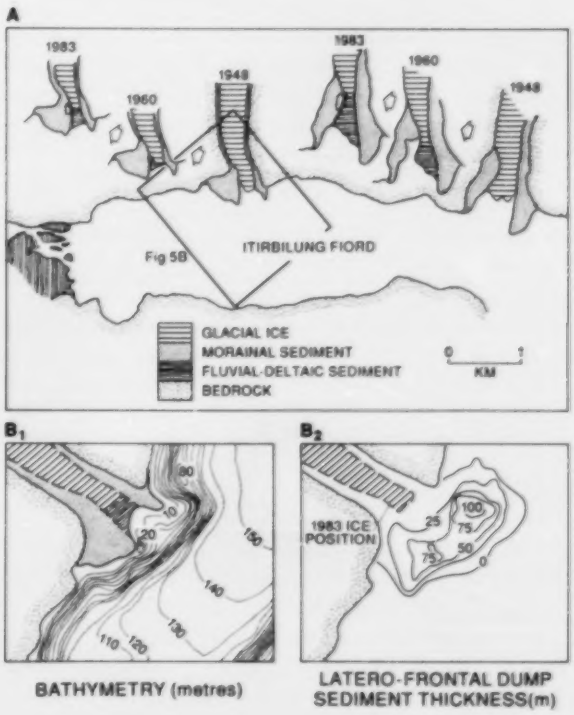

Figure 5. (A) The pattern of ice retreat of two side-entry glaciers situated on the northern margin and at the head of Itirbilung Fiord. Data based on EMR air photos T320C-199 (1948) and A-17011-16 (1960), and PCSP helicopter photography in 1983. **(B)** The present bathymetry (1) near one the side-entry glaciers and sediment thickness (2) from ice-contact sediment deposition.

conditions given by Miller et al. (1975). Corrections for evaporation and/or condensation were considered fairly small (see Østrem et al., 1967). Thus the second assumption is that the summer precipitation runoff is equal to the total summer precipitation that falls below this adjusted SFL position. The average elevation for a glaciers equilibrium position (ELA) was interpolated from the contoured data of Andrews and Miller (1972). Their given ELA altitudes during the last couple of decades are considered steady state altitudes and are thus comparable with the 30-year averaged values on climate given in Table 2. Terms t, C, g, G, B, a, and A are compiled from 1: 250 000 Canadian E.M.R. topographic maps and use of a high resolution digitizing table.

Table 3 gives the pertinent terms and model predictions for the five major hinterland drainage basins surrounding Itirbilung Fiord (Fig. 2 and 3a). Much (56%) of the freshwater discharge comes from the large sandur at the head of the fiord, and over half of this is a result of melting snow during the spring freshet (Table 3). Present data does not allow for a detailed or sophisticated check on model predictions. For instance the above model, based on 30 year-averages, predicts an annual discharge of 42.2 million m^3 for the Inugsuin River (Syvitski et al., 1984a). This may be compared to measured values of 93 million m^3 for 1965 and 64.4 million m^3 for 1967 (Østrem et al., 1967; Stanely and Land, 1968). This variation may relate to both 1965 and 1967 being subject to exceptional levels of precipitation (see Church, 1972, Table 9).

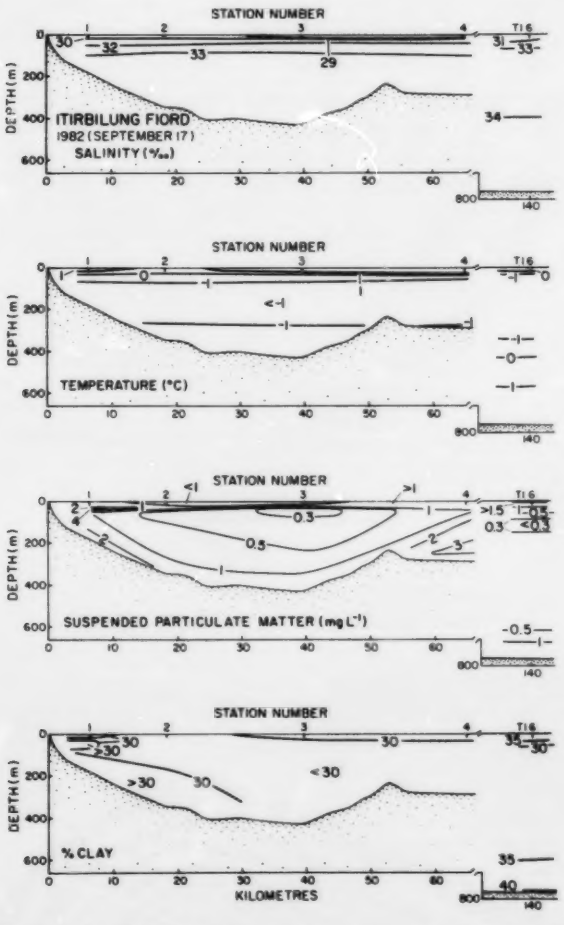

Figure 6. Salinity, temperature, suspended sediment concentration and clay fraction within SPM for four fiord stations and one deep shelf station for Itirbilung Fiord collected in September of 1982 (CTD data from Trites et al., 1983, interpretation from G.V. Winters, pers. comm., 1986).

Table 5. Geomorphological statistics of Itirbilung Fiord in comparison with other Baffin Island fiord morphologies (modified from Dowdeswell and Andrews, 1985)

	BAFFIN FIORDS (Dowdeswell & Andrews, 1985)		ITIRBILUNG
Parameter	Range	Mean	
Fiord length (km)	5-120	27.9	57
Fiord mouth breadth (km)	1-39	6.5	6.4
Max. elevation along fiord (m)	229-1905	787.1	1678
Number of bends	0-9	2.2	4
General fiord orientation (°)	0-179	77.4	110
Outer coast orientation (°)	0-178	96.3	56
Max. island elevation (m)	76-858	192.5	366
Fiord mid-breadth (km)	0.4-8	2.5	3
Fiord head-breadth (km)	0.2-5	1.3	2.2
Area (km^2)	3-853	104.7	245 (min.)
Max. depth within fiord (m)	20-950	330.8	450
Sill depth at fiord mouth (m)	2-402	146.6	275
Depth 5 km from fiord head (m)	12-512	127.2	180
Shape index	0.02-0.6	0.2	0.1
Fiord volume (km^3)	2-1220	179.7	261 (min.)

The model does not incorporate changes in the mass balance of the local ice fields, rather it assumes a steady state equilibrium. Syvitski (1987a) found that glaciers in the Itirbilung drainage basins were retreating at rates varying from 5 to 32 $m \cdot a^{-1}$. Thus, the predicted discharge component related to ice melt (Table 3) is a minimum. Where the number and size of glaciers in a drainage basin is high (>50% by area), the value of Q_i may be up to 10% too low.

Notwithstanding these concerns with respect to the climate-discharge model, a synthetic discharge curve may be constructed. To produce an appropriate discharge curve, a number of cycling factors must be determined (see Syvitski et al., 1984a). Cycling involves the number of modes and size (duration) by which a particular discharge component must be segmented. For example, Q_n is set to occur in the spring as one mode skewed towards the summertime. The duration depends on the hypsimetric integral, basin area and the number of lakes, all of which work to delay or spread Q_n over a longer time interval. Q_i is set to occur only after Q_n is complete, and is cycled by the number of clear days with high positive temperatures. (In the absence of reliable A.E.S. cloud cover data, degree days above 10°C will be used – Table 2).

Q_r is set to never overlap with Q_i (not strictly true), to occur only after Q_n is mostly complete, and is cycled by the number of significant summer precipitation events (Table 2). One event is given a peak value equivalent to 50% of the greatest rainfall in 24 hours (Table 2), and set to occur in the month with the highest standard deviation in rainfall. A base flow is maintained by distributing 10% of the total runoff over the entire discharge season.

Figure 3B is an example of a synthetic discharge curve computed for the large Itirbilung River flowing into the head of the fiord. It shows a large freshet in the early summer, followed by many short-lived discharge events that relate to rain storms or warm periods affecting the melt of hinterland ice sheets. Typical of arctic conditions, the discharge period is extremely short — of less than three months duration. The pattern is comparable to measured discharge curves (see Church, 1972; Stanely and Land, 1968; Østrem et al., 1967).

Wind

The action of wind is important to the seaward transport of aeolian material, and additionally affects the circulation, and thus sedimentation of particles, within the fiord basin. Prior to 1980, data on wind velocity within the Baffin fiords was almost nonexistent; A.E.S. weather station data is very site dependent, most being affected by local topographic features and strongly influenced by land-sea breezes. In a review of wind data, McKenna-Neuman and Gilbert (1986) note that the strongest arctic winds occur at sites where A.E.S. measurements have not been made.

In 1982, on the maiden voyage of the SAFE cruises, the C.S.S. Hudson observed winds in excess of 40 $m \cdot s^{-1}$, enough to disrupt the ongoing sampling activity in McBeth Fiord (Syvitski and Blakeney, 1983a). On the previous day, a raging aeolian storm on the Itirbilung River delta was witnessed, with dust clouds exceeding 100 m in elevation (photo interpretation). To investigate the importance of an aeolian contribution of sediment to the fiord, and to better understand local oceanographic conditions, a weather station was positioned near the high tide line within the main Itirbilung River valley (for 18 days in 1983 and for 39 days in 1985).

The winds were present almost continuously during the summer to early-autumn period of observation (Fig. 4), and either up- or down-fiord. The strongest winds were upfiord, occasionally exceeding 13 $m \cdot s^{-1}$ (47 $km \cdot h^{-1}$). The large events, sometimes lasting 5 days, were correlative between fiords and indicate the presence of large weather systems (Syvitski, 1987b). The shorter events appear to be the result of relatively strong land-sea breezes that reflect a katabatic influence, i.e. with winds developed over the hinterland ice fields.

SEDIMENT INPUTS

Glaciofluvial inputs

Except for some minor streams entering near the mouth of the fiord (Fig. 2), there is a predominantly glacier melt component, or glaciofluvial input, to the discharge of freshwater into Itirbilung Fiord. The suspended load, Q_s, may be calculated using an order-of-magnitude type rating curve. Church (1972) found daily Q_s to vary approximately with the square of the discharge for Baffin Island hinterlands not dominated by ice melt and rising to the cube of the daily discharge (Q) for hinterlands dominated by ice fields. For basins surrounding Itirbilung Fiord we use the following regression relationships (algorithms and data corrected from those outlined in Syvitski et al., 1984a):

for <30% ice fields within a drainage basin,

(5a) $Q_s = Q^2 (5 \times 10^{-3})$ where Q is in units of $m^3 \cdot s^{-1}$, Q_s is in units of $kg \cdot s^{-1}$,

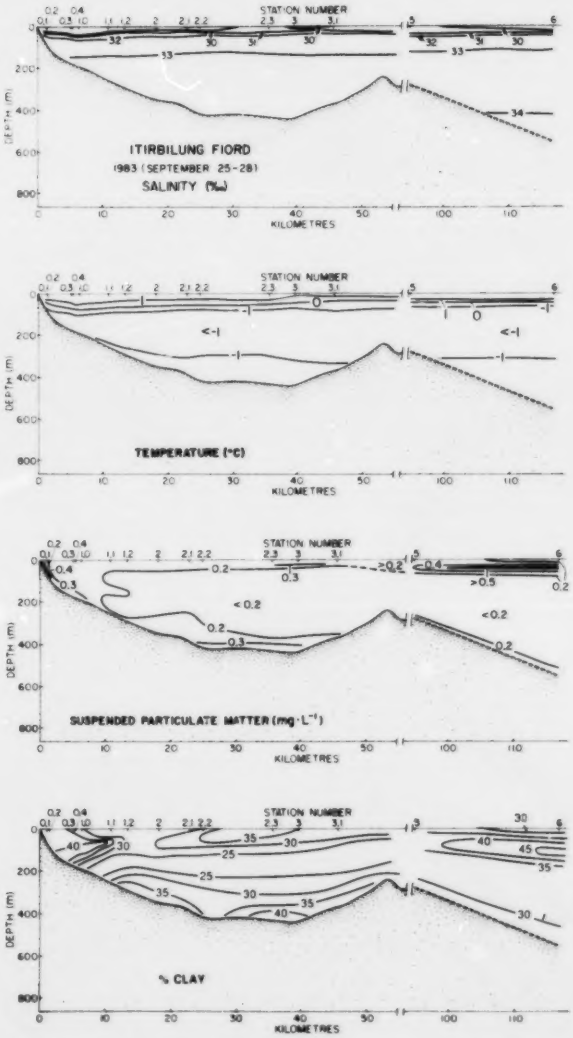

Figure 7. Salinity, temperature, suspended sediment concentration and per cent clay within SPM for 16 fiord and one deep shelf station for Itirbilung Fiord collected in September of 1983 (CTD data from Petrie & Trites, 1984; interpretation from G.V. Winters, pers. comm., 1986).

for basins with between 30 and 60% ice fields,

(5b) $Q_s = Q^{2.5} (10^{-3})$

for >60% ice fields within a drainage basin,

(5c) $Q_s = Q^3 (5 \times 10^{-4})$

and where the total sediment delivery for a basin is the average suspended load times the length of the discharge season (set to 97 days in Fig. 3). Using daily values of Q and Q_s, as compared to use of instantaneous values, will underestimate the load predictions by 5 to 20%. However the climate-discharge model (equations 1 to 4) cannot be used to predict instantaneous discharge values.

Table 4 provides the suspended sediment estimates for the five hinterland basins (Fig. 3) outlined in Table 3. The sediment yield from this data ranged from 9 to 91 $t \cdot km^{-2} \cdot a^{-1}$, values comparable to Church (1972) data for three rivers flowing into Ekalugad Fiord, ranging from 0.8 to 86.5 $t \cdot km^2 \cdot a^{-1}$ and slighly lower than those of Østrem et al. (1967), of 160 $t\ km^{-2}\ a^{-1}$ for the Decade River, a side-entry river flowing into Inugsuin Fiord. Most of the suspended sediment enters near the head of Itirbilung Fiord, i.e. basins It_2 and It_3 (Fig. 3).

Church (1972) observed on three Baffin Island fiord rivers, that the transport of bedload was as large as the transport of suspended load. Table 4 also includes this assumption of a 1:1 ratio between bedload and suspended load for the total sediment yield.

Glacial inputs

At present there are no tidewater glaciers along the margins of Itirbilung Fiord. However, as recently as the early 1950s there were four tidewater glaciers entering the fiord (Fig. 5A). Field evidence, based on lichonometry, suggests that these glaciers reached their maximum tidewater position during the Little Ice Age. Thus for at least 100 years (1850 to 1950), Itirbilung Fiord received a direct input of glacial sediment to its basin.

These hanging glaciers flow into the fiord along the steep margins. The distance they could traverse from the shoreline was dependent on the rate they could construct an ice-contact fan delta while maintaining a relatively stable ice front position. In one example considered typical of all four glaciers (Fig. 5B), the mass of latero-frontal dump of glacial debris into the fiord is estimated at about 0.7×10^9 tonnes. (This estimate was based on a volume of sediment determined from bathymetric irregularities in the otherwise smooth fiord margin slope times a bulk density for poorly sorted rubble). If we assume that the period of fan delta growth was at least 500 years, then each of these four tidewater glaciers contributed up to $1.4 \times 10^6\ t \cdot a^{-1}$, or up to one order-of-magnitude more than the sediment delivered to the fiord by fluvial discharge. The subaerially exposed lateral moraines consist predominantly of sand sized material around an inner core of glacial ice; their surface is covered in boulder sized supraglacial debris. These four tidewater glaciers were therefore responsible for a dramatic increase in the sediment delivery of coarse particles to the fiord, but for a limited time.

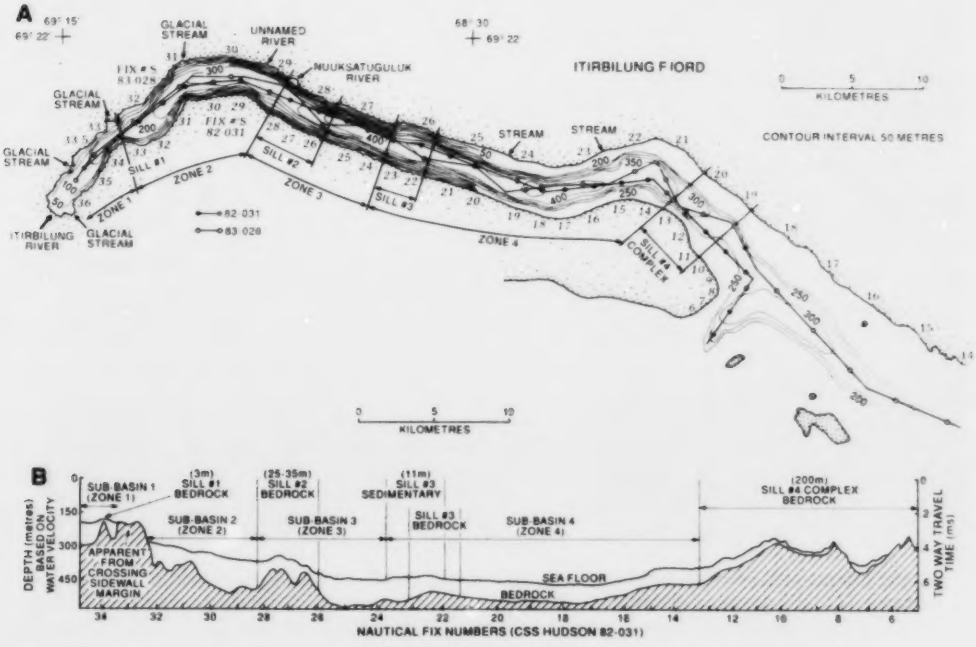

Figure 8. (A) Bathymetry of Itirbilung Fiord and ship track lines of seismic surveys. **(B)** The acoustic basement profile based on the 1982 airgun seismic survey (solid dots).

We have no direct evidence to know whether the composite stratigraphy within the Baffin Island fiords is a result of sedimentation events only since the last glaciation (i.e. the Late Foxe) or from contributions of previous glaciations (i.e. the Early Foxe). Andrews (1990) suggests that Itirbilung Fiord contained a non-erosive tidewater glacier (or possibly an ice shelf) during the Late Foxe glaciation. Thus glacial deposits identified on seismic records may relate to an early glacial period such as the more extensive Early Foxe glaciation (see supporting discussion in Gilbert, 1985).

Through indirect information on the last major glaciation, we can speculate on the contribution of sediment during that period. We know that the glaciers that occupied the Baffin fiords, flowed from an ice dome that was located over the Foxe Basin (Andrews et al., 1970b, 1985, 1989). The drainage divide during that period (from before 18 000 BP to 8000 BP) was situated some 200 km west of the present divide (Dyke and Prest, 1987). The size of the paleo-catchment areas at the heads of the Baffin Island fiords, such as Itirbilung, may have been at least five times their present size. However, the size of the hinterland along the fiord margins would not have significantly changed during this period.

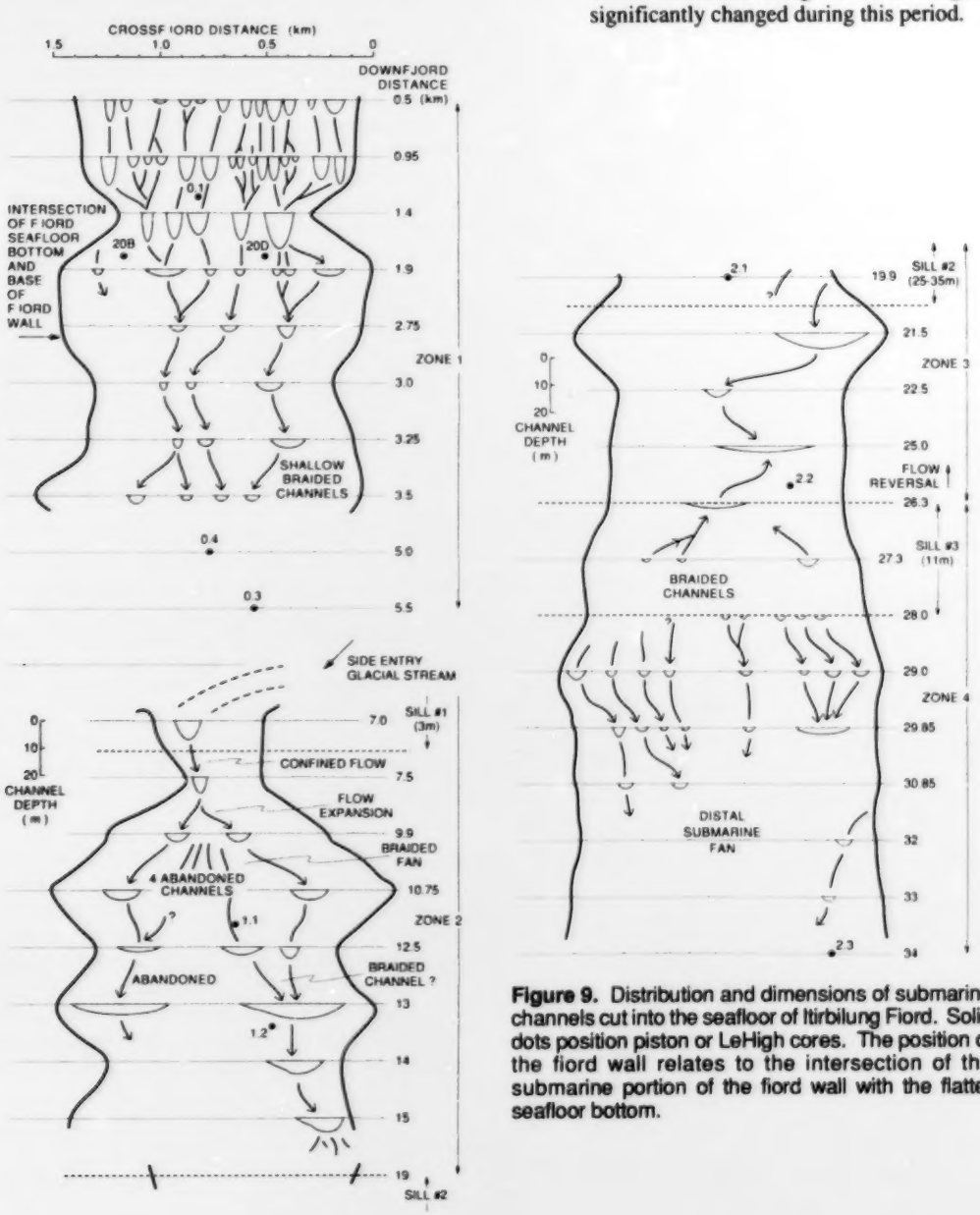

Figure 9. Distribution and dimensions of submarine channels cut into the seafloor of Itirbilung Fiord. Solid dots position piston or LeHigh cores. The position of the fiord wall relates to the intersection of the submarine portion of the fiord wall with the flatter seafloor bottom.

The climate during a period of glacial advance is one of cool summers and moist winters, associated with a concomitant increase in water storage through the formation of glacial ice. The climate during a period of glacial retreat is associated with drier winters and much warmer summers, i.e. an extended and more active season of ice ablation. If we consider only the Late Foxe deglacial period in our estimate of sediment delivery to Itirbilung Fiord, we may assume a climate similar to our present situation where glaciers are rapidly retreating from their Little Ice Age position. Thus the fluvial discharge delivered to the head of the fiord during this deglacial period would be increased both through an increase in the size of the drainage basin, and through the glacier melt contribution.

The Late Foxe deglacial period is considered to extend from 10 000 to 9000 years BP and from 8400 to 6000 years BP, separated by a small period of re-advance (Dyke and Prest, 1987). Discharge during the first portion of this deglaciation is assumed to relate primarily to the larger paleo-drainage basin with an equilibrium condition of ice

Figure 10. Detailed bathymetry (contours are in metres) of the fiordhead prodelta superimposed on a NAPL air photo showing location of hydrographic (echosounder) lines (cf. Fig. 11), location of the 1983 and 1985 weather station (W.S.) and oceanographic moorings (O.M.) (cf. Fig. 4, 14, and 15).

melt, i.e. up to five times the present level of fluvial discharge. If we assume that the meltwater is relatively clean (possibly due to a portion of the ice sheet being cold based: J.T. Andrews, pers. comm., 1989) the total sediment delivery is given by $Q_s = 2\,Q^2\,(7 \times 10^{-4})$, i.e. 3×10^5 t • a^{-1}. Determining the discharge during the latter portion of deglaciation is more complicated, as the drainage divide migrated eastward during this period (Dyke and Prest, 1987). The average basin area during this period is about 2.5 times the present drainage area. Secondly, this period of deglaciation went to completion (i.e. all of the glacial ice within the Itirbilung basin melted). Thus a nonequilibrium state of ice melt is considered: an ice volume of 3500 km^2 (paleo-drainage basin) by 2 km (ice thickness estimate: Quinlan, 1985) melted over a 2400 year period. Thus an additional 2.9 km^3•a^{-1} of ice melt must be considered, or a discharge of approximately twelve times the present level. If we again assume that the meltwater for the period 8400 to 6000 years BP is relatively clean ($Q_s = 2\,Q^2\,(7 \times 10^{-4})$), we estimate for this period that the sediment delivery to be five times the present rate, i.e. 6×10^5 t • a^{-1}.

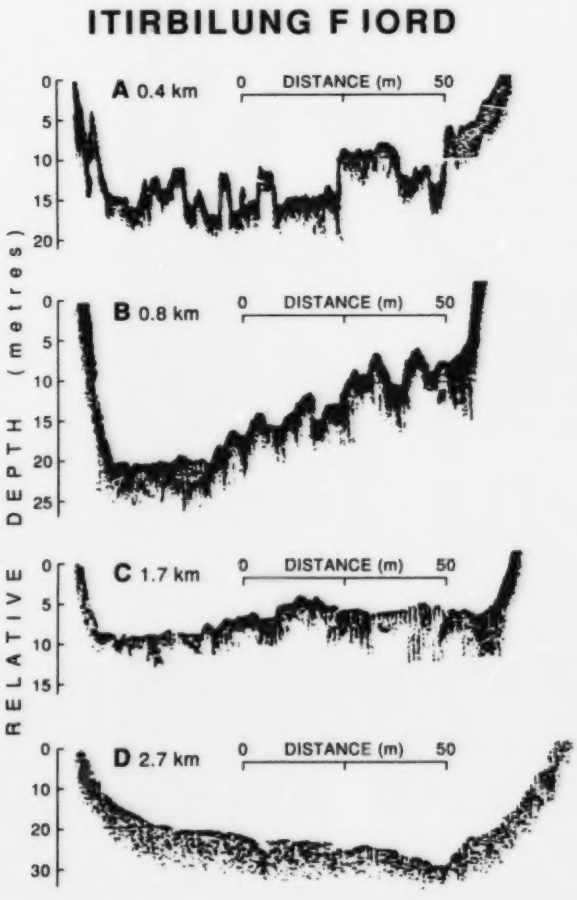

Figure 11. Echosounder profiles from the fiordhead prodelta (cf. Fig. 10 for positions).

Fluvial discharge between the period of 6000 and 150 years BP, a time of Neoglacial ice storage, is considered to be fractionally smaller than present levels. Based on estimates of maximum Holocene ice storage, discharge may be 50% less than present levels, with little bedload transport. The ice melt component would be largely reduced, thus the appropriate sediment rating is given by equation 5a.

Aeolian inputs

The importance of aeolian transport depends on having suitably strong winds to move an available supply of sediment for significant periods of time. We have witnessed and sampled aeolian storms over the Itirbilung River delta (Syvitski et al., 1983a). However, the transport of sediment from the delta to the fiord basin is difficult to estimate based on our limited wind velocity data. Whether a sediment particle is moved depends on a wind event superseding a critical or threshold shear velocity to move a particular (size, density) particle. Following Bagnold (1954), the critical shear velocity, U_{*_c}, may be expressed as

$$(6)\quad U_{*_c} = A\,[((\sigma-\rho)/\rho)\,g\bullet D]^{0.5}$$

where A is a dimensional entrainment coefficient, σ is the particle density, ρ is the density of air, g is the acceleration due to gravity and D is the particle diameter. We chose A as 0.08, a number representative of entrainment by grain impact. The modal size of all aeolian deposits on the Itirbilung delta is 0.15 mm, and needs a critical shear velocity of 14.4 cm•s^{-1} to initiate sediment transport. Lag deposits of aeolian-affected sheet sands had an upper size range of 5 mm; thus the maximum critical shear velocity to affect the entire sandur is set at 83.2 cm• s^{-1}.

Hsu (1974) notes that wind speed collected from 2 m above the sediment surface, U_{2m}, (as in our case: Fig. 4) can be used to calculate shear velocity U_*, through the relationship

$$(7)\quad U_* = 0.044\,U_{2m}$$

Thus the critical and ultimate wind velocities for the modal and lag grain sizes on the Itirbilung sandur are 3.3 m•s^{-1} and 18.9 m• s^{-1} respectively.

We are only interested in winds above the critical velocity that deliver sediment to the fiord waters (i.e. down-fiord winds). Based on our wind data (Fig. 4), only 3 events in 1983, lasting for 11% of the observational period, and 8 events in 1985, lasting for 28% of the observational period, can be considered in our calculation of aeolian sediment transport. Winds that approached the maximum critical shear velocity were not observed, and we suspect that our short periods of observation (18 days in 1983 and 39 days in 1985) are biased to the lower energy events. However, in 1982, 40 m• s^{-1} winds were recorded on our research vessel, exceeding the maximum critical wind velocity for lag deposits on the sandur.

Calculation of aeolian sediment transport is difficult without a good knowledge of the moisture content of the soil. There is no vegetation cover on the Itirbilung sandur to further

complicate the calculations. McKenna-Neuman and Gilbert (1986) note for a similar Baffin Island sandur (Weasel River), that 75% of the sediment samples had moisture contents <1% during the summer period — the time of our measurements. Thus during this period, much of the sandur would be affected by aeolian action. During the winter, snow covered the Weasel River sandur only 11% of the time. McKenna-Neuman and Gilbert (1986) speculate that reworking of the sandur surface by wind may therefore occur year-round, although the most active period is for the fall and early winter. We know that aeolian transport in Itirbilung Fiord also occurs during this period, as thick (5 to 20 cm) layers of aeolian sand interbedded with snow were located in drifts both in 1982 and 1987. In our total sediment transport calculations below, we estimate that critical winds blowing in the down-fiord direction occur 20% of the time and affect 30% of the sandur surface. Of the period of active aeolian transport, we assume that ultimate threshold conditions occur only 1% of the year.

Using the Bagnold (1954) approach to sediment transport, q (in units of grams per centimetre width per second), then

(8) $q = C\,(r/g)\,(D/d)^{0.5}\,(U_*)^3$

where C = 2.8 and is a sorting constant for poorly sorted sand, and d is a reference grain diameter of 0.25 mm sand. Through substitution of equation 7 into equation 8, then the sediment transport during critical conditions, q_m, for modal grain size and during maximum critical conditions, q_l, for lag deposits, may be expressed as

(9a) $q_m = 2.2 \times 10^{-10}\,(U)^3 \qquad 330\ cm \bullet s^{-1} < U \leq 1890\ cm \bullet s^{-1}$

(9b) $q_l = 1.3 \times 10^{-9}\,(U)^3 \qquad U > 1890\ cm \bullet s^{-1}$

We may constrain the aeolian transport predictions by assuming that there is not an unlimited annual supply of erodable sediment, i.e. that below the active layer for aeolian erosion sediment is either frozen, too moist, or too coarse to be transported by even the strongest of winds. If we choose a 5 cm mobile layer, assume 30% of the sandur surface is affected by aeolian transport, and based on an extrapolation of our wind observations with the assumptions discussed above, then the annual transport of aeolian sediment into the fiord basin is 360 000 $t \bullet a^{-1}$ (three times the estimate of fluvial transport for the Itirbilung River). It is of relevance to note that 96.8% of the aeolian sediment is predicted to be transported during 3.5 days of the year.

Marine inputs

Suspended sediment may enter or exit a fiord during deep-water flushing processes where shelf waters enter and exchange with waters within the fiord. This is of particular relevance to Baffin fiords whose waters are typically less turbid (except for the surface layer) than water masses on the shelf (Winters et al., 1985). The Baffin shelf is a high energy environment swept by the southerly-flowing Canadian current. Typical velocities range from 0.05 to 0.5 $m \bullet s^{-1}$. However, Itirbilung Fiord is protected from the direct affect of the Canadian current by Home Bay and Henry Kater Peninsula to the north (Fig. 1B).

Our oceanographic data are too sparse to attempt to discern whether on an annual basis more sediment enters or exits Itirbilung Fiord. On September 17, 1982, the fiord waters were significantly more turbid than the water in Home Bay (Station Ti6: Fig. 6). On September 25 to 28, 1983, the

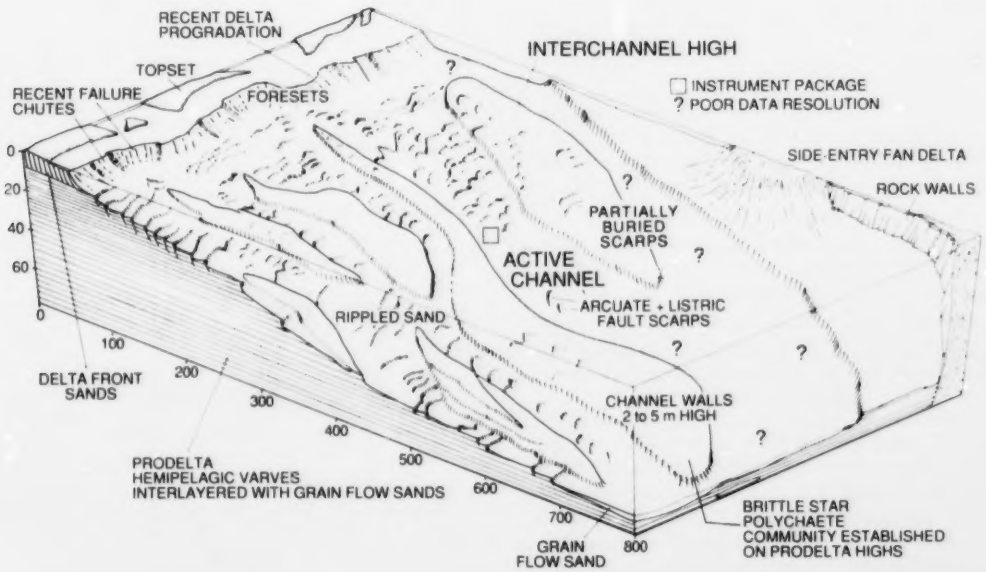

Figure 12. Interpretive sketch of sidescan sonar mosaic (combining 1982, 1983 and 1985 data) and submersible dive observations, of the prodelta of Itirbilung Fiord. The concave arcs within the channels are arcuate and listric fault scarps (after Syvitski and Farrow, 1989).

suspended particulate matter in the waters of Home Bay were at similar levels to the waters of Itirbilung Fiord (Fig. 7). For our sediment budget calculations we will assume that as much sediment enters the fiord as leaves the fiord.

Sediment may also be produced *in situ* through biologic productivity including tests of organisms (both pelagic and benthic) and mineralization of organic material. We examined grab and core sample smears with a scanning electron microscope to determine the inorganic-biogenic component. Values ranged from <0.5% in turbidite sands to 5% in some basinal muds, with a mean value of 2%. The dominant biogenic component is siliceous tests of pelagic diatoms. The carbon content of grab samples ranged from 0.2 to 1.2% with a mean fiord value of 0.6%. The total autochthonous component within Itirbilung Fiord sediments is approximately 3.5% by weight.

BASIN CHARACTERISTICS

Compared with other summary statistics of the Baffin fiords (Dowdeswell and Andrews, 1985), Itirbilung is typical, including the presence of islands at or near the fiord mouth, the presence of a shelf trough extending from the fiord mouth, and the presence of a sill at the mouth of the fiord. Dowdeswell and Andrews (1985) in their description of 227 Baffin Island fiords measured 29 parameters to geomorphologically classify the fiords. Table 5 summarizes those parameters based on interval or ratio data with comparison to Itirbilung Fiord. Itirbilung Fiord is longer than the average, less rectangular, and encompasses a larger area. Itirbilung Fiord has 4 bends, two at angles near 50 degrees and two at approximately 30 degrees (Fig. 8A). Itirbilung is much deeper than average, with a maximum depth of 450 m, and a fiord mouth sill depth of 275 m (Fig. 8A; Fig. 1.5 in Syvitski, 1984a).

Acoustic basement characteristics

Itirbilung Fiord is a narrow, possibly normal fault-bounded, 450+ m deep basin (Fig. 1B, 8). The acoustic basement comprises mixed Aphebian and Archean age bedrock of the Foxe Fold Belt (Jackson and Taylor, 1972; Henderson, 1980). A Hadrynian diabase dyke transects the fiord valley a few hundred metres upstream from the fiordhead. At the head of the fiord, the bedrock walls are Aphebian-age rocks of the Piling Group, consisting of rhythmically interbedded graphitic psammitic and pelitic metasediments, rusty weathered graphitic metapelite, and quartzite. The remaining down-fiord walls comprise predominantly Archean layered granitoid gneisses with amphibolite boudins.

The bedrock basement beneath the Quaternary basin fill was delineated using seismic reflection records obtained during the C.S.S. Hudson cruises 82-031 and 83-028 (Fig. 8A). The 1982 seismic track line was located approximately down the midline of the fiord, with fix points located at a 1 nautical mile (1.85 km) spacing (Fig. 8A). Along this profile, the bedrock has an irregular upper surface (Fig. 8B). There are four bedrock-controlled sills that separate the fiord into four basins (Fig. 8B). The innermost sill, located 6.5 km from the fiordhead and with a relief of 3 m, has ponded at least 100 metres of sediment from the Itirbilung prodelta margin. The second sill, between 11 and 16 km down-fiord and with basin relief of 25-35 m, isolates a basin containing 150 m of sediment: the sill is draped by 25 m of sediment. The third sill, between 20 and 24 km down-fiord with relief of 11 meters, has framed a basin with >150 m of sediment-fill. This 'sedimentary sill' (Fig. 8B) is displaced about 1 km up-fiord from the underlying bedrock high (Fig. 8B), reflecting up-fiord progradation of a wedge of sediment possibly derived from the third sill. The fourth sill, with 200 m of relief, occurs at the fiord mouth.

Present seafloor morphology

Itirbilung Fiord can be divided into four basins (Fig. 8, 9). Basin 1, bounded by sill 1, receives sediment from the Itirbilung River, and secondarily by three side-entry glacial streams (Fig. 2, 8). Basin 2, located between sills 1 and 2, receives sediment mainly by a glacial stream and a submarine valley that dissects sill 1. Secondary inputs include a smaller side-entry glacial stream on the north side of the fiord located midway down the basin, and an unnamed river at the eastern end of the basin, up-fiord from the second sill. Basin 3, constrained between sills 2 and 3, receives sediment predominantly by the side-entry Nuuksatuguluk River and its associated submarine channel which dissects sill 2. Basin 4, located between sills 3 and 4, is the largest basin within the fiord, nearly 16 km in length. It is fed by two side-entry streams on the north side of the fiord.

The seafloor of Itirbilung Fiord is dissected by submarine channels that decrease down-fiord in number (from 15 at the fiord head to 1 near the outermost sill) and size (176 m wide and 13 m deep at the head to 28 m wide and 1 m deep near the outermost sill). Four cross-section sounder profiles

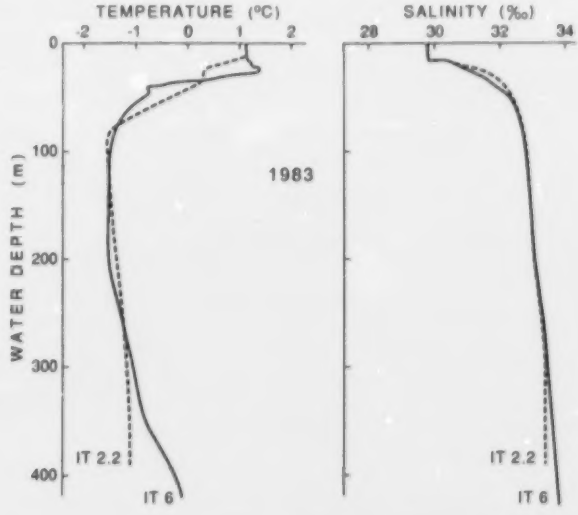

Figure 13. Salinity and temperature profiles collected in September of 1983 for an inner fiord (station It2.2) and an outer fiord (It6) station (cf. Fig. 7 for station location).

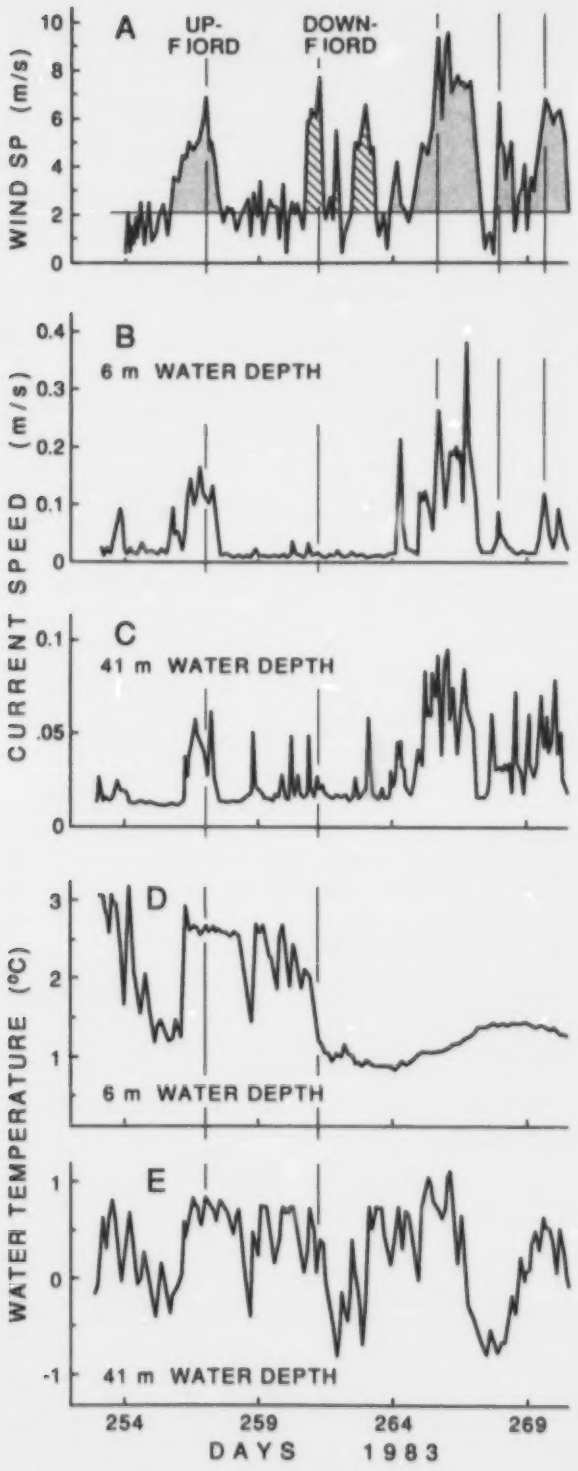

(Figure 11, with positions in Fig. 10) show these down-fiord trends in the number and size of submarine channels. Four styles of channels on the basin floor are recognized (Fig. 9 and 11): (1) straight, U-shaped, 1 to 10 m deep, prodelta channels 0 to 7 km down-fiord, which become less dissected, and have more relief down-fiord (Fig. 9); (2) straight, U-shaped, 6 to 10 m deep, channels in sites of confined flow, 7 to 10 km down-fiord (Fig. 9, 11 and 12); (3) broad, meandering or straight channels, 2 to 7 m deep, 13 to 15 km down-fiord and 21.5 to 25 km down-fiord (Fig. 9); and, (4) shallow, braided channels, 1 to 5 m deep, 3.25 to 3.5 km down-fiord, 9.9 to 13 km down-fiord (Fig. 9), and 28 to 32 km down-fiord. Channels originating on sill 3 direct sediment into the third basin, in an up-fiord direction (Fig. 9).

Synoptic oceanography

Baffin fiords experience three oceanographic seasons (Syvitski, 1989; Syvitski et al., 1990). The first is the winter season (= October 1 to June 15), a time of sea ice growth wherein salt is rejected during the crystallization process and super-saline "salt fingers" sink through the water column. The salinity of the sea ice decreases through the winter season from an initial value of about 30 ppt, to about 5 ppt by the spring melting. The rejected brine establishes isohaline circulation and initiates the break down in water stratification and the formation of large circulation cells (for review see Syvitski, 1989).

The second oceanographic season occurs during the spring to early summer (about June 15 to July 15), when the seasonal surface layer is re-established through a combination of nival melt, sea ice melt, and warming of the surface waters. In terms of annual freshwater input, fluvial discharge accounts for 0.47 km^3 (49%), while melting of the seasonal sea ice (ice thickness times fiord surface area) contributes 0.49 km^3 (51%) of freshwater. Examination of 17 Landsat images of Itirbilung Fiord indicate that the sea ice melts progressively from the head of the fiord to its mouth. Wind strength is at a minimum for this period (based on Clyde Inlet weather station data) and wind mixing of the surface waters is considered minor; water stratification is expected to remain well developed.

The third oceanographic season extends through the summer into the fall (about July 15 to October 1), a time of surface layer thickening through wind mixing (cf. Fig. 4).

Figure 14. Aanderaa current meter mooring data and associated wind data (cf. Fig. 4 for details) collected over 18 days in August of 1983 (cf. Fig. 10 for mooring location). The data has been massaged using a 0.5 hour filter and averaged over 1 hour. The surface meter was located 6 m below the sea surface, the deep mooring was located 41 m below the sea surface, and 2 m above the seabed. **(A)** Wind speed with up- and down-fiord direction indicated. **(B)** Current speed (6 m). **(C)** Current speed (41 m). **(D)** Water temperature (6 m). **(E)** Water temperature (41 m). (For details see Syvitski et al., 1984b).

In a similar Greenland fiord, wind dominates the energy budget during this period (Nielsen and Ottesen-Hansen, 1980). Itirbilung Fiord is comprised of three thermal layers (Trites, 1985; Fig. 6 and 7): a relatively warm surface (seasonal) layer (about 0 - 3°C) of about 25 m in thickness (Fig. 13), a cold intermediate layer (< -1°C) of about 230 m thickness, part of the Baffin Island current, and a warmer deep layer (>1°C below 580 m) in the Home Bay Trough.

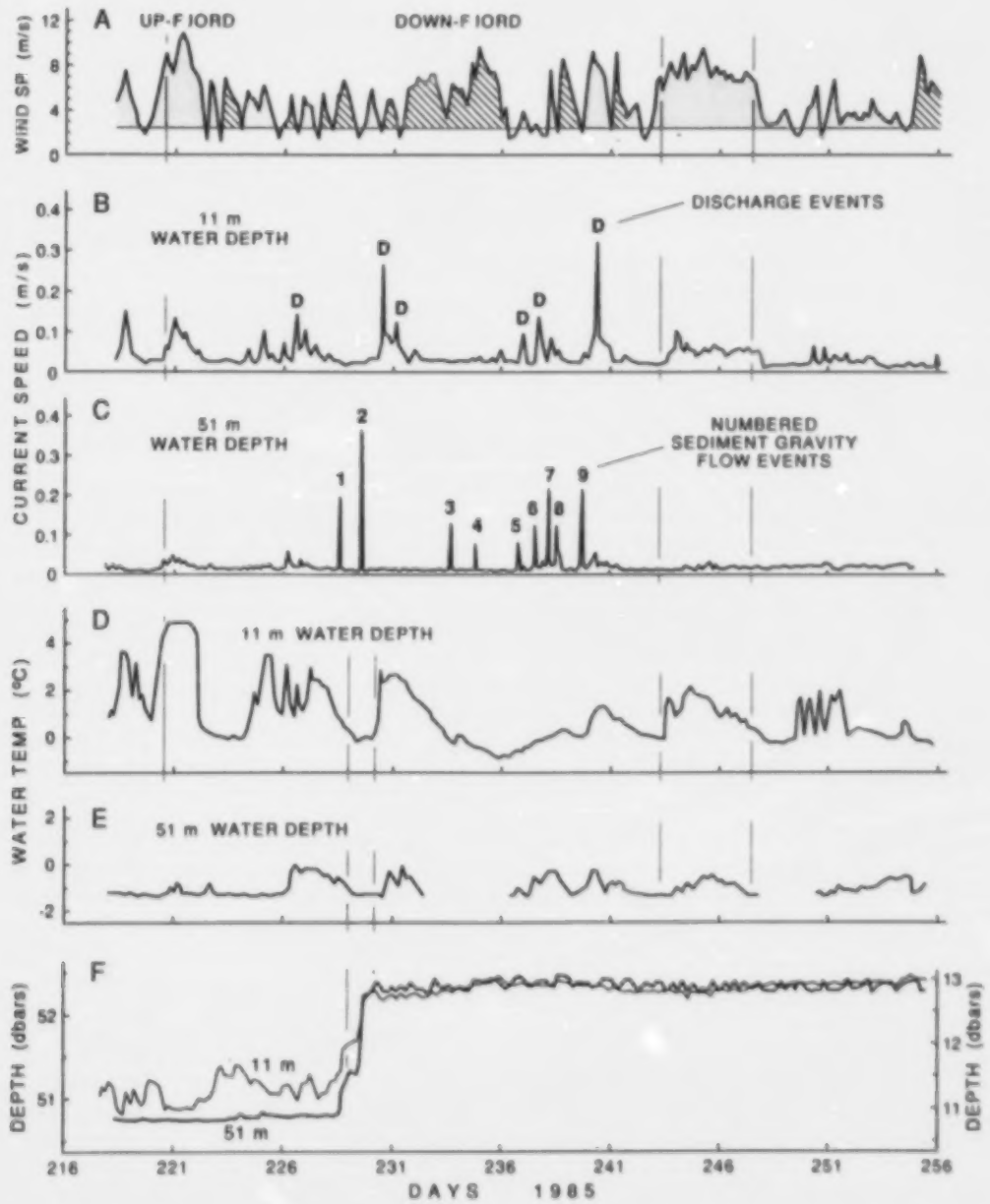

Figure 15. Aanderaa current meter mooring data and associated wind data (cf. Fig. 4 for details) collected over 39 days in July and August of 1985 (cf. Fig.10 for mooring location). The data has been massaged using a 0.5 hour filter and averaged over 1 hour. The surface meter was located 11 m below the sea surface, the deep mooring was located 51 m below the sea surface, and 2 m above the seabed. **(A)** Wind speed with up- and down-fiord direction indicated. **(B)** Current speed (11 m). **(C)** Current speed (51 m). **(D)** Water temperature (11 m). **(E)** Water temperature (51 m). **(F)** Pressure measured in dbars a proxy indicator of depth (m) showing the mooring translation into deeper water as a consequence of the first and second turbidity current event. (For details see Syvitski, 1987b.)

These water layers were verified with four CTD profiles collected along the axis of Itirbilung Fiord (on 11/17/82), one profile (station TI6) from Home Bay Trough (Fig. 6; Trites et al., 1983), and sixteen CTD profiles along the axis of the fiord (09/25-28/83), of which one station (IT6) represents the water characteristics of the deep shelf (Fig. 7; Petrie and Trites, 1984). The surface layer of the shelf water was thicker than that found in the fiord, based on temperature profiles (Fig. 13), an indication of more vigorous mixing.

If currents within Itirbilung Fiord are similar to fiords found elsewhere, then the strongest currents are confined to the seasonal surface layer and over sills (Syvitski, 1989). Current energy within the fiord decreases rapidly with depth (based both on submersible observations: Syvitski et al., 1985 and current meter moorings located on Fig. 10). Currents are largely driven by meltwater discharge during the summer, wind-generated drift during the late summer and fall, deep water exchanges during the fall, isohaline-generated circulation of winter, and tides which operate over the entire year.

In 1983 and 1985, sediment traps and oceanographic moorings were emplaced into about 50 m water depth near the fiordhead using a Bell 206B helicopter (for details see Syvitski et al., 1984b; Syvitski, 1987b). In both experiments, a near surface and a near seafloor Aanderaa current meter was used to ascertain prodelta dynamics during the summer season – 18 days in 1983 and 39 days in 1985 (Figs. 14 & 15). Up-fiord winds were accompanied by water advected up-fiord, initiating downwelling at the fiordhead. This is associated with temperature increases, i.e. with the downwelling of warm surface water. After a particularly strong wind event ends, an internal seiche is set up the period of which is equal to the diurnal tide (e.g. Fig. 14D and E). This is evident in the water temperature but not the current velocity. Conversely, down-fiord winds bring about a dissipation of the internal seiche, thus stabilizing the water column. In 1983, the currents at the 41 m water depth varied linearly with the 6 m currents, but were extremely weak.

Syvitski et al. (1984b) evaluated short term (3 days) tidal records collected within Itirbilung Fiord. They found that the predictions based on Clyde River data needed to be reduced

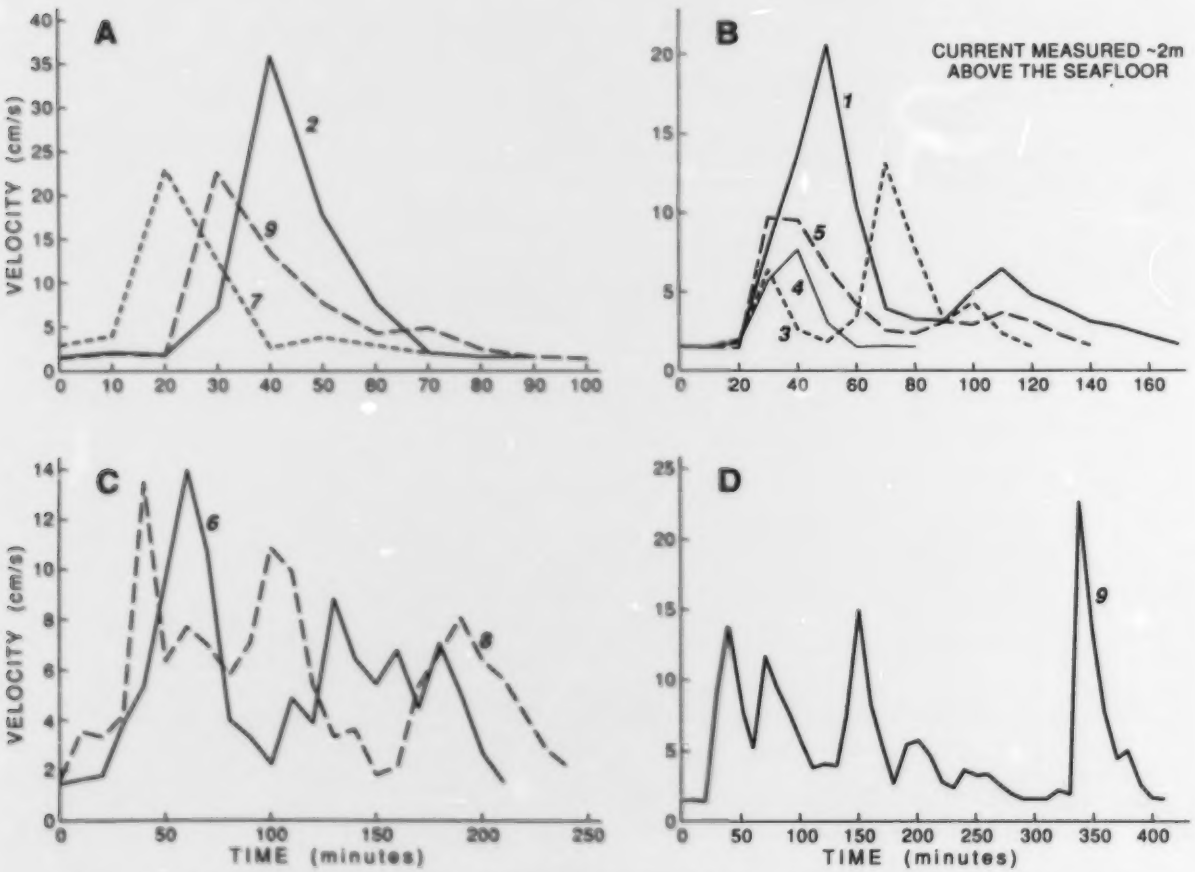

Figure 16. Details of the current speed of the turbidity current events identified on Figure 15C. The complexity, i.e. multiflow events, and duration increases from (A) to (D).

by 0.2 m with a positive time shift of 3.2 hours. Tidal predictions based on these corrections provided large tides of 1.19 m HHW (high high water) to -0.04 m LLW (low low water), and average tides of 0.96 m HHW to 0.14 m LLW around a mean sea level of 0.55 m.

In both 1983 and 1985, the near-surface water currents ranged from quiet water conditions to 0.35 $m \cdot s^{-1}$ (Fig. 14B and 15B). A tidal component, although present, has little effect on the major velocity events. The major events are correlatable to both up-inlet winds and discharge events: the former is best recognized by a temperature increase (associated with downwelling at the delta front); the latter is best identified in the lateral ,v, component (down-fiord) of the deconvoluted current velocity (Syvitski, 1987b).

The deep current meter in 1985 was positioned 2 m above the seafloor within a submarine channel. Predominantly very low currents (< 0.01 $m \cdot s^{-1}$) were recorded (Fig. 16C) except for 9 gravity flow events best registered on the down-fiord (v) component of the current velocity (Syvitski, 1987b). Each event lasted between 1 and 5 hours (Fig. 16). The maximum

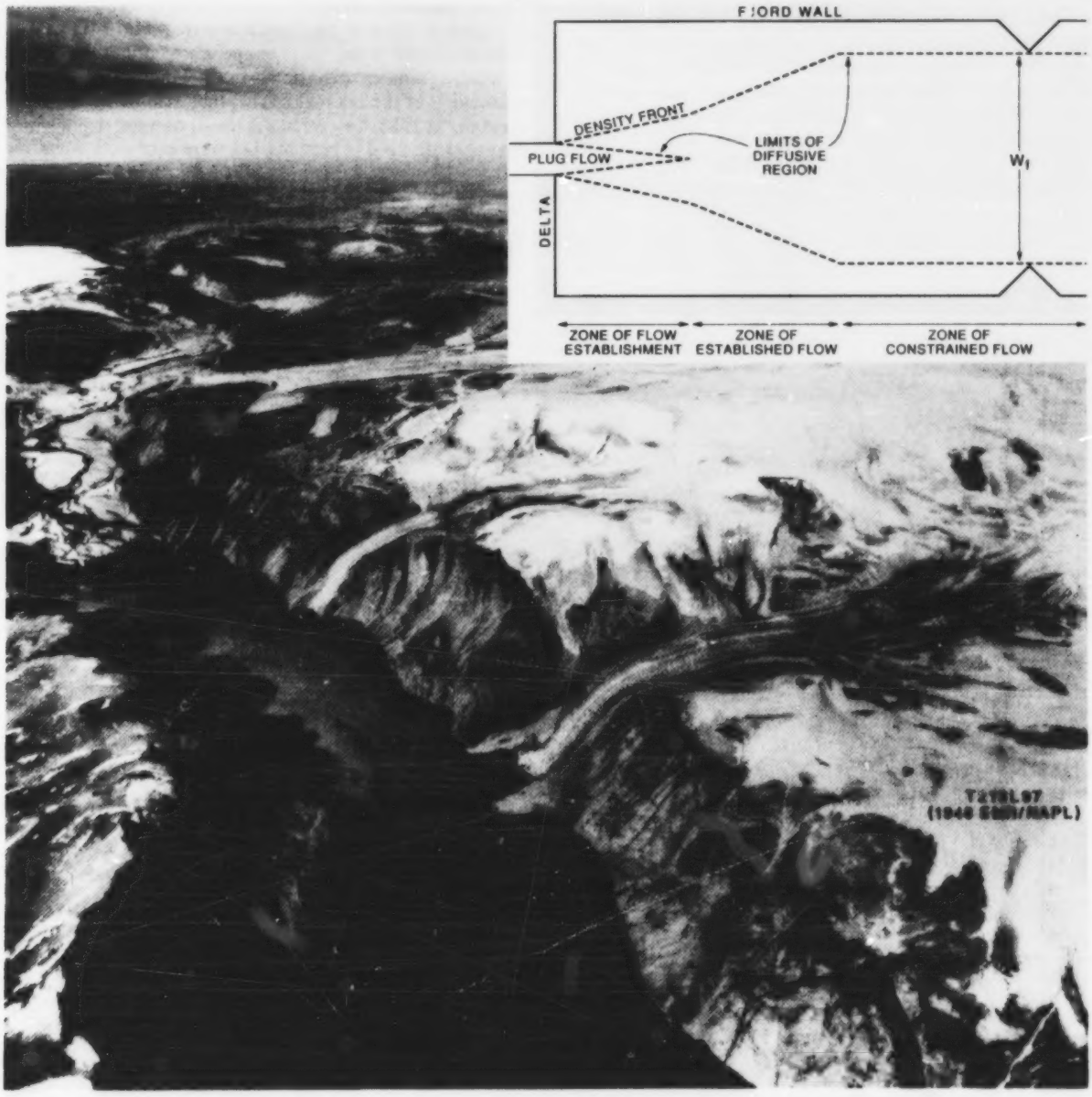

Figure 17. NAPL air photo (# T219L97, 1948) of the head of Itirbilung Fiord showing the river plume flowing down-fiord. The narrows near a side-entry glacier constrain the plume and initiate vorticy shedding. Note the plume dimensions are similar to the schematic of a theoretical model given as an inset (after Syvitski, 1989).

current detected was 0.36 $m \cdot s^{-1}$. Two types of events were identified: (1) powerful single events (which may represent coarse grained delta front chute* failures); and (2) weaker multi-events (which may represent retrogressive slide failures of the prodelta muds). In addition, each sediment-gravity flow event was also associated with a slight bottom water temperature increase (i.e. the bringing down of warm surface water in sediment/water mixtures). The first and second (the largest) sediment-gravity flow events were apparently powerful enough to move the mooring array into deeper (1.6 m) water. These events registered on the pressure sensors of both the shallow and deep current meters (Fig. 15E and F). Given a slope of 3°, the cumulative downslope translation of both events was 31 m.

Suspended particulate matter

During the summer, the surface river plume is very turbid. One sample collected on August 5, from the Itirbilung River mouth, contained 153 $g \cdot m^{-3}$ of mostly silt and clay sized particles (lab no. 2837: Syvitski et al., 1987b). This value is within the predicted range of equation 5a. Also on August 5 and sampled within minutes of Itirbilung River mouth sample, the second glacier stream from the head of the fiord and the Nuuksatuguluk River mouth were discharging a suspended sediment concentration of 88.6 $g \cdot m^{-3}$ (lab no. 2835 Syvitski et al., 1987b) and 152.1 $g \cdot m^{-3}$ (lab no. 2826 Syvitski et al., 1987b), respectively. Five weeks later, during late September, the suspended sediment concentration of the Itirbilung River had decreased to 1.3 $g \cdot m^{-3}$ of mostly clay sized particles (lab no. 3494 Syvitski et al., 1987b).

The Itirbilung River plume width is constrained by down-fiord narrows that cause the shedding of plume vortices (Fig. 17). Based on 25 satellite and airphoto images of the suspended plume in Itirbilung Fiord, little suspended sediment escapes the fiord via surface plumes. The highest suspended sediment concentrations during the fall are confined to the surface layer and near the head of the fiord, although both 1982 and 1983 surveys noted an elevated concentration near the seafloor (Fig. 6 and 7). This near seabed turbidity may relate to resuspension events associated with a possible influx of shelf water causing resuspension of fines from over the outer sill complex. LeBlanc et al. (1988) provide scanning electron photomicrographs of many of the water samples examined. Of particular relevance is the appearance of mud chips suspended in water near the seafloor – these were interpreted as being further evidence of seafloor resuspension, although the mechanics of resuspension remains unknown.

SEDIMENTARY ENVIRONMENTS

We have divided the fiord system into five sedimentary environments: fiordhead delta, fiordhead prodelta, basin margins (sidewall slopes), deep basin, and outer sill and approaches. Herein, we describe each environment in terms of their sediment types, landforms and bedforms, acoustic signature (sidescan), bathymetry or topography, with observations from submersible dives, aerial and underwater photography.

Grain size analytical methods have been discussed in detail in Clattenburg et al. (1983) and Asprey et al. (1983). Results are reported in the four SAFE data reports (Syvitski and Blakeney, 1983a; Syvitski, 1984a; Syvitski and Praeg, 1987; LeBlanc et al., 1988) with corrections to size statistics of some samples given in Praeg and Prime (1987). Unless otherwise indicated, moment measures are given in units of phi (Ø). A complete list of all grab and core samples, including water depth and core length, is provided in Table 6. Sample locations and dive transects are shown on Figure 18. A variety of sidescan tow-fish were used as part of the SAFE cruises – HU82-031, HU83-028, and PA85-062. They have been described in detail in Syvitski et al. (1983b), Syvitski (1984b), and Syvitski et al. (1984b). Sidescan systems insonify swath widths between 150 m and 3 km.

Underwater photography was carried out using a U-MEL stereo camera-package, the unmanned submersible and the manned submersible Pisces IV (see Syvitski et al., 1983c for the submersible capabilities). Most of the manned dives were observational, although the external manipulator arm was used to obtain short sediment cores or to recover suspended particulate matter. The submersible dives investigated geomorphic features observed on the sidescan sonar records from the 1982 and 1983 cruises, for which there were questionable interpretations. In Itirbilung Fiord, 5 dives were conducted on the steep proximal prodelta slope, on the seafloor adjacent to a side-entry glacier, along the walls and floor of a 400-m deep basin, and on bedrock outcrops exposed along the outer sill. Transcripts and details of the dives are published in Syvitski et al. (1985) and videotapes are available for inspection at the Bedford Institute of Oceanography, Dartmouth, Nova Scotia.

Delta

The Itirbilung River sandur is one of the largest on Baffin Island, over 20 km in length, 2 km in width, with slope of 0.0065 (Fig. 19). Three prominent side-entry glaciers have affected the sandur surface through their advance onto the sandur during the Little Ice Age. Although they have since retreated, their massive deposits, mostly push moraines and stagnation deposits (Fig. 20K), affect the modern hydraulic regime of the Itirbilung River. These deposits supply copious amounts of sediment for transport through fluvial and aeolian action. Based on lichonometry (Stravers, pers. comm., 1987), the lake identified on Figure 19 was filled to well over 100 m above its present level about 100 years ago. It apparently experienced a catastrophic drainage when the most westerly of the side-entry glaciers melted back. This jøkolhlaup event armoured much of the present sandur with very large gravel waves ($\gamma = 20$ m, $h = 2$ m, **where γ and h are defined for**

* Chutes are concave and listric slip surfaces found along the lip of a delta, and may extend from low-low water to the base of the delta foresets; their origin relates to loading or liquefaction failute of the foreset sand beds.

the remainder of this paper as symbols indicating wavelength and wave height, respectively), moving boulders in excess of 1 m (Fig. 20I, J). Many of the boulders are subrounded at best, suggesting that fluvial transport was limited to this short-lived jøkolhlaup. This event, coupled with higher than normal discharge associated with the melting of these side-entry glaciers, appears to have eroded much of the raised glacial-marine terraces that dominate most other Baffin fiordhead deltas. Raised terraces are presently confined along the margins of the sandur (some 50 to 100 m wide) (Fig. 20L).

In support of the calculated high rate of aeolian sediment transport, the delta surface is covered with the effects of wind transported sediment. Ventifacts decrease down-fiord away from the side-entry moraines, suggesting the moraines act as a source of sediment affected by wind (katabatic) drainage off the plateau ice sheets. The central portion of the sandur is covered with rippled sand ribbons over a pebble deflation lag (Fig. 20F). Where the pebble lag is absent, the delta surface is being actively eroded by wind (Fig. 20H). During our fall surveys (1982, 1983, 1985), frozen topset beds were polished flat due to sand blasting, revealing the intricate structures of lingoid current (fluvial) ripples. Aeolian sinks on the delta include: (1) snow drifts which as act as blotters

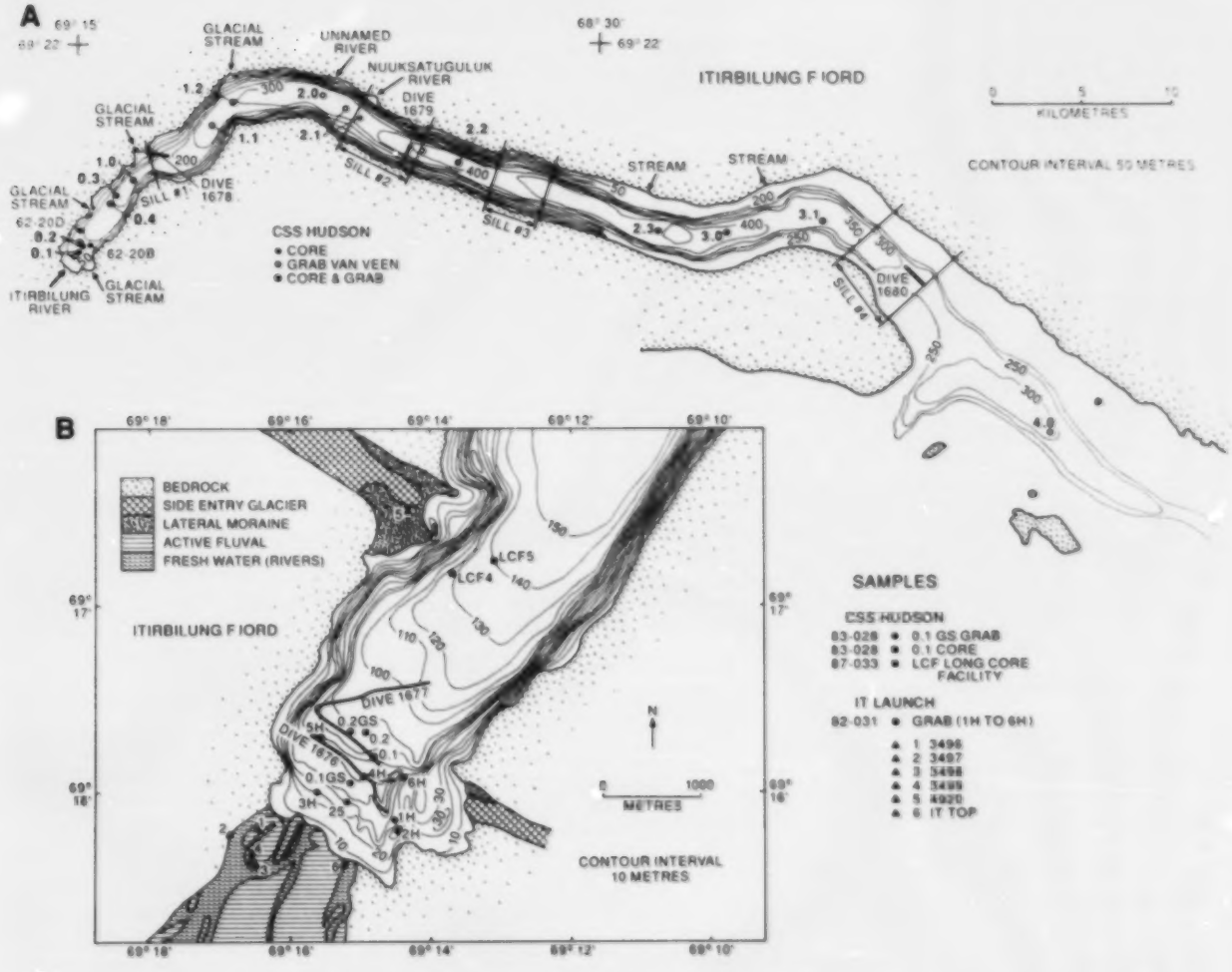

Figure 18. Sample locations for onshore and offshore Itirbilung Fiord grabs and cores collected between 1982 and 1987. **(A)** Bathymetry with sample stations and submersible dive tracks. **(B)** detailed map of fiordhead, showing bathymetry, distribution of Quaternary and bedrock outcrops, active fluvial tract, with sample stations and submersible dive tracks. See Table 6 for sampling details.

to the wind blown sand (Fig. 20 F), (2) the lee of fluvial channel banks (Fig. 20D) and raised terraces (Fig. 20E), (3) river water (Fig. 20D), and (4) the troughs of gravel waves and polygons (Fig. 20I, J). Aeolian sand is typically between 3.2 Ø and 3.5 Ø in mean size, although aeolian sheet sands may be as coarse as 0.8 Ø.

The architectural structure of the sandur is controlled by the migration and bifurcation of the braided river channels (Fig. 19, 20C). Gravel armours the river bed, suggesting a bedload-dominated system. As on the Ekalugad sandur (Church, 1972), grain size decreases rapidly downstream. The intertidal flats show the conflicting effects of fluvial channel migration and wave-generated linguoid bars parallel to the delta front. These bars have a typical length of 50 m and height of 20 cm (Fig. 20B), and indicate substantial landward movement of sediment over the tidal flats during the fall storm season. Tidal action appears to have little effect on the transport of sediment.

An examination of DEMR/NAPL airphotos taken in 1948, 1958, and 1960, and SAFE photos (1982, 1985) gives an average rate of delta front progradation of 2.6 $m \cdot a^{-1}$ (Syvitski, 1987a). The delta front is 900 m wide and has a submerged foreset thickness of 10 m (Fig. 10). Therefore the rate of sediment accumulation is 23400 $m^3 \cdot a^{-1}$. If we assume a particle density of 2700 $kg \cdot m^{-3}$, and a porosity of 40%, then the effective bulk density is about 1600 $kg \cdot m^{-3}$. This accounts for a mass of 3.7 x 10^4 $t \cdot a^{-1}$. The estimated bedload transport for the Itirbilung River (Table 4) is 6.1 x 10^4 $t \cdot a^{-1}$.

Table 6. Sample information for grab and core samples, Itirbilung Fiord. Cruise reference: HU is C.S.S./Hudson, PA is M/V Pandora II. L: Lehigh core, LCF: Long Core Facility, P: piston core.

Station number	No. of grab	Grab water depth (m)	Core type	Core water depth (m)	Core Length (m)	Cruise	Reference
Delta	5					HU 82-031	12
Delta	2					PA 85-062	Cruise Data Sheets
IT H1-H6	6	10 - 70				HU 83-028	13,8
IT0.1	1	55	L	73	2.25	HU 82-031	3,5,8,9
			P	73	2.66		10,11,13
IT0.2	1	88	L	88	0.45	HU 82-031	10,11,13
62-20D			L	85	0.34	PA 85-062	5
62-20B			L	91	0.94	PA 85-062	5
LCF4			LCF	124	6.55	HU 87-033	15
LCF5			LCF	139	5.49		
IT0.4	1	148	L	155	1.40	HU 83-028	3,5,8,9,
			P	155	3.25		10,13
IT0.3	1	155	L	155	1.43	HU 83-028	3,5,8,9,
			P	155	4.27		10,13
IT1	1	167	P	167	6.32	HU 82-031	1,2,7,10,11,13
IT1.1	1	256	L	256	0.48	HU 83-028	3,5,9,10,
			P	256	7.93		13
IT1.2	1	293	L	293	1.17	HU 83-028	3,5,8,9,
			P	293	6.24		10,13
IT2	1	320				HU 82-031	2,10,11
IT2.1	1	310	P	325	2.50	HU 83-028	3,4,5,10,13
IT2.2	1	420	L	420	2.11	HU 83-028	3,5,9,10,13
			P	420	3.84		
IT2.3	1	424	L	424	2.29	HU 83-028	3,5,9,10,13
			P	424	8.40		
IT3	1	417	L	417	2.40	HU 82-031	2,6,10,11,13
Dive 1680	3	270				PA 85-062	14
IT3.1	1	365	L	365	2.46	HU 83-028	3,5,9,10,13
			P	365	4.59		
IT4	1	303				HU 82-031	2,10,11

1: Cole and Blakeney, 1983; 2: Clattenburg et al., 1983; 3: Gilbert, 1984; 4: Gilbert and Horvath, 1984; 5: Hein, 1987; 6: Hein and Longstaffe, 1983; 7: Mothersill and Tabrez, 1987; 8: Praeg et al., 1987; 9: Reasoner and Hein, 1984; 10: Schafer et al., 1984; 11: Syvitski, 1982; 12: Syvitski et al., 1983a; 13: Syvitski et al., 1984a; 14: Syvitski et al., 1985; 15: Vilks and Powell, 1987.

Recognizing the large uncertainty in the latter, the implication is that 61% of the fluvial bedload is used in delta front progradation, the remainder is moved offshore by slumping and turbidity currents.

Prodelta

The Itirbilung prodelta consists of well defined foreset beds, sediment-gravity flow channels, interchannel terraces, and more distal slope deposits. It is an excellent example of a seafloor experiencing semi-continuous delta front failures. As calculated above, 4.8 x 10^5 $t \cdot a^{-1}$ of sediment enters the fiordhead delta: 75% through aeolian transport, 12% as fluvial bedload, and 13% as fluvial suspended load. The delta lip occurs at about 0.5 to 1 m below the low tide line. Along the delta lip there are numerous re-entrant chutes cut into the 15° to 25° foresets (Fig. 21); smaller chutes occasionally lie within larger chutes (up to 15 m wide). The chutes are commonly separated by sharp crested ridges. The foreset seafloor merges with the more gentle bottomset beds (8.5° to 0.4°) at a water depth of 10 m. There the chutes converge into a number of distinct channels that may reach 170 m in width and 8 m in depth (Fig. 22).

The channel walls can be near vertical, with relatively flat floors. Levee deposits line the walls of some of the channels (Fig. 23). The cumulative channel area (channel width times channel height) decreases downslope after an initial increase, as does the number of channels, until the channel form disappears (Fig. 24). The initial increase in channel area out from the delta front is not associated with an increase in

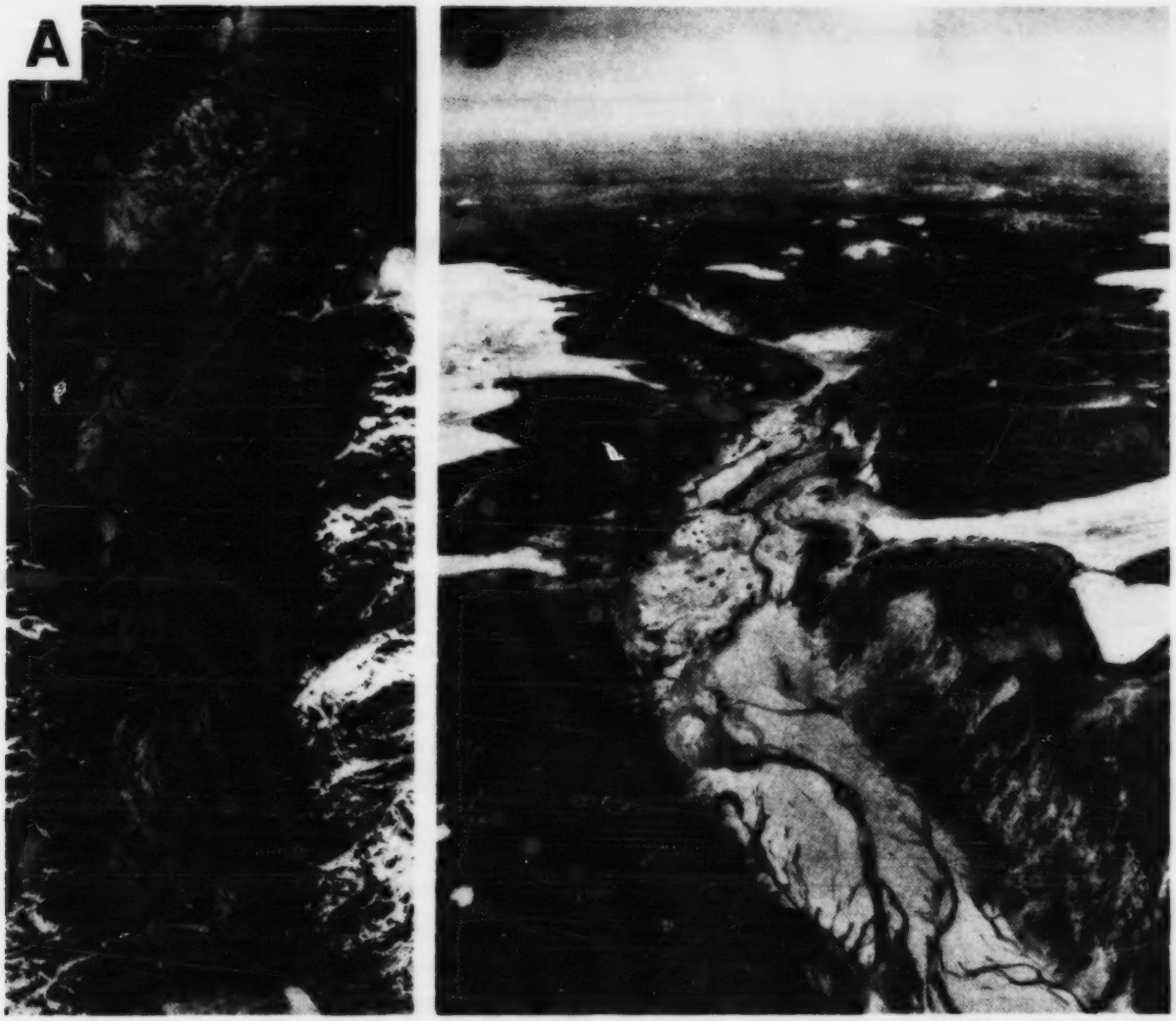

Figure 19. (A) DEMR - NAPL airphoto (A-16221-80), taken in July of 1958, showing photograph locations shown on Figure 20 (A through L). **(B)** DEMR - NAPL airphoto (T320L-197), taken in August of 1948, showing an oblique perspective of side-entry glaciers that fed directly into the Itirbilung sandur. Also note the position of a lake that was once much higher (>100 m) and apparently drained catastrophically within the last 100 years.

prodelta slope and may relate to slope failure of the bottomset beds. The channels are of low sinuosity and may converge with or truncate one another (Fig. 12). In general, within basin 1 the sand content decreases down-fiord from >70% to <10% (Table 7).

Two Pisces IV dives (1676 and 1677, Syvitski et al., 1985) were conducted on the prodelta slope (30 to 90 m water depth), to verify channel features identified on sidescan sonagrams (Fig. 12). During dive 1676, a passing turbidity current reduced our visibility and confirmed the role of sediment gravity flows in the seaward transfer of delta front sand. Bottom sediment within the active channels was found to be 90% sand in the form of current ripples (e.g., Fig. 18, IT-2B: μ, σ = 3.0 Ø, 1.3 Ø, respectively **where μ and σ are defined for the remainder of this paper as symbols indicating mean size and standard deviation of the sediment sample and not population statistics**). Concave arcuate features were observed along the floors of the sandy channels (Fig. 12, 21, 22). Originally interpreted on sidescan images as bedforms (Syvitski et al., 1984b), submersible investigations identified them as arcuate and listric fault scarps (Fig. 25B, D), with a surface relief of 1 to 3 m, often broken by crevasses. Associated longitudinal ridges were decimetres in height and metres in length. Other dislocation features within the sandy channels included longitudinal fractures, parallel to channel axes, and conjugate fractures, oriented at 20° to the main channel axes. Most of the fractures were fresh, without superimposed bedforms, were not draped by fine sediment, and were unpopulated by benthic fauna. Bedforms were found in the main channels in protected areas along the sidewalls, in the protective lees of interchannel terraces, and within secondary, mainly inactive channels. These small bedforms included oscillation ripples (h = 3 to 5 cm; γ = 10 cm) and three-dimensional linguoid current ripples (h = 3 to 9 cm; γ = 15 cm). Linguoid ripples were oriented at oblique angles or parallel to the axes of the channels.

The interchannel 'islands' or terraces are covered by poorly sorted silty mud from the hemipelagic fallout from under the river plume (e.g. IT5H: μ, σ = 5.4 Ø, 2.5 Ø). These submarine terraces are densely colonized by epifauna (e.g. Fig. 25A: polychaetes, brittle stars, anemones and scallops), as they are somewhat protected from the episodic turbidity currents that are initially contained within the channels. Some of the interchannel terraces have buried (lower relief) fault scarps (Fig. 12). The sides of the interchannel terraces are marked by scarps (up to 10 m relief), some of which have a cutbank and terrace topography (with 7 or 8 rises), with small fault-like dislocations parallel to the crestlines of the cutbanks.

Further downslope, between 50 and 100 m water depth (Dive 1677), the seafloor was composed of fine sandy silt, some areas with ripples, other areas with abundant worm traces and small bottom undulations of about 1 to 2 m in height. Epifaunal populations are sparse, marked by low numbers of small sea anemones and gastropods; less commonly dense patches of small brittle stars occur. The walls of submarine channels are cusp-shaped, a result of post-incision localized slumping along the channel walls. Further seaward (station IT1: Fig. 18), in 175 m of water, the benthic community is well established away from the submarine channel system (Fig. 25C).

In 1985, sediment traps were moored for 39 days contemporaneously beside the oceanographic mooring, identified on Figures 10 and 12. (For details on trap

Table 7. Water depth, distance from the head of the fiord, and four textural parameters for submarine grab samples collected in Itirbilung Fiord. See Figures 1 and 18 for sample locations. Mean and standard deviation are calculated by the method of moments. (Sand+silt+clay = 100%)

Sample ID	Depth (m)	Distance (km)	Sand (%)	Clay (%)	Mean (Ø=-log$_2$mm)	St. Deviation (Ø)
Prodelta (basin 1)						
IT1H	47	0.6	71	5	4.0	1.7
IT2H	39	0.5	45	12	4.9	2.6
IT3H	30	0.4	52	8	4.6	2.1
IT4H	60	0.7	46	12	5.0	2.3
IT5H	70	0.9	41	17	5.4	2.5
IT6H	42	1.0	70	6	3.9	2.0
IT0.1	55	0.8	30	22	6.0	2.5
IT0.2	88	1.6	34	14	5.3	2.1
IT0.4	148	4.1	11	43	7.5	2.6
IT0.3	155	4.8	6	46	7.9	2.5
IT1	167	6.0	11	39	6.9	2.4
Basin 2						
IT1.1	256	11.2	17	43	7.3	3.0
IT1.2	293	12.9	8	50	7.9	2.6
IT2	320	17	70	11	4.1	2.3
Inner sill 2						
IT2.1	310	18.4	70	14	4.3	2.8
Basin 3						
IT2.2	402	25.3	24	38	6.9	3.1
Basin 4						
IT2.3	424	37.0	12	43	7.3	2.3
IT3	417	41.5	6	48	7.6	2.1
Outer Sill (4) Complex						
IT3.1	356	50.5	74	14	4	2.7
IT4	303	72.5	40	22	5.5	2.6
IT5	175	102.5	74	4	3.6	1.7
IT6	502	124	41	17	5.4	2.4

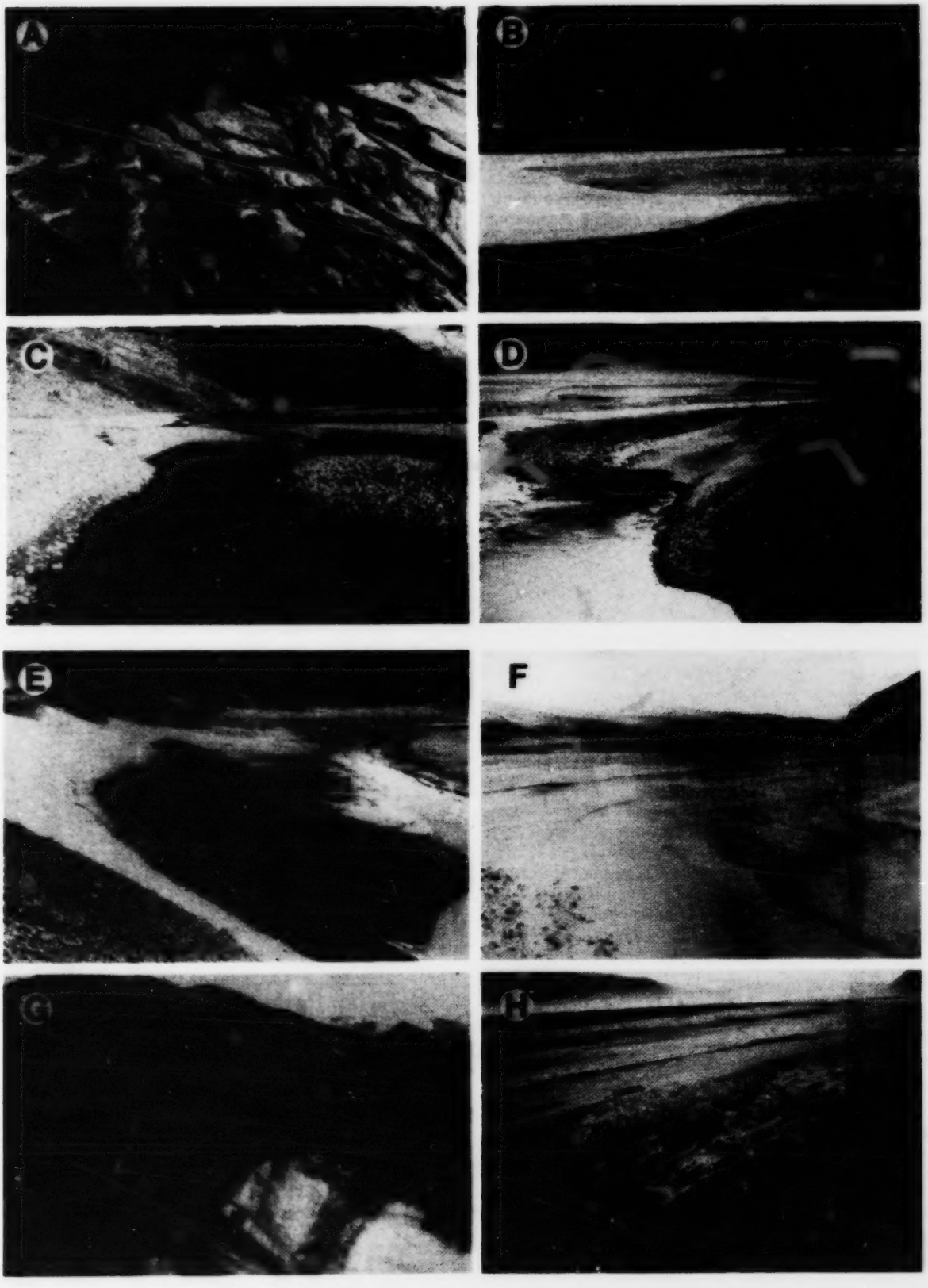
A
B
C
D
E
F
G
H

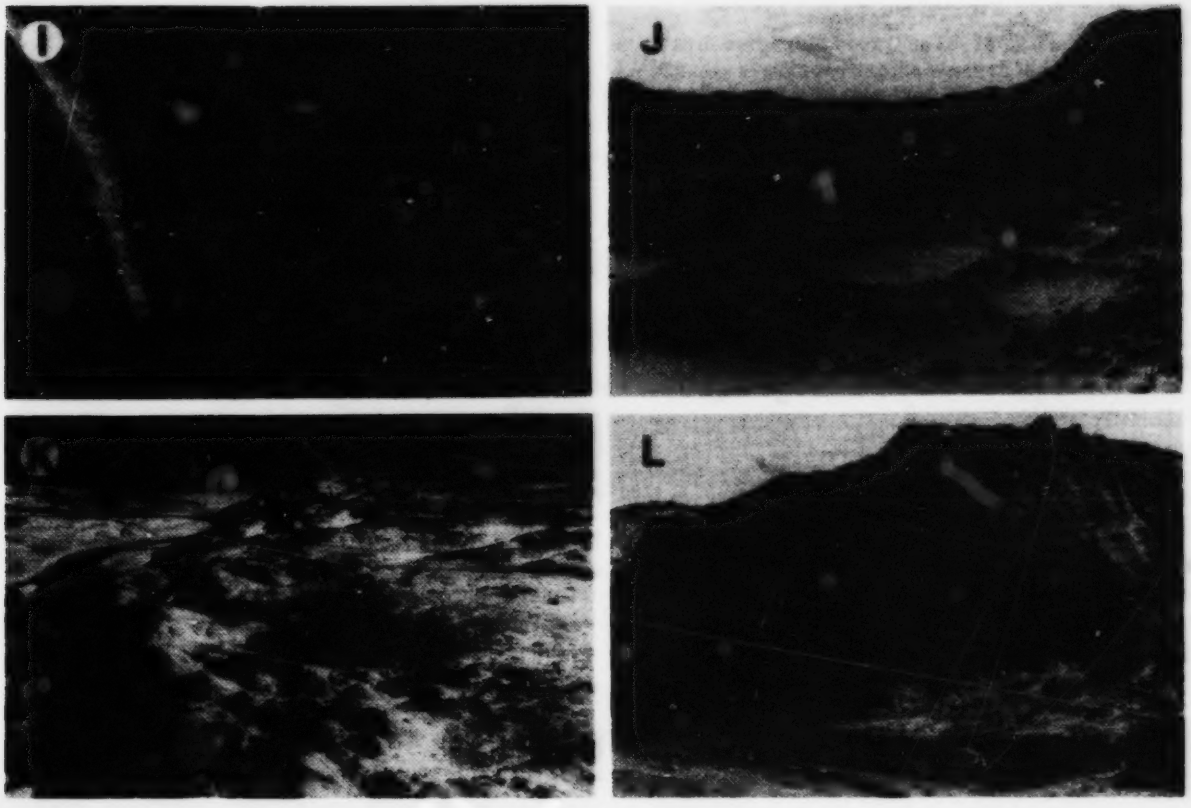

Figure 20. Twelve photographs demonstrating a variety of sedimentological features on the Itirbilung delta (cf. Fig. 19 for location). **(A)** The delta front (0.5 km across photo) dominated by braided fluvial channels and transverse wave-generated linguoid bars. **(B)** Close up of one of the many linguoid bars (note person for scale). **(C)** Main fluvial channel at low discharge stage (pebbles in foreground are about 4 to 8 cm in diameter). **(D)** Wind blown sand accumulation along the lee (down-fiord) of river bank. **(E)** Wind blown sand accumulating on the up-fiord lee of raised deltaic (late Holocene) terraces. The dark coloured sediment in the foreground is wet sand covering snow deposits (see circled person for scale). **(F)** Aeolian rippled sheet-sands covering pebble deflation lag on delta surface. **(G)** Close up of (E) showing thick (5 to 30 cm) accumulation of aeolian sand covering a snow drift both deposited during the previous winter. **(H)** Sand drifts on wind blasted surface. Note wind storm clouds in the distance. **(I)** Gravel sand waves deposited during a jøkolhlaup event and since filled with aeolian sand. Also note the sand-filled polygons (200 m across photo). **(J)** Close up of (I) showing sand wave troughs filled with aeolian sand (note metre stick beside boulder for scale). **(K)** Ice-cored Little Ice Age moraine (stagnation deposit) that contributes significant aeolian and fluvial sediment to the sandur (300 m across photo). **(L)** An example of raised glacial-marine deposits exposed through fluvial cannibalism (cliff is 35 m high).

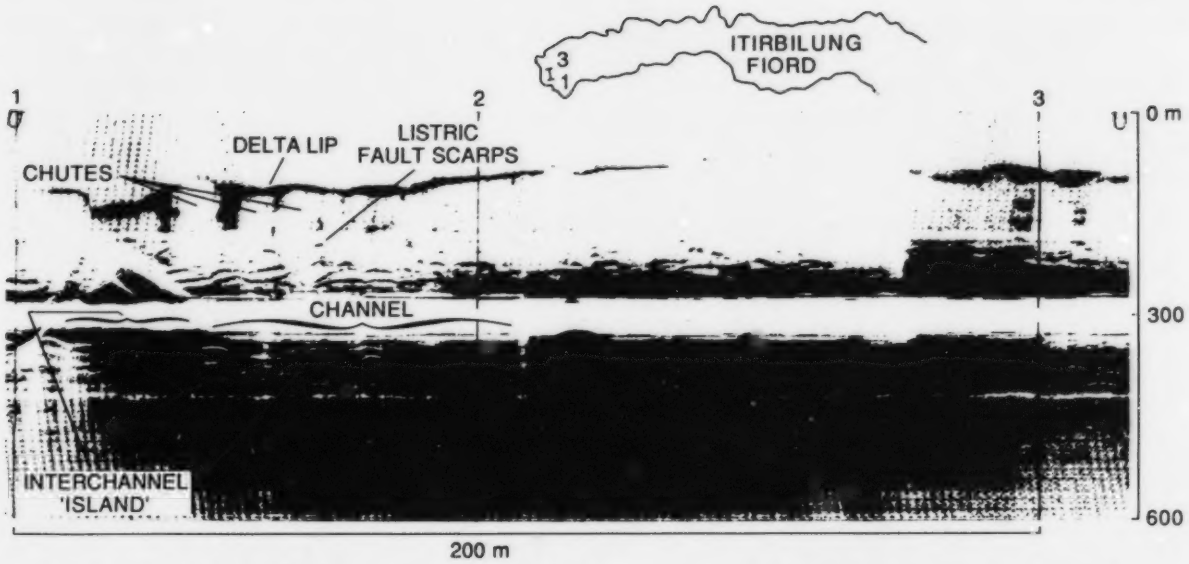

Figure 21. Klein® (421T: 100 kHz, band width 20 kHz) sidescan sonagram collected in 1982 parallel to the foresets of the Itirbilung prodelta environment, about 180 m offshore (see map inset). Note the position of the delta lip, the interchannel islands and listric fault scarps identified and illustrated in Figure 12. (after Syvitski and Blakeney, 1983b).

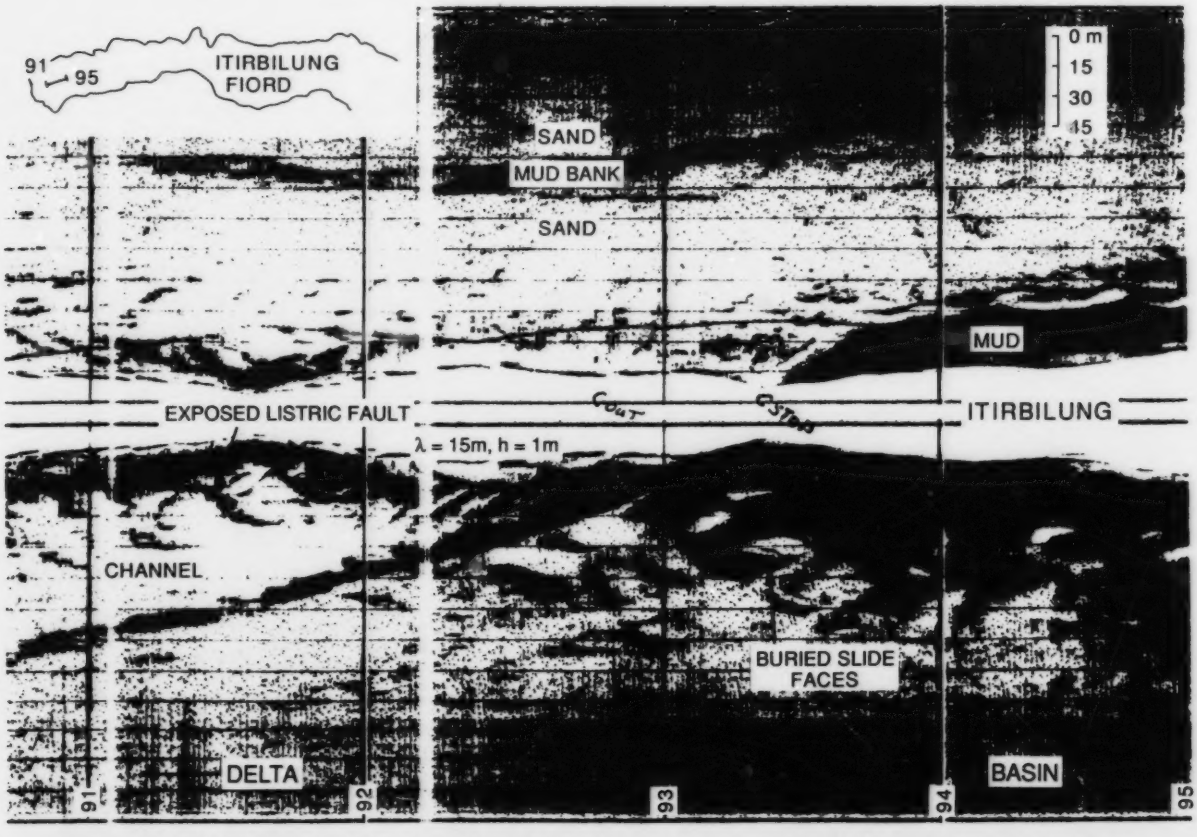

Figure 22. Klein® (421T: 100 kHz, band width 20 kHz) sidescan sonagram collected in 1983 perpendicular to the front of the Itirbilung delta (see map inset). Note the channel running the length of the record and the exposed (in the channel) and partly buried slide faces (on the interchannel islands). (after Syvitski et al., 1984b).

construction and deployment see Syvitski, 1987b). The surface trap was situated 10 m below sea level, 43 m above the seafloor. The bottom trap was located within a 6 m deep channel, 1.8 m above the channel floor, and 51 m below the sea surface. The surface trap collected sediment at 0.428 $kg \cdot m^{-2} \cdot day^{-1}$ with a measured bulk density of 1223 $kg \cdot m^{-3}$, a sand-silt-clay content of 4%, 69.9%, and 24.1% respectively (μ, σ = 6.7 Ø, 2.4 Ø). The bottom trap collected sediment at 1.225 $kg \cdot m^{-2} \cdot day^{-1}$ with a measured bulk density of 1221 $kg \cdot m^{-3}$, a sand-silt-clay content of 41.9%, 43.6%, and 14.6% respectively (μ, σ = 5.2 Ø, 2.5 Ø). In addition, the layered sediment recovered in the bottom trap was sampled every 3 mm for a total of 10 samples. In these layers the sand content ranged from 7.9% to 60.5% (μ = 7.4 Ø to 4.5 Ø). Sediment in the lower trap apparently collected turbidite sand interlayered with hemipelagic mud. The surface trap only collected mud from sedimentation under the river plume.

Sidewall environment

Fiord margins are locales for the temporary and typically unstable storage of sediment, deposited as particles settling from under the fluvial plumes, or from prograding side-entry deltas, alluvial fans and talus cones. The basinward transport of marginal sediment is a result of semi-continuous current action and benthic foraging, and episodically through unstable (oversteepened) sediment accumulation. Morphological features of fiord margins have been discussed by Boulton et al. (1984), Boulton (1986), and Syvitski et al. (1987a).

The submerged portion of the Itirbilung fiord walls typically have slope angles between 10° and 30°, although portions of the margins can approach vertical. Towards the mouth of the fiord, where the fiord widens, the slope angles concomitantly decrease to less than 10°. Side-entry glaciofluvial fan deltas, and margins near the head of the fiord, contain thick Quaternary deposits that typically show failure features on sidescan sonar imagery. These include major slide surfaces (Fig. 26A, 27), rotational slump scars (Fig. 28B: Syvitski et al., 1983b) and debris flow deposits (Fig. 27). The remaining fiord margins are typically in the form of exposed bedrock (Fig. 27, 28A), thinly mantled with silty clay and bordered at the seashore and at the base of the fiord wall with talus (Fig. 26B, 27, 28A).

Dive 1678 occurred near a side-entry glacier along the north wall of the fiord, water depth 162 m to 6 m on top of a submerged lateral moraine (cf. Fig. 18, 5A). The fiord bottom was relatively flat and composed of a thin layer of silt overlying sand. Local drop stones (Fig. 29C) were associated with erosion holes excavated on the down-current side and lee dunes. Epi- and infaunal populations were relatively dense, with up to 70% of the bottom covered by "feather worms"; less common were small brittle stars, basket stars, crinoids, and worm tubes. Above 150 m water depth, crinoids became abundant, along with pockets of shell hash (*Hiatella arctica*), large brittle stars, and rare gastropods. By 140 m water depth, on the lateral moraine, the bottom was marked by many small stones on a steep slope. Pectins increased in abundance to the surface, with densities of 10 to 20 per 10 m^2 (Fig. 29B).

Dive 1679 occurred on the floor and along the wall of a deep basin within Itirbilung Fiord (Fig. 18). The dive commenced in the middle of the basin (393 m) and terminated

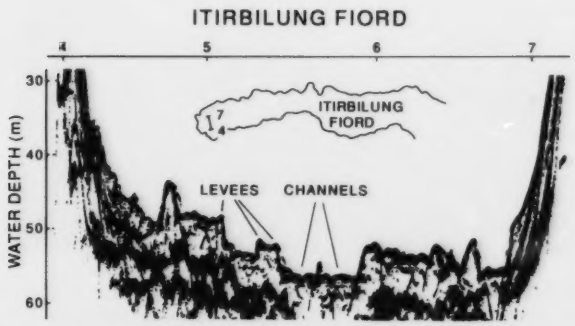

Figure 23. Ross® acoustic profile (192 kHz, band width 18kHz) of the seafloor collected in 1982 parallel to the foresets of the Itirbilung prodelta, about 200 m offshore (cf. Fig. 21 and map inset). Note the levees identified on the banks of the channels.

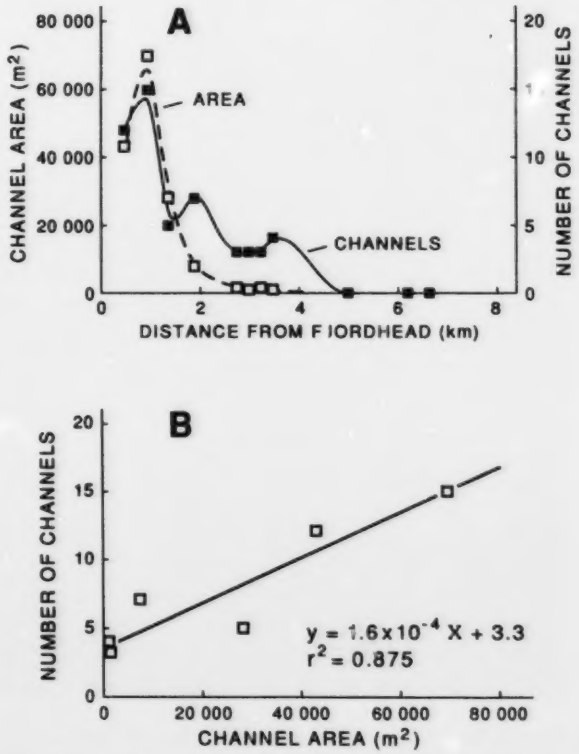

Figure 24. (A) The change in total (cumulative) channel area and the number of channels identified in any one crossfiord transect with distance from the Itirbilung delta front. **(B)** Linear relationship between number of channels and the cumulative channel area over the Itirbilung River prodelta.

on the south wall at a depth of 15 m. Bottom sediment was sandy throughout the basin, with larger concentrations of pebbles and small boulders on the lower slope of the south wall. Bottom fauna were sparse, and showed a relatively homogeneous distribution, mainly sea anemones and polychaetes. Other less common invertebrate species included basket stars, brittle stars, snails, crinoids, and sea urchins. Large red shrimp occurred in intermediate water depths, between 50 to 200 m, most often nestled in burrows 2 to 3 cm in diameter. Lithothamnion algae occurred on rock surfaces beginning at water depths of 44 m.

Basin

Except for incised submarine channels (cf. Fig. 9), the basin floors are flat, with sediment ponded between the fiord walls. The axial seafloor slopes, not including those associated with the four sills, generally are <1°, most less than 0.2° (for details see Syvitski et al., 1984c). The primary sediment inputs include hemipelagic sedimentation of mostly mud-sized particles from under the surface fluvial plumes issuing from the fiordhead and from side-entry glaciofluvial fan-deltas, sediment-gravity flow sands that travel down the submarine channel network, debris flows and slumps (mixtures of mud and talus boulders) off the steep fiord margins, and aeolian sand and silt.

The seafloor sediments within each of the four basins (cf. Fig. 8) vary in sand content from as high as 70% to <10% (Table 7). In the deeper parts of basin 1, the sand content is lowest (6% to 11%). In basin 2, sand content is very high (70%) in the deeper parts of the basin, fed by the Nuutsitlaguluk River. In basin 3, sand content is still moderately high (24%). In the most distal basin (4), the sand content is relatively low (6%). Portions of each basin that are outside the influence of sediment gravity flows contain seafloor sediments where the clay content exceeds 40% (Table 7).

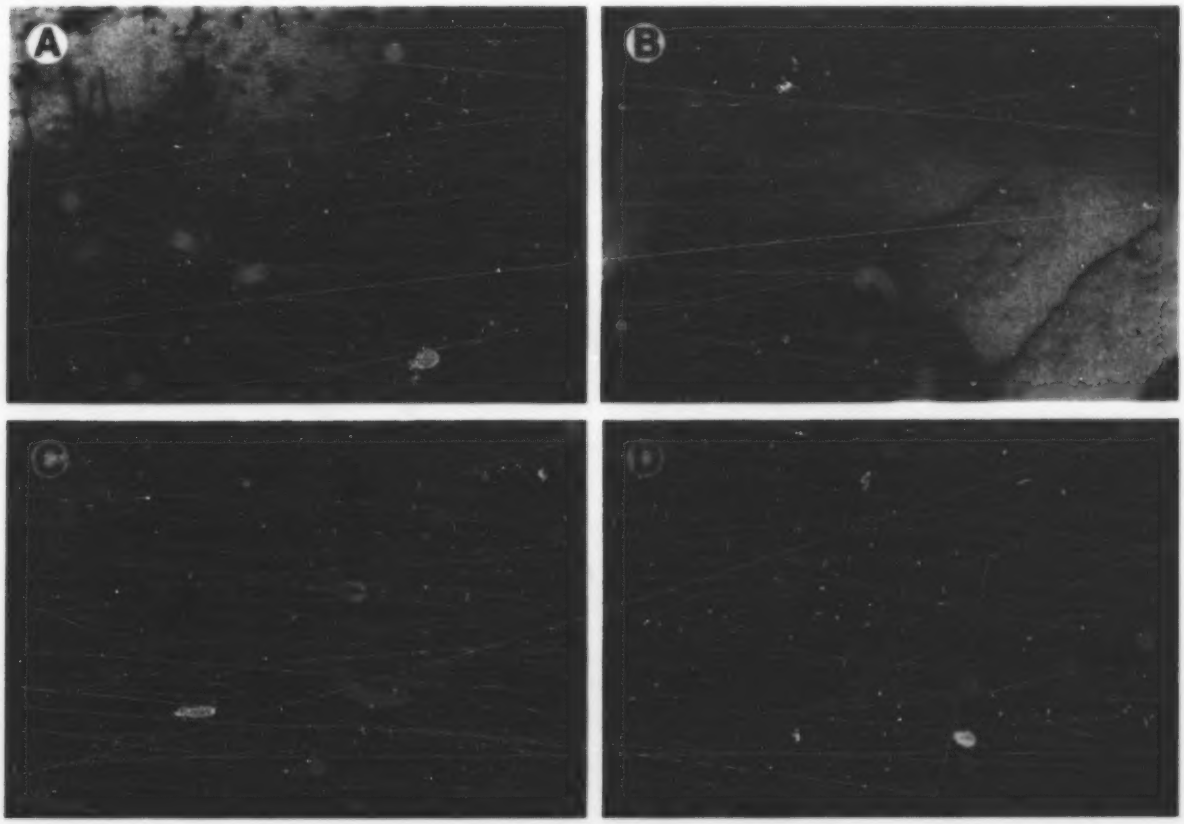

Figure 25. Pisces submersible photographs (except for C) of the Itirbilung prodelta environment. (**A**) Stable benthic environment of agglutinated polychaetes, scallops and brittle stars, on an interchannel "island" on the Itirbilung prodelta, an environment protected from delta front sediment gravity flows (water depth is 60 m). (**B**) Bedding plane steps of an exposed 3 m high fault scarp trending parallel to the Itirbilung delta front. Located within an active prodelta channel, the inundation of gravity flows has effectively eliminated all benthic fauna (water depth 65 m). (**C**) U-MEL collected photograph of anemones and abundant ophiuroids on a current swept portion of the seafloor (IT1, water depth 175 m). (**D**) Exposed fault scarp (2 m high) within an active Itirbilung prodelta channel (water depth 70 m).

If the sand content can be considered a proxy indicator of sedimentation rates (this assumes that the sand is related to rapid delta front progradation and failure), then the present rate of sedimentation decreases down the fiord. Gilbert (1984) arrived at a similar conclusion for Itirbilung Fiord, based on an exponential (down-fiord) increase in the number and weight of drop stones collected in grab samples. Andrews and Syvitski (in press) similarily found a seaward exponential decrease in sedimentation rate, based on ^{14}C dated sediment cores. Finally, Syvitski et al. (1990), used the organic carbon content of grab samples as an inverse proxy indicator of sedimentation rates, confirming this trend.

The basin floors of Itirbilung Fiord are dominated by a macrobenthic Maldanid Association (Syvitski et al., 1989) which includes a large number of deposit feeders including *Nuculana pernula, Macoma calcarea, Yoldila* sp., Sabellids, and the scavenging Buccinid gastropods. Sea floor gouges and pits of about 1 m^3 have been interpreted as mammalian feeding traces, probably caused by whales (Hein and Syvitski, 1989). Through a simple hindcasting technique Hein and Syvitski (1989) suggested that these foraging sea mammals could resuspend 10% of the annual suspended sediment supplied by rivers to the Itirbilung Fiord.

Sills and the outer sill complex

Inner sills 1 and 3 are mantled by hemipelagic deposits and thus tend to be muddy, showing little variation in their benthos compared to the surrounding basin sediments. Sill 2 is very sandy (70%) affected by the sediment flux emanating from the Nuutsitlaguluk River. The outer sill (4) complex is also very sandy (Table 7), with bedrock outcrops common (Fig. 30). Dive 1680, on this sill, reached a maximum water depth of 278 m (Fig. 18). Most of the seafloor consisted of a granule-pebble to cobble-boulder-strewn bed (Fig. 29D). A moderate, steady easterly current (about 10 cm/s) swept the bottom.

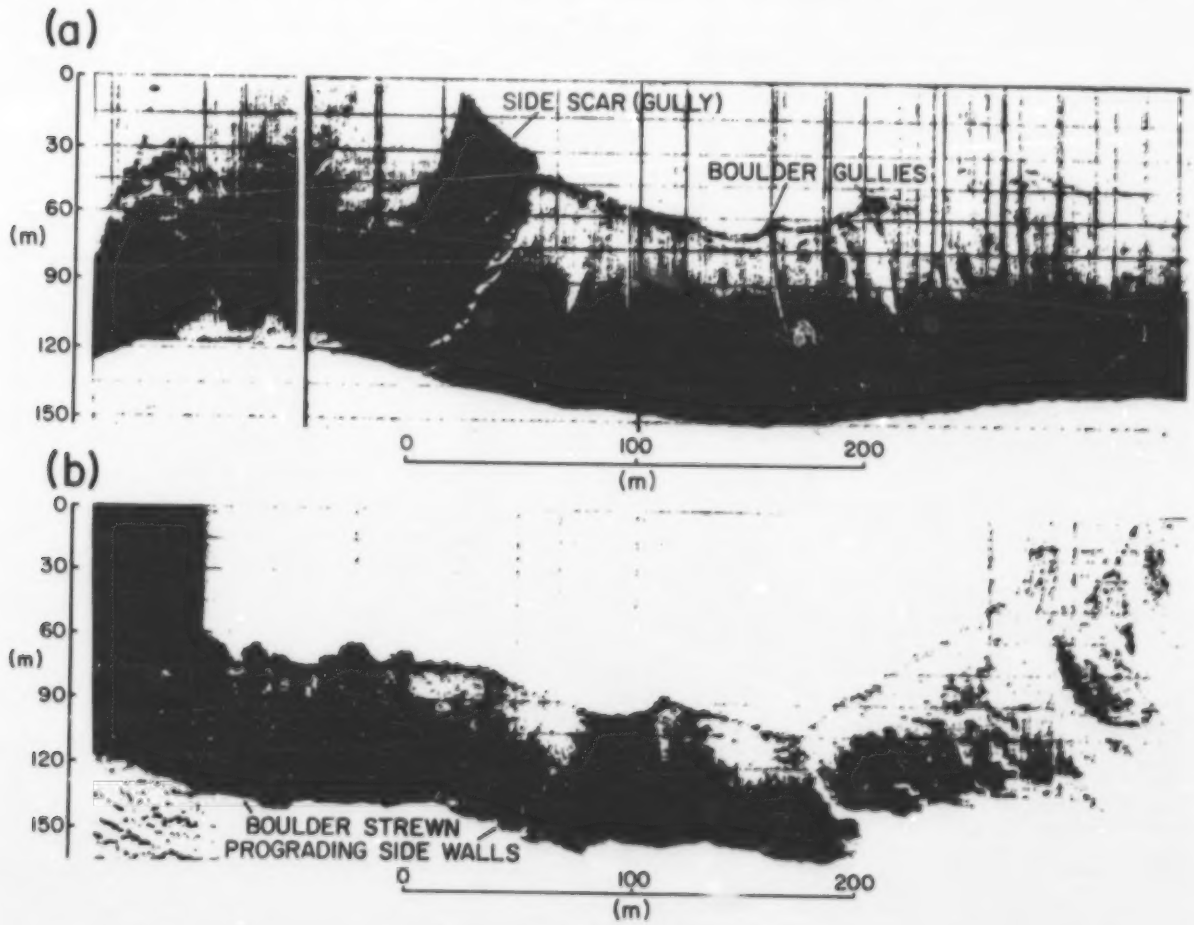

Figure 26. Sidescan sonographs (Klein®421T: 100 kHz, band width 20 kHz) of the fiord walls near the head of Itirbilung Fiord. **(a)** Fresh slide chute and boulder gullies identified on the north wall about 1.2 km from the fiordhead. **(b)** Rock debris from subaerial talus cones that have accumulated on the south wall about 0.9 km from the fiordhead.

Most of the boulders (up to metres across) were clean; a few were covered with silt. The boulders supported a moderately dense and diverse epilithic population, consisting of sabellid polychaetes, alcyonaceans, brittle stars, small white sponges, sea urchins, crinoids, and large basket stars. Encrusting forms included sponges and bryozoans. Abundant shell hash was scattered about. The density and diversity of the faunal populations varied mainly as a function of the current strength. For example, by 270 m water depth, the diversity and density of the fauna was steadily decreasing, marked by an increase in free-standing large sponges and Buccinid gastropod shells. A blue encrusting sponge coated many of the rocks. The bottom sediment was muddy between the boulders. In regions of higher current, there was a marked loss of muddy sediment. A bedrock ledge encountered between 243 and 240 m showed large striations (possibly glacial in origin), on its near vertical rock wall. Sediment on the rock ledge included fine gravel, coarse cobbles, and boulders with scattered shell debris. The larger boulders were covered with a diverse and dense epilithic community. Small brittle stars reached densities of 10 to 20 per square metre.

The seaward approaches to Itirbilung Fiord showed numerous bedrock outcrops (covering about 50% of the seafloor) with sand and mud occurring in pockets between these outcrops (Fig. 31, cf. Fig. 1(B) for location). Many of the outcrops in the distal portions of the approaches appear very rough in relief. Possible glacial striations, seen both on the sidescan images (Fig. 30) and from the submersible or the outer sill, are not present in the outer approaches (Fig. 31).

FACIES ANALYSIS

Data base and facies definition

The sedimentary facies data base for Itirbilung Fiord includes 12 Lehigh cores, 10 piston cores, and 2 cores obtained by the Long Core Facility, for a total accumulated recovery length

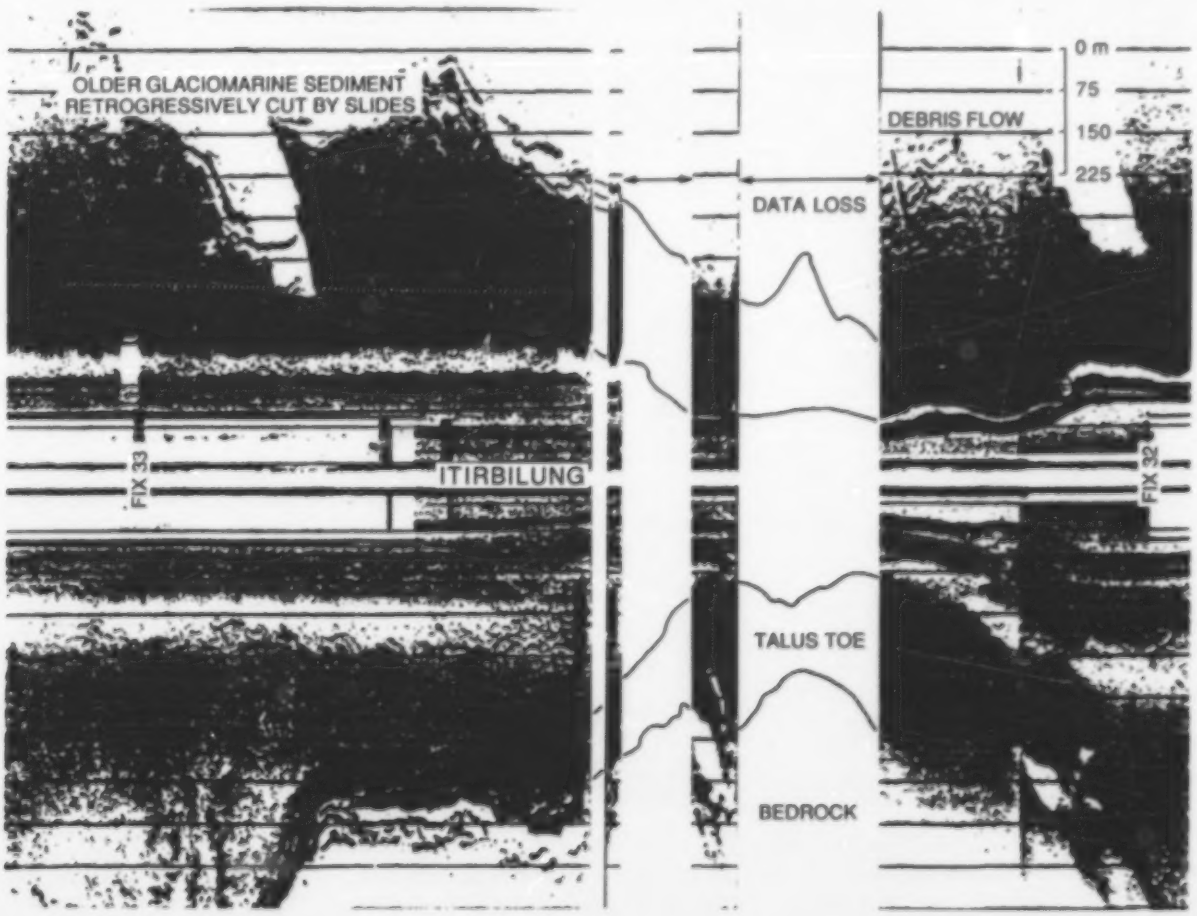

Figure 27. AGC (72.5 kHz, bandwidth of 1 kHz) sidescan imagery coverying a swath of 1.5 km across the fiord, between fixes 32 and 33 of HU83-028 (cf. Fig. 8A). Note the older glaciomarine sediment retrogressively cut by slides (top left), the debris flow deposit (top right) and the talus cone at the base of the bedrock wall (lower right).

exceeding 76 metres of sediment (Table 6, Fig. 18). With the exception of 2 piston cores (IT1 and IT2), 1 Lehigh core (IT0.2) and the two cores obtained by the Long Core Facility (LCF4, LCF5) , all of the cores were logged on a mm to dm scale, depending on bed thickness variation. Detailed log descriptions of split core, photographs of peels from split core, and X-radiographic interpretations are given in Cole and Blakeney (1983), Hein and Longstaffe (1983), Gilbert and Horvath (1984), Reasoner and Hein (1984), Syvitski et al. (1984d), Praeg et al. (1987), and Hein (1987). Preliminary facies description is given in Hein and Longstaffe (1985) and Hein and Syvitski (1987).

Grain size analyses were completed on 358 selected samples from representative facies within core and grab samples, using sieve and pipette analysis and computerized sedigraph and settling tube systems at the Atlantic Geoscience Centre. For a review of the methods see Clattenburg et al. (1983) and Hein and Longstaffe (1983). Supplementary textural data has been supplied by Gilbert (1984) on the coarse fraction obtained in grab samples, by Mothersill and Tabrez (1987) for IT1 piston core and Andrews (1990) on piston cores IT 1.1, 2.3, and 3.1. Grain size frequency plots and tables of moment statistics for individual analyses are given in Clattenburg et al. (1983), Gilbert (1984), Hein and Longstaffe (1983), Reasoner and Hein (1984), Schafer et al. (1984), Mothersill and Tabrez (1987), and Praeg et al. (1987). Some of the original moment statistics were in error and are corrected by Praeg and Prime (1987).

Sediments were classified into facies following the rationale of DeRaaf et al. (1965). The main distinguishing criteria include sediment texture and trends, physical and biogenic sedimentary structures, and the presence or absence of grading, observed in split core sections with reference to X-radiographs and sedimentary peels. Facies data are presented in two ways: (1) as a correlation chart with respect

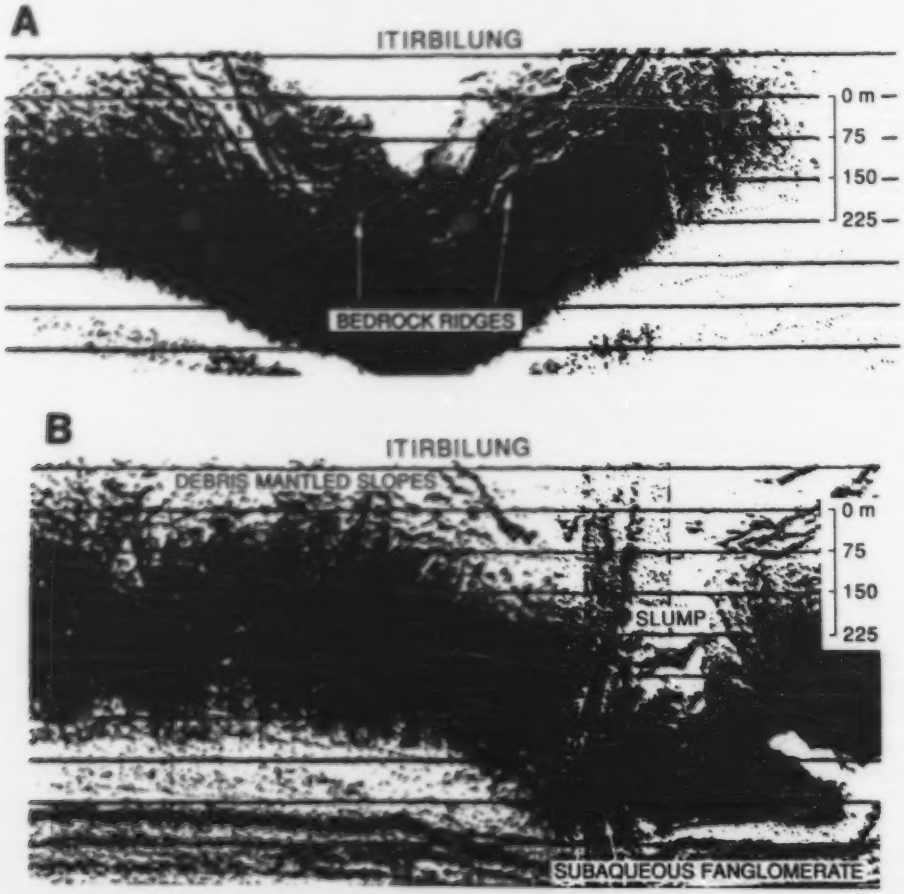

Figure 28. AGC (72.5 kHz, bandwidth of 1 kHz) sidescan imagery of: **(A)** a bedrock wall (located at fix 28 of HU83-028 of figure 8A) showing the exposed rock ledges that appear as arcuate banding (cf. Fig 29A) [the arcuate nature is a simple reflection of the ship approaching the sidewall]. Also note the toe of the wall is covered in accumulated talus; and **(B)** debris mantled slope partially covered by a slump deposit and a subaqueous fanglomerate (located at fix 29 of HU83-028 of Figure 8A) that has partially cut through the slump deposit.

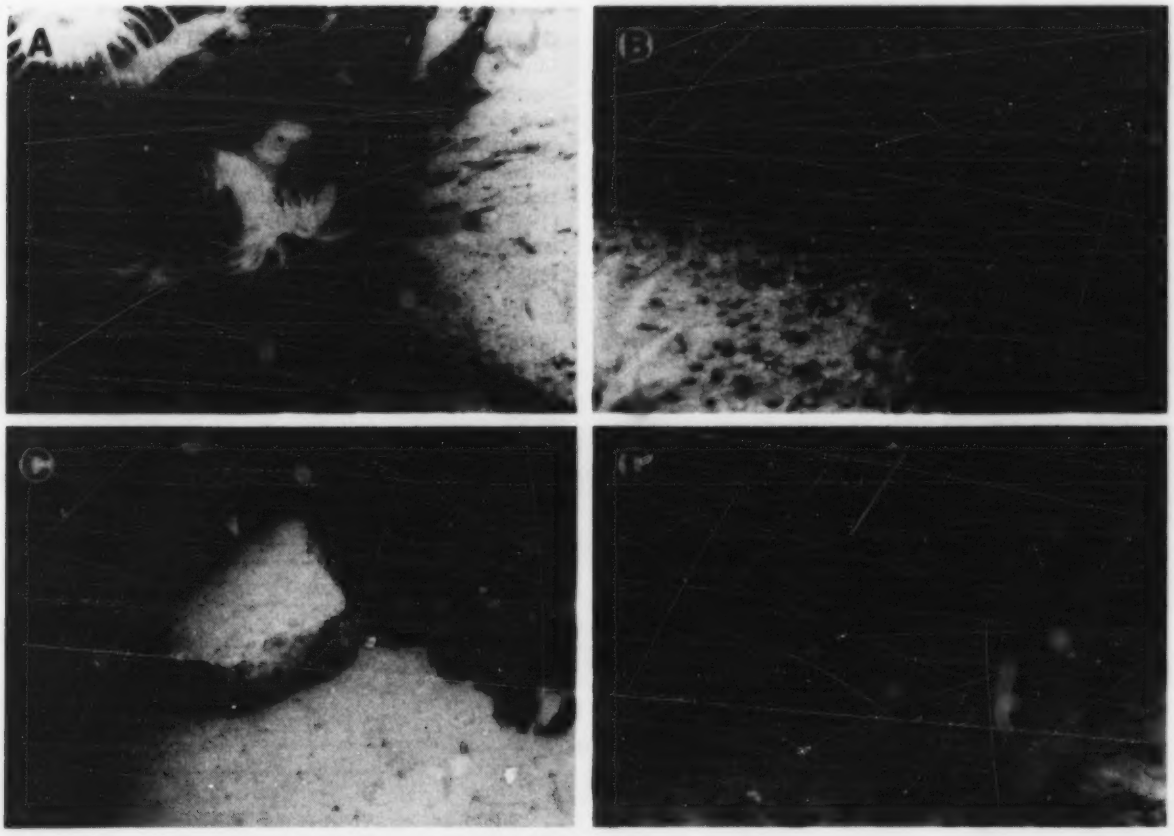

Figure 29. Pisces collected photographs of the sidewall margins and sill (#4) crest. **(A)** Overhang of bedrock, protected from the vertical rain of SPM, is occupied by solitary corals and two large anemones (water depth 310 m, photo from fiord wall in McBeth Fiord equally applicable to the Itirbilung margins. **(B)** Highly mobile crinoids on steep sidewall slope littered with pectin shells and a few gastropods and brittle stars. Also note *Laminaria* debris in water depth of 70 m (Dive 1678). **(C)** Recent dropstone trapping *Laminaria* on steep sidewall slope that, except for the crinoid, contains no epilithics. The recent mantling of sediment suggests that the boulder was emplaced in recent weeks (water depth 60 m, dive 1678). **(D)** Pebble-boulder field representing the outer fiord sill or shelf environment in Itirbilung Fiord (water depth 268 m, dive 1680).

to depth, showing the general distribution of facies in shallow versus deep-fiord sites (Fig. 32 and 33), and (2) as detailed facies logs with respect to bathymetry in sites with good core control, bathymetric contouring, and seismic records (see later discussion).

Huntec and air gun records were the principal data used in establishing our seismo-stratigraphic units. Survey lines were run at speeds of 4 to 11 km/h, and were positioned by fixes from radar (±50 m). Air gun seismic reflection profiles were collected using a Bolt Associates model 600B gun with a 0.655 L chamber fired at 1900 PSI at a 2 to 3 second rate. The single channel, 6 m long, NSRF hydrophone was towed about 20 m astern. Air gun records have a 3 to 10 m vertical resolution and a 4 to 10 m horizontal resolution, and provide penetration to the bedrock surface everywhere.

Huntec® deep tow seismic reflection profiles were collected from a tow-fish containing a 375 Joule (1982) or a 1000 Joule (1983) high resolution boomer fired at a 0.75 second rate and two single channel hydrophones, internal (maximum resolution) and external (maximum penetration). The fish was towed up to 400 m astern and 50 to 250 m above the seabed to a maximum depth of 200 m. The signal returns from the broadband energy source (0.8 to 10 kHz) were typically filtered into two graphic recorders (internal hydrophone: 0.5 to 10 kHz, and external hydrophone array: 0.5 to 3 kHz). Huntec records provide up to 100 m of high resolution (30 to 50 cm vertical, 1 to 2 m horizontal) subbottom information.

Throughout this paper, thicknesses are reported in metres, for conceptual ease. Thicknesses were calculated using an assumed velocity of 1.5 km/s (approximately the speed of sound in water). Masson and Locat (1987) provide the only measured sediment velocity data for Baffin Island fiord

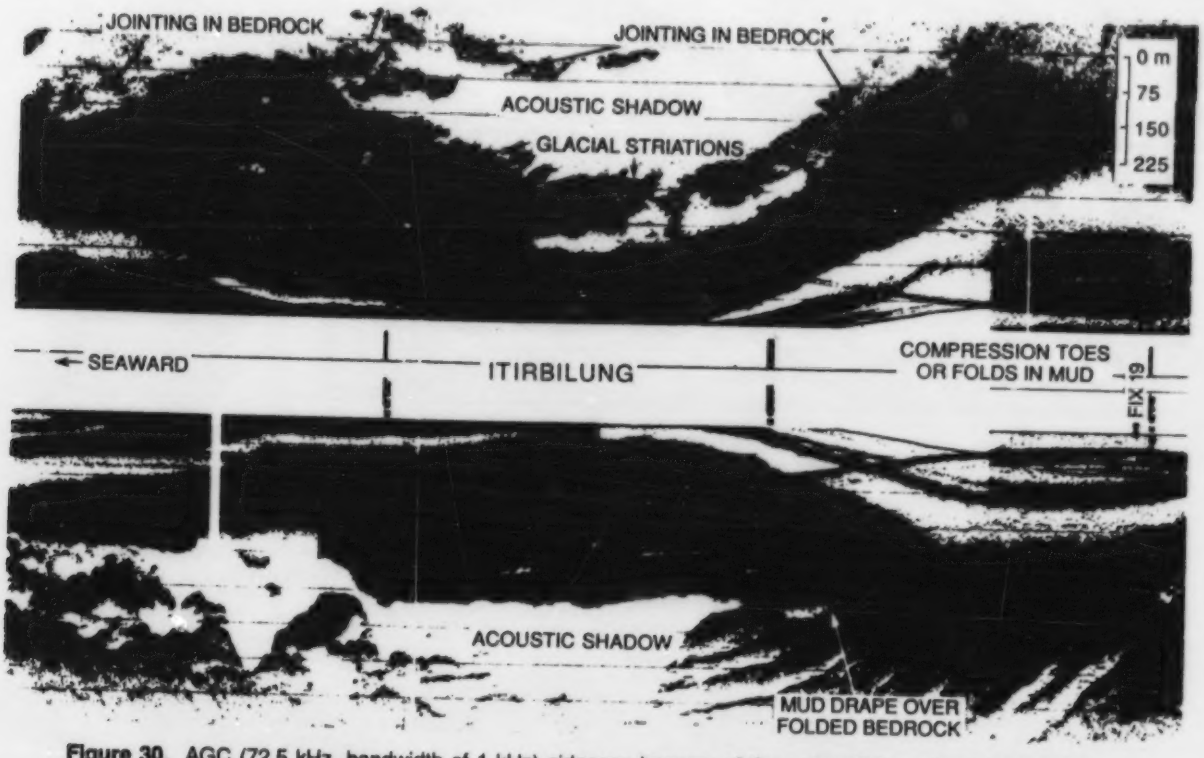

Figure 30. AGC (72.5 kHz, bandwidth of 1 kHz) sidescan imagery of the outer sill bounding Itirbilung Fiord (cf. Fig. 1 for location). Interpretations include mud folds leading into the outer fiord basin, glacial striations oriented down-fiord, apparent jointing in the bedrock, and mud-covered large scale folds of the Archean?

sediments with a mean value of 1.65 km/s for near-surface sediments. Thus our thickness values represent minimum estimates. Over 200 line kilometres of seismic profiles were examined.

Seismo-stratigraphic units are defined as successive intervals that can be recognized and traced on the basis of distinctive acoustic attributes, bedding styles, and/or unit geometry (for rationale and details see Syvitski and Praeg, 1989). Units were established in a typical section, and then traced laterally to establish a regional stratigraphy within which units often display facies variability in their acoustic attributes, bedding style, and geometry (Syvitski and Praeg, 1989).

Regional acoustic units

Five seismo-stratigraphic units are commonly recognized within a given glacial/deglacial sediment deposited within glaciated continental shelves (e.g. Gilbert, 1985; Syvitski and Praeg, 1989; Syvitski, in press). Based on these previous studies, the lowermost unit (1), overlying 'basement', is an unconsolidated layer whose upper and lower bounding surfaces are complex. The unit may be subdivided into a depositional facies (unit 1a), e.g. till (drift), moraines and eskers, and an ice loaded facies (unit 1b) where sediments deposited prior to an advancing ice terminus are over-ridden but not completely eroded. Both subunits have moderate acoustic tone and tend to be acoustically unstratified (incoherent). Major internal reflectors are usually interpreted to indicate erosional surfaces, possibly from ice load and scour, especially when these reflectors are unconformable to both the basement bathymetry and the normal bedding planes (observed in more surficial units).

Unit 2, characterized by strong, closely-spaced reflectors, may represent the rapid deposition of sediment proximal to a glacier terminus and directly influenced by submarine glaciofluvial discharge. The overlying unit 3 is characterized by distinctive very low tone, weak stratification and a conformable bedding style. Unit 3 may represent ice distal accumulation of glaciomarine sediment from the hemipelagic deposition under turbid surface plumes. Unit 4 is characterized by strong and dense acoustic stratification and generally ponded bedding style, although the unit may be distally conformable over unit 3. The unit commonly contains deposits relating to submarine slides and sediment-gravity flow deposition. Unit 4 may represent the paraglacial period of local land drainage and deltaic progradation during the melting of terrestrial-based ice caps during a period rapidly falling sea level. Unit 5 is typically characterized by low tone and weak reflectors that may range from conformable to onlapping in geometry of the deposit. Near modern deltas, unit 4 may grade continuously into unit 5. Unit 5 reflects the postglacial period where sea level

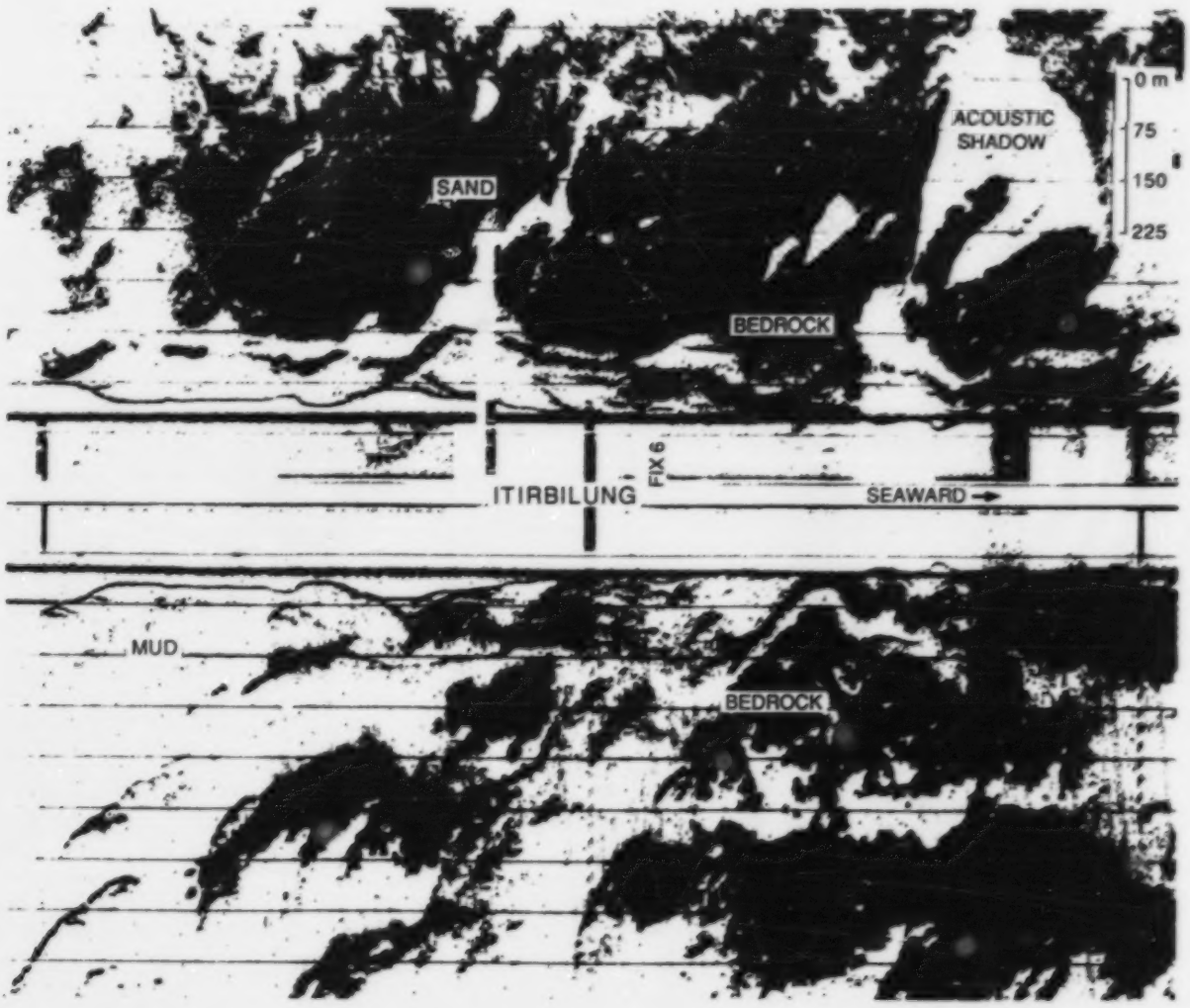

Figure 31. AGC (72.5 kHz, bandwidth of 1 kHz) sidescan imagery of the outer approaches to Itirbilung Fiord (cf. Fig. 1 for location). Pockets of sand are distinguished from mud drapes based on acoustic absorption characteristics. The bedrock outcrops have a very rough surface morphology.

is more or less stable, the major ice sheet has retreated from the drainage basin. It is within units 4 and 5 that our marine cores have penetrated.

Figure 34 provides the down-axis distribution of these seismo-stratigraphic units, except for unit 5 which is too thin to be identified on airgun records. Our interpretation varies from that of Gilbert (1985) in the placement of some unit boundaries; particularly in defining the relationship between units 1 and 2, and in the interpretation of units over the outer sill complex. On a replay of the original analog tapes through a Kronite® filter (300 to 1200 Hz), boundaries between units were more easily resolved. Figure 35 provides examples of a portion of the replayed 1982 record (fixes 11 to 25).

There appears to be only local ice contact (unit 1a) deposits, located in depressions of sill 2, within ice push features (unit 1b), and as undifferentiated drift over the outer sill complex. Stravers and Syvitski 1991 have interpreted similar features in Cambridge Fiord as morainal banks, through correlation with similarly positioned terrestrial deposits. Unfortunately the ice cover in the Itirbilung hinterland is so extensive, that correlative deposits relating to the waning phase of the Late Foxe glaciation can not be identified. Of the ten Baffin Island fiords surveyed within the SAFE Project, the ice push features identified (Fig. 34 and 35) are unique to Itirbilung Fiord. They show an intimate relationship with the interpreted ice proximal sediments of unit 2, that together account for 50% of the basin fill within Itirbilung Fiord, dominating the fill of

Table 8. Facies percentages (on the basis of thickness) for core samples collected in Itirbilung Fiord. See Figures 1 and 18 for sample locations.

			FACIES						
Core	Depth (m)	Distance (km)	A	B	C	D	E	F	G
0.1L	55	0.8	0.0	29.3	14.6	53.0	3.0	0.0	0.0
0.1P	55	0.8	0.0	3.6	1.8	67.4	0.0	25.1	2.1
0.2L	88	1.6	0.0	33.3	0.0	66.7	0.0	0.0	0.0
62-20D	85	0.16	0.0	5.7	0.0	94.3	0.0	0.0	0.0
62-20B	91	0.18	0.0	17.2	0.0	80.6	0.0	0.0	2.2
LCF4	124	3.1	4.7	13.0	0.0	3.1	0.0	79.3	0.0
LCF5	139	3.45	3.6	24.1	2.9	13.9	0.0	55.5	0.0
0.4L	148	4.1	16.4	35.6	14.4	25.3	0.0	8.2	0.0
0.4P	148	4.1	6.1	5.8	3.3	21.0	0.0	63.9	0.0
0.3L	155	4.8	12.3	39.2	28.5	10.4	0.0	7.7	1.9
0.3P	155	4.8	1.0	14.4	0.0	0.0	0.0	84.7	0.0
1.0P	167	6.0	3.2	36.6	0.0	31.0	1.6	29.3	0.0
1.1L	256	11.2	5.4	79.7	0.0	0.0	0.0	14.9	0.0
1.1P	256	11.2	7.2	87.1	0.0	0.4	0.0	5.3	0.0
1.2L	293	12.9	15.2	54.3	0.0	12.4	2.9	11.4	3.8
1.2P	293	12.9	0.0	24.1	3.6	5.0	3.6	63.7	0.0
2.1P	310	18.4	0.0	8.5	0.0	0.0	0.0	91.5	0.0
2.2L	402	25.3	34.1	56.6	3.8	0.0	0.0	5.5	0.0
2.2P	402	25.3	0.7	86.1	1.2	0.0	0.9	11.1	0.0
2.3L	424	37.0	22.5	64.2	6.9	0.0	0.0	4.9	1.4
2.3P	424	37.0	0.0	93.6	0.9	0.0	0.0	5.1	0.4
3.0L	417	41.5	1.9	98.1	0.0	0.0	0.0	0.0	0.0
3.1L	356	50.5	16.6	73.5	7.6	0.0	0.0	2.2	0.0
3.1P	356	50.5	0.0	78.7	0.7	17.9	0.0	1.0	1.6

basins 3 and 4; with a maximum thickness of 85 m. Not surprisingly, slump deposits are commonly associated with the interfingering of units 1 and 2.

Unit 3 has a more even distribution: it drapes over sills, with a range in thickness from 30 to 70 m. Acoustic stratification within unit 3 becomes stronger towards the head of the fiord. It also contains evidence for large submarine slides, such as identified on Figures 34 and 35. Details of one of these slumps is interpreted from the boomer record (Fig. 36): failure has occurred along the surface of a morainal bank over which ice distal sediments (unit 3) were deposited. This slumped deposit shows little internal reflection and was interpreted incorrectly by Syvitski (1984b) and Boulton (1986) as representing till (which is present but much farther down in the section).

Units 4 and 5, undifferentiated on Figure 34, thin from >100 m near the fiordhead prodelta region (basin 1) to less than 5 m over the outer sill complex. Side entry inputs are common and occur in the form of slumps and debris flows off the margin walls and from fluvial inputs from tributary rivers (Fig. 37). Sidewall-generated slides may fail more than once (Fig. 38), because of their steep slopes and the thin cover of sediment over local basement rocks. The result of sidewall slides is usually a complete remolding of the affected

sediment mass (cf. Fig. 37 and 38). Differentiating unit 5 from unit 4 is difficult, even using boomer data. This can be attributed to the fact that because the Itirbilung hinterland is 32% covered in glacier ice (Gilbert and MacLean, 1983), and thus the region is not yet postglacial but remains within a paraglacial framework. Except for certain small portions of the fiord dominated by bioturbated hemipelagic deposits (e.g. IT2.3), unit 5 can not be established.

The prodelta region provides the most dramatic evidence of changes in the style and rates of basin fill. Although the total thickness is unknown, due to lack of airgun data, a thick highly reflective unit in the lower part of the section has been identified as glaciomarine sediment (Fig. 39). It may be either unit 3 or unit 4 within our seismo-stratigraphic framework because it predates the growth of the local marginal icecaps and their production of side-entry fanglomerate deposits (Fig. 39). Based on its strong, closely-spaced reflectors we favour its identification as unit 4. Overlying this unit is an aggrading prodelta wedge with a retreating hinge line[1] (Fig. 39). We interpret this to represent a decreasing sediment supply, because the associated effects of the known falling sea level should advance the hinge line given a constant sediment supply. As such, we suggest that the period of decreasing sediment supply could be reasonably assigned to the Neoglacial period of lowered sediment yield (see glacial input section above). This interpretation is supported by noting that the prodelta wedge was largely deposited during the earliest stage in the growth of the side-entry ice-contact deltas (which are Little Ice Age deposits, cf. Fig. 5).

Overlying this unit is a massive, 8 m thick, ponded slide mass (Fig. 39). We suggest that this deposit relates to the major jøkolhlaup discharge event (about 1890) discussed earlier (see delta environment description). Our sediment trap-determined sedimentation rates of about 90 mm• a^{-1} further support this interpretation, considering the 6 to 10 m of overlying sediment. The surficial unit is characterized by strong, closely-spaced reflectors. These sediments have experienced and, as submersible observations suggest, continue to experience failure along listric riders and concomitant thrust toes (Fig. 39). There is some evidence that a deep-seated growth fault may control these retrogressive slide scarps (Syvitski and Farrow, 1989). Failure along these scarps is the obvious mechanism in generating the muddy turbidity currents.

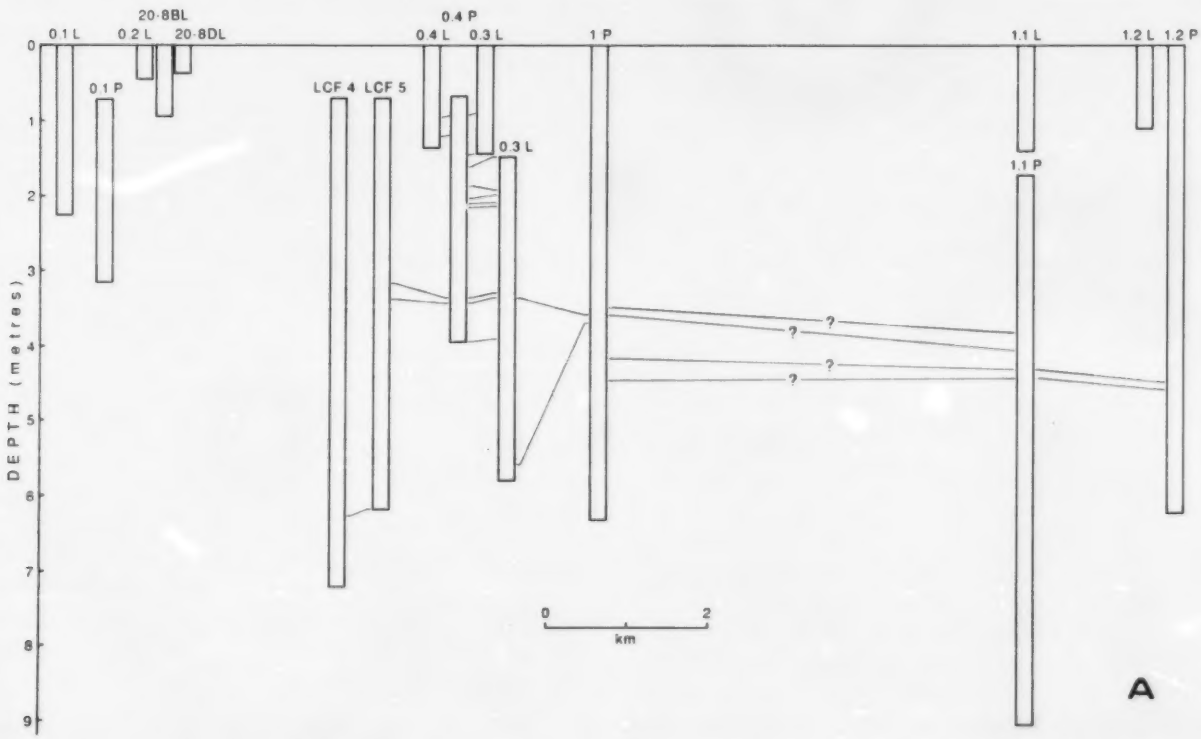

Figure 32. Correlation chart of interpreted lithologic facies of all marine cores collected within basins 1 and 2 (cf. Fig. 8 and 18, Table 8). **(A)** Cores positioned in terms of distance and vertical height. **(B)** Facies interpretation.

[1] A prodelta hinge line is defined as a marked change in slope within a seismic package of a delta.

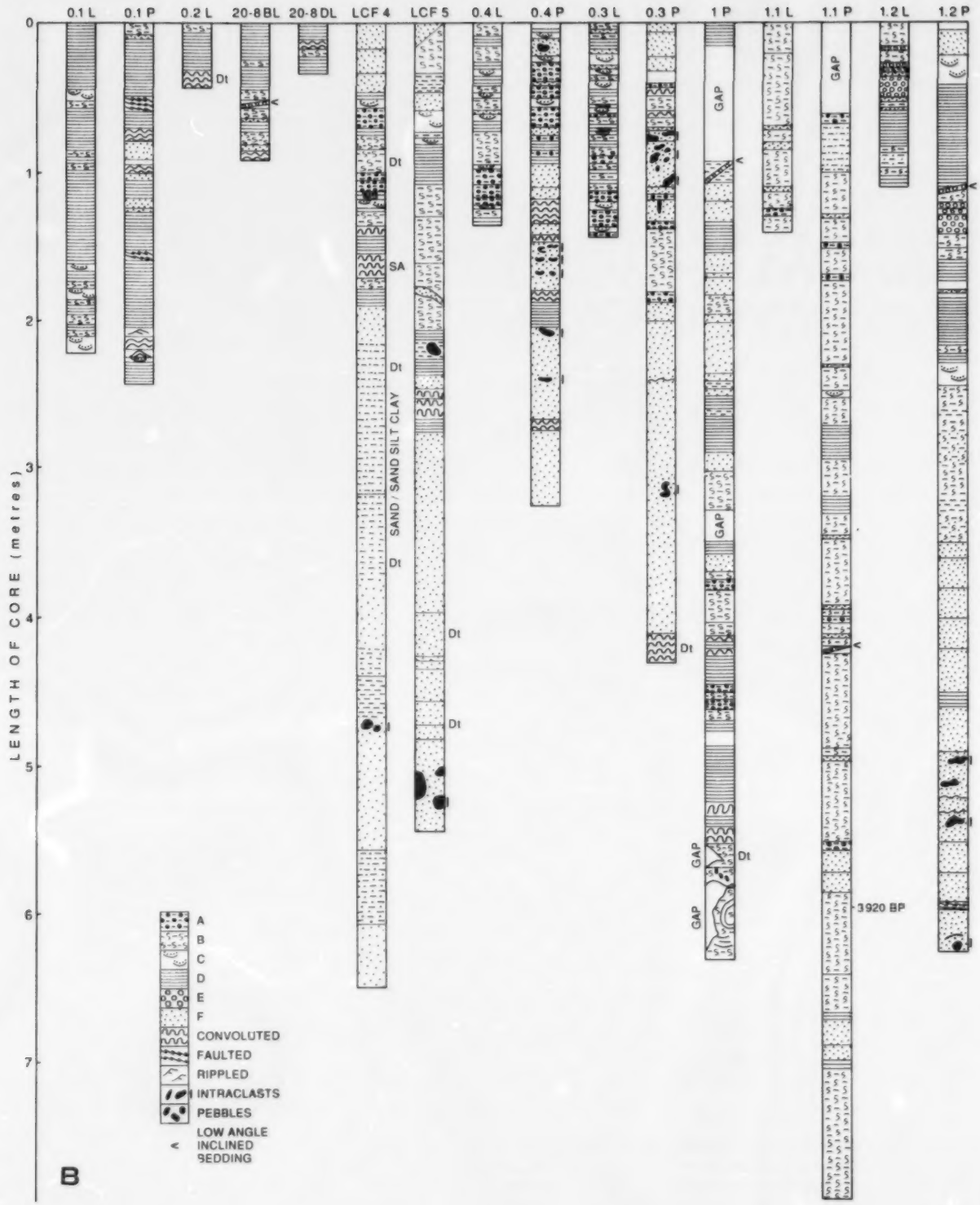
0.1 L
0.1 P
0.2 L
20-8BL
20-8DL
LCF 4
LCF 5
0.4 L
0.4 P
0.3 L
0.3 P
1 P
1.1 L
1.1 P
1.2 L
1.2 P
LENGTH OF CORE (metres)
0
1
2
3
4
5
6
7
Dt
SA
SAND / SAND SILT CLAY
GAP
3920 BP
A
B
C
D
E
F
CONVOLUTED
FAULTED
RIPPLED
INTRACLASTS
PEBBLES
LOW ANGLE INCLINED BEDDING
B

Figure 32B

Table 9. Average textural characteristics of facies for core samples collected in Itirbilung Fiord. See Figures 1 and 18 for sample locations. Mean and standard deviation are calculated by the method of moments.

Facies	Ave. mean (Ø)	Ave. std. dev. (Ø)	Gravel (%)	Sand (%)	Mud (%)	No. analyses
A	6.52	2.99	1.1	26.1	72.7	19
B	6.99	2.56	0.1	19.1	80.5	31
C	5.37	2.43	0.1	49.2	50.7	6
D	5.14	2.09	0.1	48.1	51.8	67
E	1.53	1.48	9.4	78.1	12.4	5
F	3.97	1.61	0.1	69.0	30.9	121
G	3.61	1.83	0.1	83.5	18.4	7

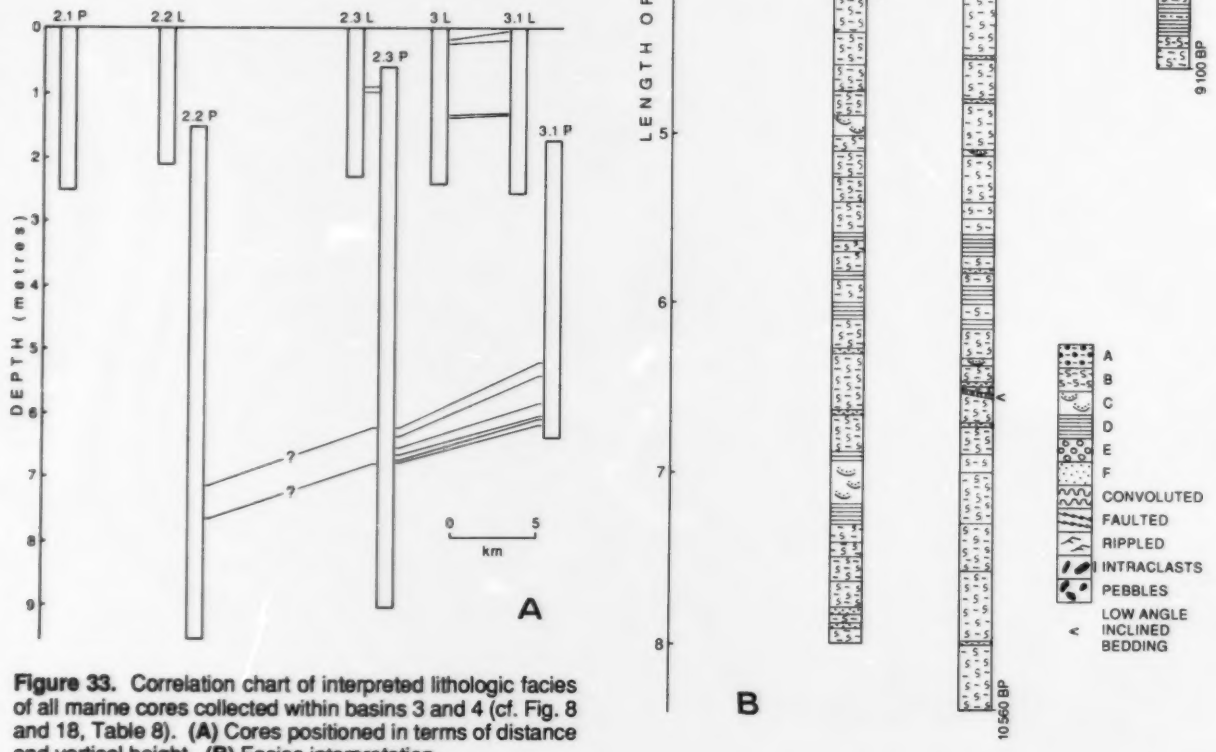

Figure 33. Correlation chart of interpreted lithologic facies of all marine cores collected within basins 3 and 4 (cf. Fig. 8 and 18, Table 8). **(A)** Cores positioned in terms of distance and vertical height. **(B)** Facies interpretation.

Sedimentary facies

Facies A. Pebbly-sandy-mud (Fig. 40, 41, 42): This facies is rare and occurs sporadically throughout the cores, although it is mostly in the upper third of the piston cores, or lower portion of the Lehigh cores (Fig. 32, 33). Facies A has an average thickness per core of 6.3% (range: 0 to 34%, Table 8). Sediment sorting is very poor (average $\sigma = 2.99$ Ø, Table 9). Facies A has a dominant mode in the medium to fine sand range (1.5 to 2.5 Ø) (Fig. 42), with a tail in the silt and clay sizes (>4 Ø). This facies consists of layers that average 5 cm thick (range 0.00 to 0.18 m, Core IT2.2P, Fig. 33). The mud is commonly dark olive green, and may be completely bioturbated. Pebble size is up to 3 cm, averaging 1 to 2 cm in length, within a finer grained sandy, silty matrix. Rare downwarped convolute structures (i.e. soft sediment deformation structures of underlying sediment around the base and sides of pebbles) are interpreted as 'dropstone structures'. The occurrence of out-sized pebbles, the very poor sorting, the absence of stratification and the occurrence of dropstones suggests that the coarse clastic component of this facies was derived from the meltout of material from debris-laden ice.

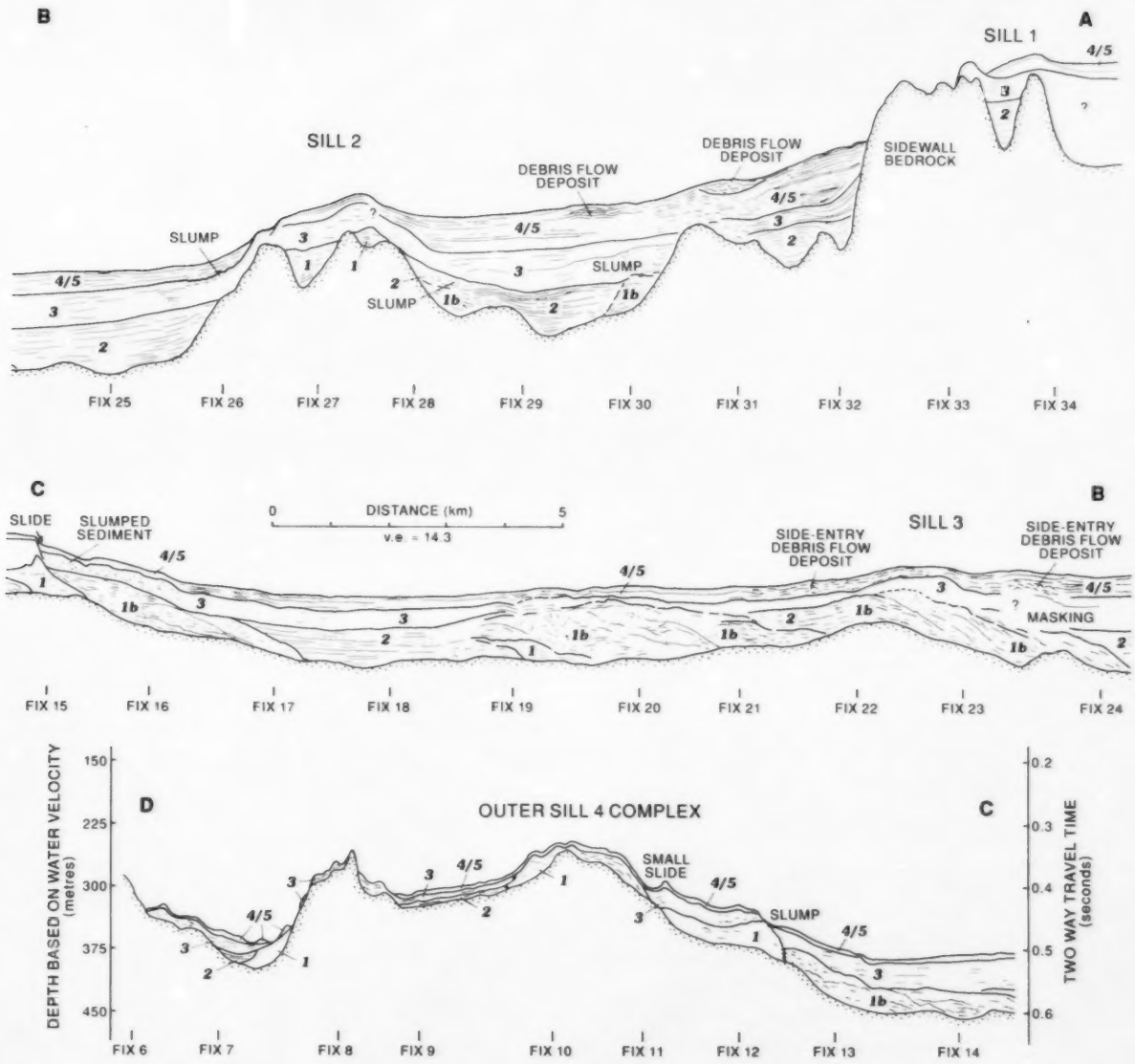

Figure 34. Seismo-stratigraphic interpretation of 1982 airgun profile (cf. Fig. 8 for location). See text for description of seismic units, and Figure 35 for portion of seismic record.

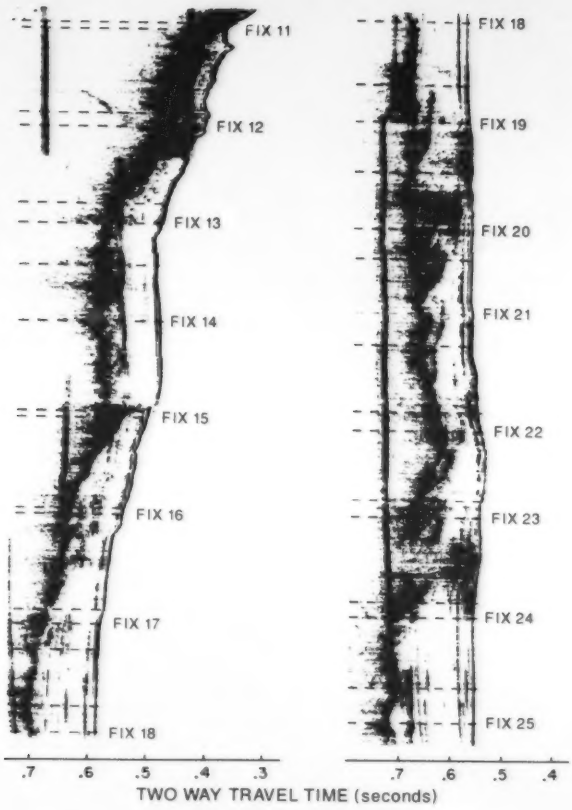

Figure 35. Airgun reflection seismic record from fix 11 to 25 (cf. Fig. 8). For interpretation see Figure 34.

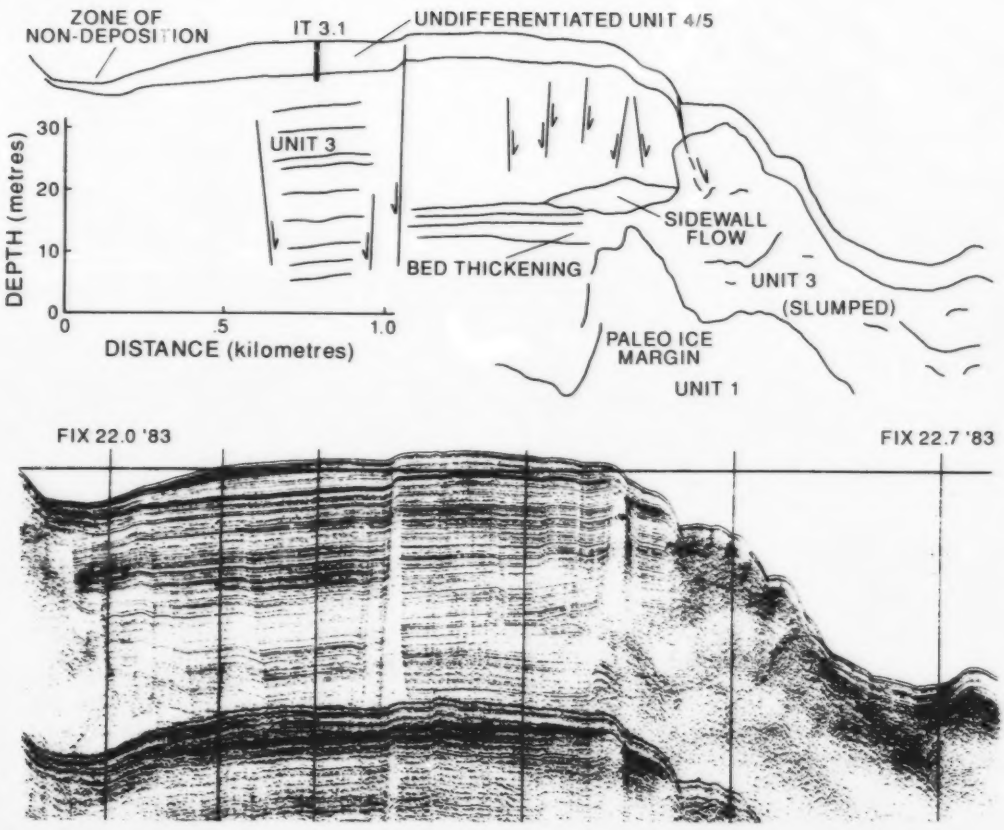

Figure 36. Huntec profile with interpretation of a paleo ice marginal position and subsequent slump generated after retreat of the terminus (cf. Fig .8 1983 track for position of fix 22 and 22.7 for position).

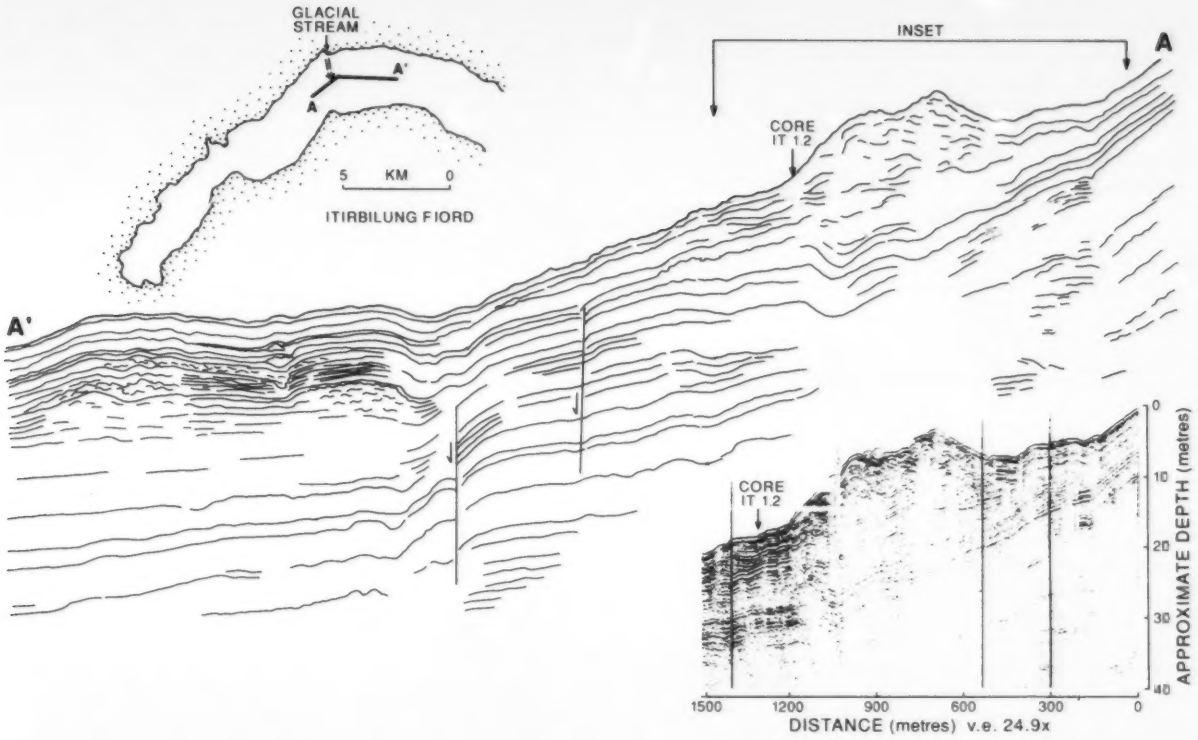

Figure 37. Interpretation of Huntec profile over sidewall generated slump with associated debris flow deposits (note inset of portion of actual Huntec record). Note core location of It 1.2.

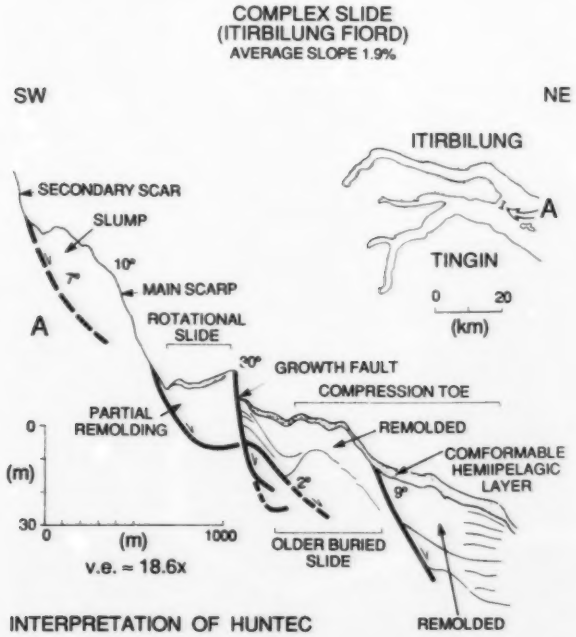

Figure 38. Example of a slide complex from the margin of the basin based on interpretation of high resolution Huntec DTS reflection seismic record.

Gilbert (1984) in his study of coarse particles (>2 mm) in grab samples from Cambridge, McBeth and Itirbilung fiords shows that dropstones are a minor to moderate component of the sediments obtained in grab samples. In Itirbilung Fiord the numbers of large pebbles per grab sample increase rapidly downfiord from the head to about 35 km. Most of the pebbles greater than 8 mm in diameter are angular or subangular, and are interpreted as glacial (iceberg drop or dump) in origin. Some of the angular pebbles may also be derived from colluvial inputs, including landslides. The petrography of the stones indicates a dominant local source for the clasts (Gilbert, 1984), with most of the clasts corresponding to the local bedrock composition. In one sample, IT5 in northern Home Bay outside the mouth of the fiord, there were some Phanerozoic sedimentary rock fragments, including a well rounded limestone pebble that was interpreted as being transported by sea ice from a beach in Lancaster Sound or from sites to the north or west. Thus, most of the coarse, out-sized particles in Facies A within Itirbilung Fiord originated as dropstones from icebergs and sea ice of local origin. Outside the mouth of Itirbilung Fiord, other sources for the coarse clasts may be important.

Facies B. Burrowed/mottled mud (Fig. 41, 43): This facies is predominant in the longer piston cores from deeper parts of the fiord (i.e. cores IT1.1P, 2.2P) and in both the Lehigh and piston cores within the outermost basin 4 (Fig. 8, 18) (i.e. cores IT2.3L, P; IT3L, IT3.1L, P, Fig. 37). Facies B has

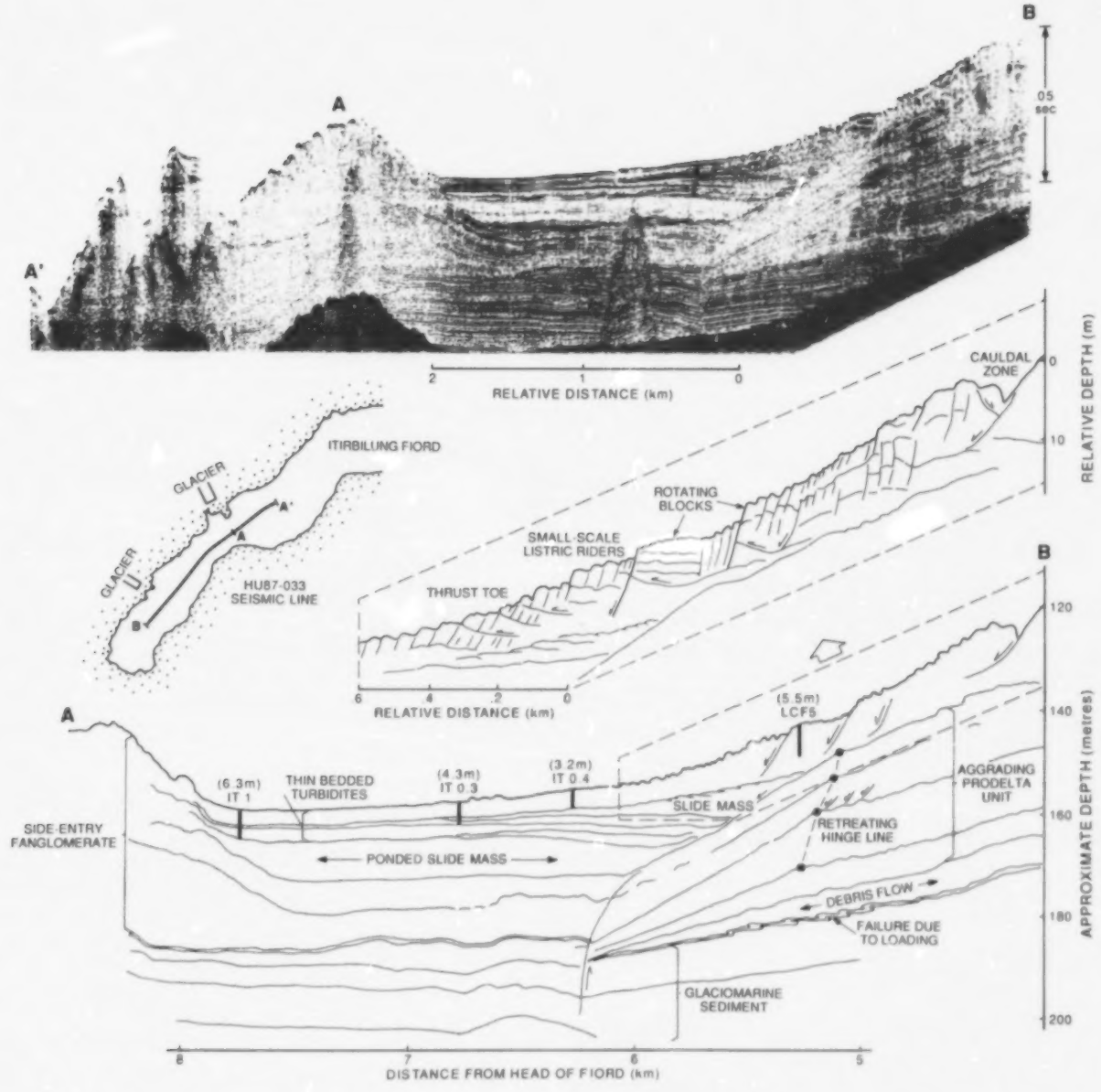

Figure 39. Huntec profile of the prodelta region of Itirbilung Fiord (basin 1) with associated interpretation of the major units and aspects of the main slide.

an average thickness per core of 44.3% (range: 0 to 98%, Table 8), ranging in thickness from about 0.1 to 1.0 m (average about 0.3 m, Fig. 32, 33). Sorting is very poor (average $\sigma = 2.56$ Ø, Table 9). Facies B has size distributions truncated toward the coarser sizes (<4 Ø), with a secondary mode in the fine sand to very fine sand range (3 Ø), and with most of the distribution skewed towards the silt and clay sizes. Burrow infills are generally dark, reduced silty-mud, rarely sand. Most of the mottles are irregular in shape, with sharp, well-defined boundaries. More distinct burrow types are commonly *Planolites* (IT1.1P, IT2.2P, IT2.3P, IT3.1P); less commonly, in sandier beds, *Skolithos* (IT1.1P, IT2.2P, IT2.3P); and, rarely, in muddy sediment, *Asterosoma* (IT2.3P), *Chondrites* (IT2.3P), *Thalassinoides* (IT2.2P), and *Rhizocorralium* (IT2.2P) (cf. Ekdale et al., 1984).

The nearly complete obliteration of primary sedimentary structures by bioturbation implies that locally the rate of biological mixing exceeds the rate of sedimentation. The general lack of coarse sediment size (<4 Ø) and the skewness toward the fine sizes (i.e. silt and clay), suggests

that most of the sediment was originally emplaced by deposition from fluvial plumes of fine silt and clay, or from hemipelagic fallout of aeolian-transported sand and silt. The bioturbation patterns within this facies resembles Howard's (1978) model in which there is slow, continuous sedimentation accompanied by complete bioturbation. Most of the identificable traces belong to the *Cruziana* ichnofacies (cf. Ekdale et al., 1984), which imply depositonal conditions of low- to moderate-energy level (Frey and Seilacher, 1980). The local occurrences of *Chondrites* indicate dysaerobic to anaerobic conditions within the sediment itself, and need not imply similar conditions of the overlying water column (cf. Ekdale et al., 1984). This fact supports the electro-chemical measurements of pE within Itirbilung Lehigh cores (e.g. Fitzgerald, 1984).

Facies C. Wispy laminated/ mottled mud (Fig. 41, 44): This facies is uncommon, and occurs sporadically throughout the cores, although it is more common in cores having a thicker proportion of laminated layers (Fig. 32, 33). Facies C has an average thickness per core of 3.8% (range: 0 to 29%, Table 8). Sediment sorting is very poor (average $\sigma = 2.43$ Ø, Table 9). Facies C has textural distributions similar to Facies A, with a coarse mode in the fine sand size (2 to 3 Ø), and a fine (muddy) tail (>4 Ø). Laminae consist of wispy-sands about 2 to 5 mm thick (range: 0.3 mm to 40 mm) (Fig. 35). These laminae alternate with silty mud, and sandy-silty-mud in units up to 1.3 m thick (IT2.2P, Fig. 33). The sand commonly occurs as a tan-white, mica-rich quartz sand, within a medium to dark olive green or grey silty mud. The bases of the sand lenses are sharp, and often show delicate scour marks. The tops of the lenses are most often gradational and may be mottled. The sand lenses are discontinuous, and thinner laminae may appear as coarser 'streaks' within a muddy sediment.

Figure 40. X-radiographic print of Facies A pebbly-sandy-mud, core IT0.3P, showing the random distribution of pebbles within a silty mud. Core depth shown is 183-203 cm.

The scoured bases of the sands, and their intimate, normal grading into the overlying muds suggest that this facies represents largely suspension fallout of clayey and silty mud from fluvial or aeolian plumes, which is intermittently punctuated by sudden, rapid erosion and deposition by fine grained, sand-laden currents. Carey and Roy (1985) in their study of laminated shales show that such wispy lamination may occur in silt and clay-laden currents which are decelerating during deposition, with current velocities in the range of 12 to 28 $cm \cdot s^{-1}$ for such flows. Thus the sediment-laden currents interpreted to have deposited these intermittent laminations are likely fine grained turbidity currents resulting from failures of small volume (possibly from the sidewalls of the basin, or from the many steep scarps of the prodelta region).

An alternate explanation may have the thin sand lenses related to the meltout of aeolian sand initially transported onto the sea ice cover of winter. Fine grained, mica-rich, quartz sand perfectly describes the aeolian deposits that partly cover the Itirbilung sandur. The associated scoured bases may then relate to undercurrents set up by the rapid introduction of sediment through melt-pools formed during the early summer disintegration of the sea ice cover.

Facies D. Laminated sand and mud (Fig. 41, 45, 46): This facies is most common in the upper part of cores near the head of the fiord (IT0.1L, P; 0.2L, 20-8BL, 20-8DL; 0.4L and 0.3L, Fig. 32, 33), where in some cores >90% of the core consists of this facies. Other laminated layers occur farther downsection, at different stratigraphic intervals within the piston cores (Fig. 32, 33). Facies D has an average occurrence per core of 21% (range: 0 to 94%, Table 8). Within Facies D, sediment sorting is poor to very poor (average $\sigma =$ 2.0 Ø, Table 9), although this may be an artifact due to the difficulty in sampling individual laminae. Facies D has size frequency distributions similar to Facies A and C, with a coarse mode in the fine sand size (2 to 3 Ø) and a tail in the finer fractions (>4 Ø). By comparison, sediment trap data 11 m below the sea surface shows a similarly shaped distribution to these facies, but the distribution is shifted toward the fine end, with a coarse silt mode (about 4 Ø) (Fig. 46). The data recovered from the sediment trap represented hemipelagic deposition associated with a relatively low stage in fluvial discharge. Laminae consist of sands, silts or sandy/silty muds about 1-2 mm thick (range: 0.3 mm to 8 mm), which alternate with silty mud and mud in stacked units up to 1.7 m thick (IT0.1P) (Fig. 32). Some laminae become progressively coarser, then finer upsection; whereas other

stacked laminae define fining-upward units. No consistent patterns of upward coarsening or fining between cores was noted.

In this facies primary lamination is preserved, with corresponding minor disruption by bioturbation. This implies that the sedimentation rate greatly exceeded the bioturbation rate. The variable coarsening and fining-upward trends within intervals of Facies D suggests that currents either gradually increased or decreased over time. The lack of persistent trends either within single cores or between adjacent cores suggests that these currents were variable in time and in space. There is a marked similarity of the size distributions in Facies D samples with those distributions obtained from sediment traps beneath proximal fluvial plumes (Fig. 46). Facies D occurs within cores located near glaciofluvial inputs (i.e. IT0.1L and P, IT0.2L and P, 20-8BL, 20-8DL near Itirbilung River; and IT0.4, IT1 and IT1.2P near side-entry glacial streams, Fig. 18, 32). The textural pattern of this facies (Fig. 44) indicates that both silt and clay were hydraulically sorted within the flows prior to deposition.

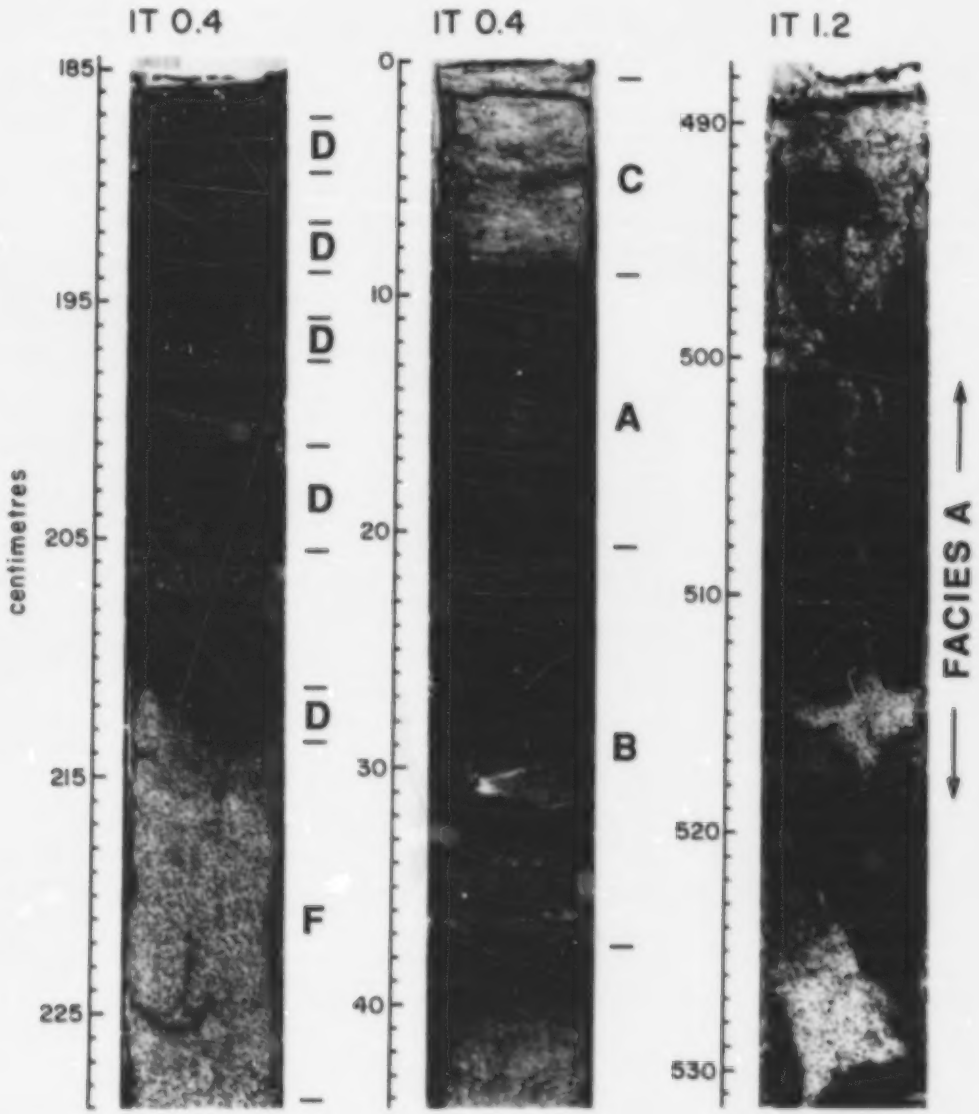

Figure 41. Photographs of split core, showing Facies A pebbly sandy mud and disturbed (Dt) sections, core IT0.3P; Facies B bioturbated silty mud, core IT0.4L; Facies C, wispy laminated sand and mud, Facies D laminated sand and mud, Facies E thin gravel, thin Facies F sand, core IT0.4P; thick Facies F sand with distorted silt and mud intraclasts, core IT1.2P. Tick marks are each one cm long.

Thus, Facies D is interpreted as representing high-sedimentation fallout of sand and mud from hypopycnal discharge plumes (Syvitski, 1987a). The variable trends of Facies D grain size and lamina thickness within individual cores reflect the time-variation, perhaps diurnal and seasonal variability, of discharge events from the glacial ice fields. The lack of correlation in Facies D patterns between adjacent cores may reflect the spatial variability of turbid plumes across the fiord. R. Gilbert (pers. comm., 1980) provides excellent documentation on the migration of the fluvial plume issuing from a Baffin Island sandur over a ten hour period. The transport of sand-sized particles, some 1 to 2 km out from river mouths, is not unexpected, considering the high flow velocities associated with high gradient streams (especially the side-entry streams). Schafer et al. (1983) have related discharge levels of the Saguenay River to both sand concentration and sand modal size within similar hemipelagic laminations observed in a core collected 2.5 km from the river mouth.

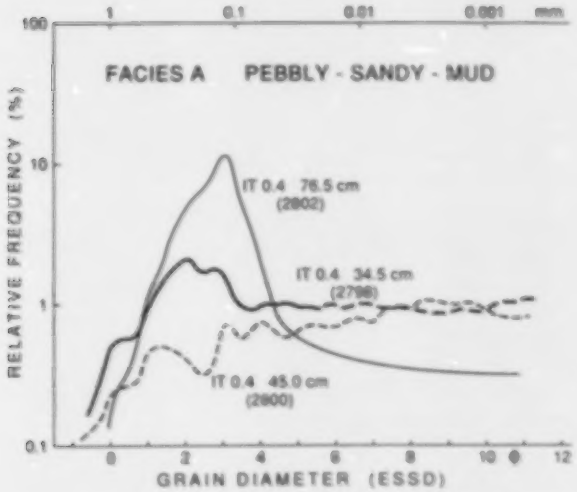

Figure 42. Representative grain size-frequency distribution curves for Facies A pebbly sandy mud. Core numbers, sample depths, and lab numbers are labelled beside the curves. ESSD = equivalent spherical sedimentation diameter.

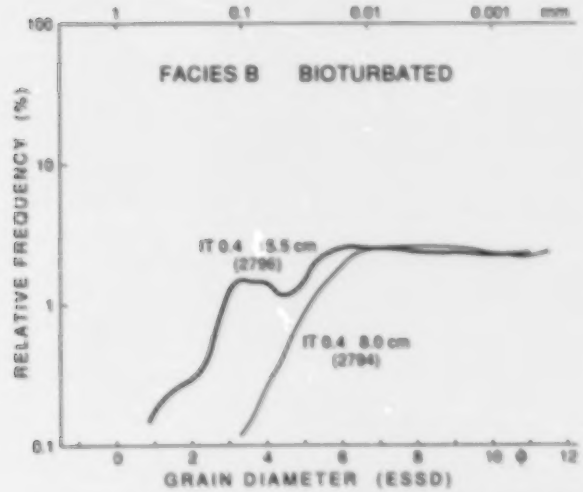

Figure 43. Representative grain size-frequency distribution curves for Facies B bioturbated mud. Core numbers, sample depths, and lab numbers are labelled beside the curves.

Facies E. Coarse Sand/gravel (Fig. 41, 47): This facies is extremely rare, with only one good occurrence in core IT1.2P (Fig. 37). Facies E has an average thickness per core of 0.5% (range: 0 to 4%, Table 8). Sediment sorting is poor (average σ = 1.48 Ø, Table 9). Facies E has a very irregular textural distribution patterns, with modes in the coarse sand and fine sand ranges. Many of the distributions are multimodal, and the tail of the finer fraction may be truncated or show a positive skewing (Fig. 47). These irregularities most likely represent the mixing of samples from different lamina or stratification bands. In core IT1.2P, the Facies E coarse pebble layer occurs as a normally graded, 0.25 m thick bed. Grain size varies from 8 to 10 mm at the base, to 5 to 6 mm at 0.1 m above the base, to a pebbly sand and sand at the top. The bed has a scoured and loaded base, and is well stratified throughout. The lower portions of the bed are clast-supported, openwork gravel. Upper bed portions are clast-supported, matrix-infilled gravel, with a sand matrix infill. The interpretation of this facies is similar to Facies F given below.

Facies F. Pebbly Sand and Sand (Fig. 41, 48, 49): This facies comprises between 50 and 90% or more of some of the cores (LCF4, LCF5, IT0.4P, IT0.3P, IT1.2P, IT2.1P, Fig. 32, 33). Facies F has an average thickness per core of 24% (range: 0 to 92%, Table 8). Sediment sorting is poor (average σ = 1.61 Ø, Table 9). Facies F sediments generally lack fine material, and

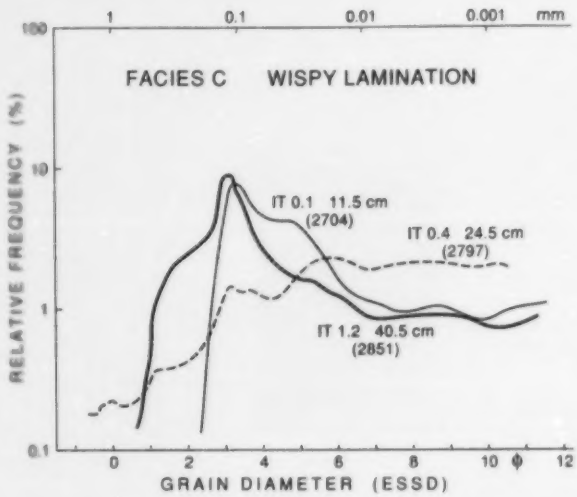

Figure 44. Representative grain size-frequency distribution curves for Facies C wispy laminated sand and mud. Core numbers, sample depths, and lab numbers are labelled beside the curves.

show a somewhat better sorted distribution, with modes in the coarse, medium and fine sand sizes (Fig. 48). Complications may arise in the interpretation of the distribution curves due to the incorporated fine material as mud intraclasts or dissemminated mud material (Fig. 49). Individual beds range from 0.05 m to >3 m in thickness (IT0.3P). Stacked units exceed 4.5 m in thickness (LCF4, Fig. 32). Pebbles may occur dispersed throughout a finer grained sand bed; or may occur as concentrated bands near the base of beds. The sand-sized material is mica-rich clean quartz sand. Variable grading patterns occur: many beds are ungraded; others show normal, inverse, or inverse-to-normal grading. Deformed intraclasts are commonly dispersed within the upper bed portions of individual beds (Fig. 41) (LCF4, LCF5, IT0.4P, IT0.3P, IT1.2P, IT2.1P, Fig. 32, 33). Some of these clasts occur within stratification bands, whereas others show a random orientation. Liquefaction structures, including fluid escape tubes and dish structures, occur in sandy cores near the head of the fiord (IT0.4P, IT0.3P, Fig. 32). Generally, the pebbly sand and sand of this facies lacks stratification. Rare convolute lamination and synsedimentary folds occur.

The generally massive character of Facies E and F, the random distribution of coarse outsized clasts within a finer-grained matrix, the absence of dropstone structures, the occurrence of distorted intraclasts, and the variable grading patterns (including normal, inverse-to-normal and inverse) suggest that these deposits were emplaced very rapidly from highly concentrated, viscous sediment-gravity flows. The one good coarse gravel Facies E bed in core IT1.2P is normally graded and stratified, with a scoured and/or loaded base. This deposit is virtually identical to many ancient deep-sea conglomerates, interpreted to have been deposited from high-concentration, large-volume turbidity currents (cf. Hein, 1982; Hein and Walker, 1982; Walker, 1975). The occurrence of dish and pillar structures within some of the Facies F beds suggests that liquefaction was important either during or after deposition, associated with

Figure 45. X-radiographic prints of Facies D laminated sand and mud, and Facies G, crossbedded sand, core IT0.1P, showing the fine scale of lamination and the interbedding of these two facies. particulary in core lengths 146-166 cm and 186-206 cm.

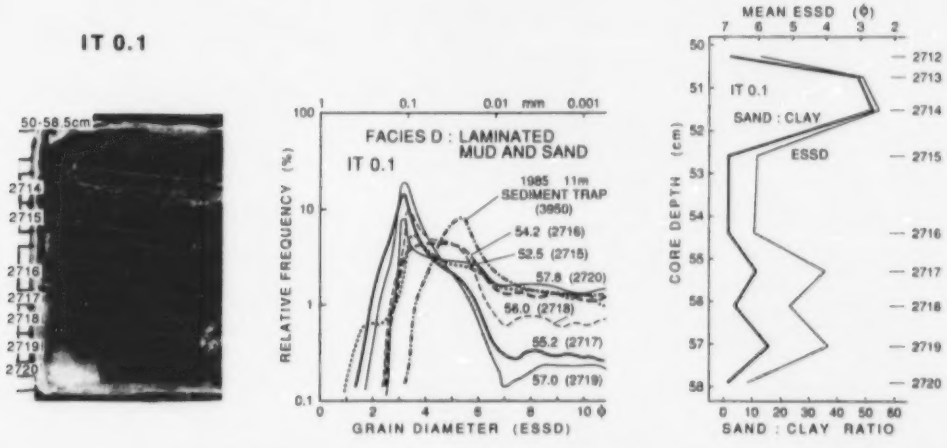

Figure 46. Core IT0.1P: Photograph of a sedimentary peel of Facies D laminated sand and mud (tick marks are each 1 cm long), showing the sample locations for textural analyses (left), with representative grain size-frequency distribution curves (middle). Mean grain size and % sand with core depth shown to the right. Sample depths and lab numbers are labelled beside the curves. By comparison, sediment trap data (lab no. 3950) is shown.

consolidation and dewatering of individual sandy beds. Fluid escape features can also develop due to postdepositional liquefaction associated with coring, sudden loading or shock (for example, by earthquakes or sea waves).

The textural features of the Facies F samples and of the cores dominated by Facies F (Fig. 48) indicate little segregation of silt and clay prior to deposition. This implies *en masse* deposition of the coarse and fine grained fractions, probably at the base of large turbidity currents. If most of the conglomerate, pebbly sand and sand is emplaced *en masse* from concentrated basal dispersions, these are most likely the type of basal dispersion Bagnold (1973) described for saltation of grains under bed load transport. Here, grains are maintained above the bed by dispersive pressure, in which the saltating layer is a 'modified grain flow' (cf. Middleton, 1966a, b, 1967) where the overriding fluid applies the shear stress for the generation of dispersive pressures.

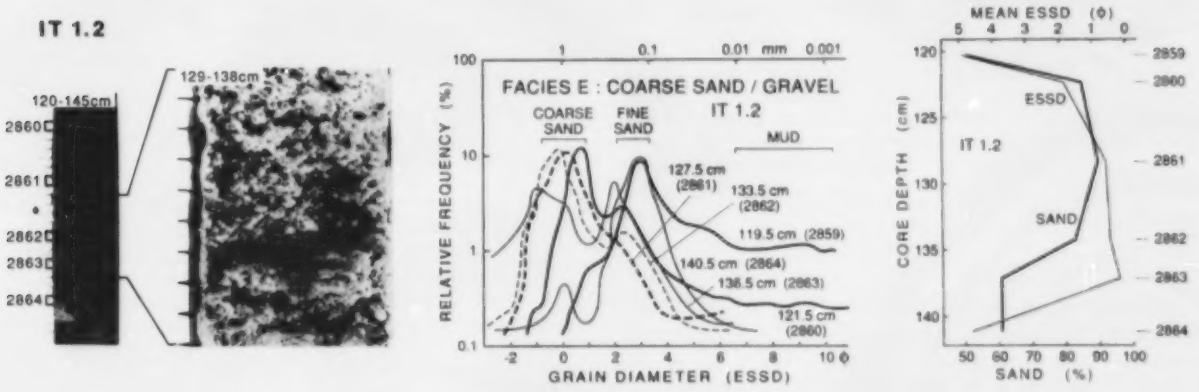

Figure 47. Core IT1.2P: Photograph of core (left), showing the sample locations for textural analyses; and a photograph of a sedimentary peel (right), showing in detail the features of Facies E graded-stratified gravel, core IT1.2P. Tick marks are each 1 cm long. Representative grain size-frequency distribution curves of Facies E gravel (left). Mean grain size and per cent sand with core depth shown to the right.

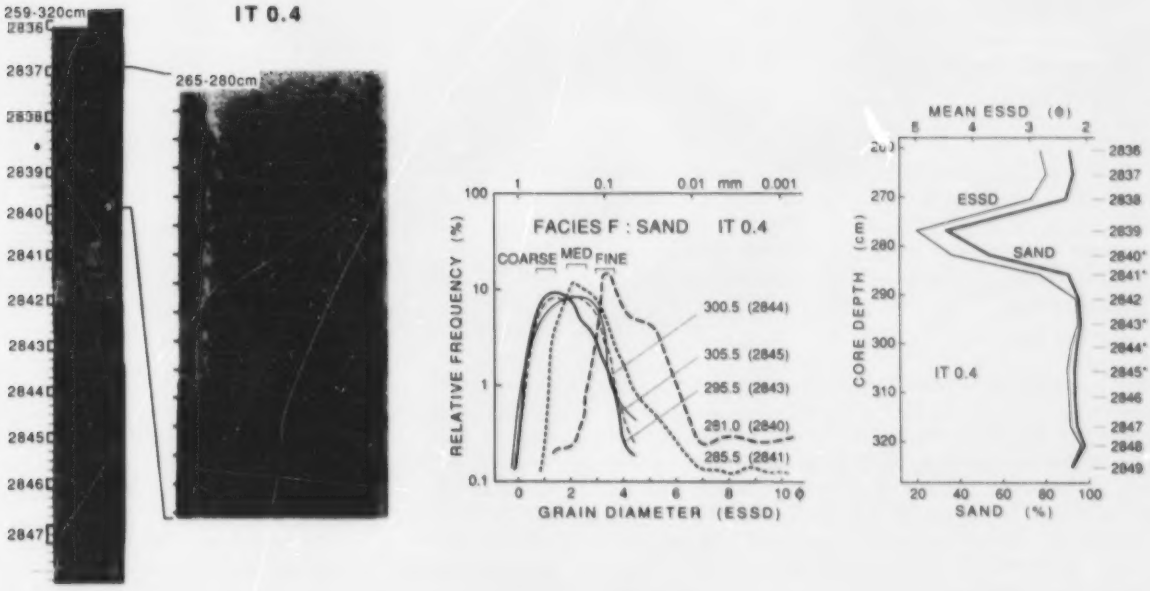

Figure 48. Core IT0.4P: Core photograph and an enlarged photograph of a sedimentary peel of Facies F sands (tick marks are each 1 cm long), showing the sample locations for textural analyses (left), with representative grain size-frequency distribution curves (middle). Mean grain size and sand % with core depth shown to the right. Sample depths and lab numbers are labelled beside the curves.

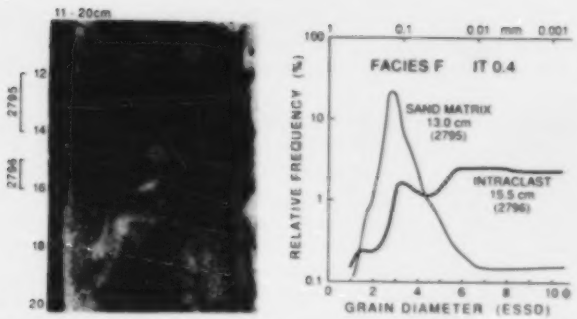

Figure 49. Core IT0.4P: Core photograph and an enlarged photograph of a sedimentary peel of Facies F sands with a large silty mud intraclast (tick marks are each 1 cm long), showing the sample locations for textural analyses (left), with representative grain size-frequency distribution curves (right). Sample depths and lab numbers are labelled beside the curves.

The thickness of such modified grain flows can be calculated as follows (Hein, 1982). Using the sediment trap measured bulk density for deposited sediment, ρ_s = 1.2 g•cm^{-3}, we estimate a sediment-gravity flow density, ρ_f = 1.1 g•cm^{-3}. The only major source of sand and gravel is from failure of nearshore (foreset) deposits. We use the average prodelta bottomset slopes as estimates of bottom slope. The bottom sediment trap and current meter, at 1.8 m above the sea floor, obtained data from 9 turbidity currents which were travelling at substantial velocities. Thus, for confined flows within the submarine channels, we use a conservative thickness of 3.6 m for average flows (1.8 m x 2 = 3.6 m). Using an average prodelta slope of 4.5°, shear stress at the base of a turbidity current is given by

(10) $\tau_0 = \Delta\rho \bullet g \bullet d \bullet S$

where g = 981 cm•s^{-2}, S = 0.079, and $\Delta\rho$ = 0.08 g•cm^{-3}, and d = 3.6 m. This results in a basal shear stress of about 223 N•m^{-2}. In order to calculate the thickness of the modified grain flow layer beneath the turbidity current, one must examine the behaviour of cohesionless grains under shear. Firstly, from Bagnold's (1956, with modifications in 1973) experiments,

(11) $T \bullet P^{-1} = 0.6$

where T = total shear stress at the sea bed and P = the dispersive pressure of the flow. Secondly, true grain flows can only move on high slopes (i.e. 30°), so for much lower slopes the down slope component of the shear stress due to gravity is virtually nil, and true grain flows cannot operate. Thus, all of the shear stress (T) must be provided by the fluid shear stress (τ_0). If this basal shear stress is totally transferred to the grains in the basal dispersion, then τ_0 becomes T and the dispersive pressure is given by

(12) P = T/ 0.6 = (223 N•m^{-2})/0.6 = 372 N•m^{-2}

This dispersive pressure balances the vertical component of the gravitational force acting on a column of dispersed grains, where the height of the column, h, can be calculated as follows

(13) $P = \Delta\rho \bullet g \bullet h$,

where $\Delta\rho$ is the difference in bulk densities between the basal dispersion and sea water. If we assume P = 372 N•m^{-2} and $\Delta\rho$ = 0.5 g•cm^{-3}, then a modified grain flow layer only 0.08 m thick can be maintained at the base of a turbidity current 3.6 m thick. The above calculations show that if a modified grain flow layer does exist at the base of the turbidity currents, it comprises a very thin zone at the base of the flow. Facies E gravel beds average 0.25 m and Facies F sand beds average 0.5 m thick. Thus, aggradation on the bed must be stepwise with gradual buildup from successive modified grain flow layers.

One can estimate the head velocity of average turbidity currents using the theoretical and experimental results of Middleton (1966a, b, 1967), where the velocity of the head is given by

(14) $V = 0.7\ [(\Delta\rho/\rho_1)\ g \bullet d_2]^{0.5}$

where d_2 is the thickness of the head (approximate thickness of flow = d = 3.6 m) and ρ_1 = 1.02 g•cm^{-3}. This results in an average velocity of the head of 12 cm•s^{-1}. This value compares very well with our measured velocities for turbidity

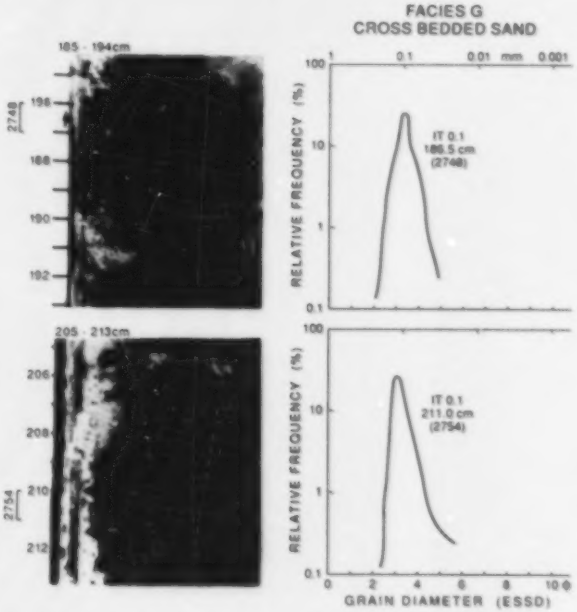

Figure 50. Core IT0.1P: Enlarged photographs of sedimentary peels of Facies G crossbedded sands (tick marks are each 1 cm long), showing the sample locations for textural analyses (left), with representative grain size-frequency distribution curves (right). Sample depths and lab numbers are labelled beside the curves.

currents (Fig. 17). In most cases only the peak surges exceed 12 cm• s^{-1} (up to 36 cm• s^{-1}, with most of the measured current flows in the range of 2 to 14 cm• s^{-1}). This suggests that the above calculations regarding the thickness of the modified grain flow used reasonable estimates of thickness and differences in bulk densities for the estimated turbidity current flows.

Many of our seismic records show evidence of slide/slump/debris flow deposits (see Figure 37 for examples). However, most of our coring was too shallow to penetrate these units. The acoustic records of the bottom of IT1 and most of IT2.1 (see later discussion) may penetrate what appear to be debris flow deposits. It is very difficult to distinguish coarse, sandy deposits from the basal dispersions of turbidity currents or deposits of sandy debris flows, particularly in narrow-diameter cores. These associations suggest that most of Facies F is deposited from viscous sediment-gravity flow deposits, either as turbidity currents or as sandy debris flows.

Facies G. Crossbedded sand (Fig. 50): This facies is rare, although it tends to be more common in those cores in which there is a thicker proportion of Facies D laminated layers (see below) (Fig. 32,33). Facies G has an average thickness per core of 0.6% (range: 0 to 4%, Table 8). Sediment sorting is poor (average σ = 1.83 Ø, Table 9), reflecting the interlamination of coarse and fine sands within the crosslaminated units. Facies G sands tend to have truncated distributions, with both coarse and fine tails absent (Fig. 50). Modal values fall within the fine sand size category. Compared with other distributions, Facies G units are more leptokurtic (i.e. more peaked). Crosslaminae consist of rippled sand, averaging 30 mm thick. The sand occurs as a tan-white, mica-rich quartz sand. The bases of the sand lenses are sharp, and often show delicate scour marks. Some sand lenses are inclined at a low angle to the core (about 10 to 12°). However, with the narrow diameter of the cores, it is difficult to ascertain whether these represent low-angle cross-stratified units, or sands deformed (rotated) during folding or coring.

The occurrence of well defined small-scale trough crossbedding (as ripple form sets, and small festoons), the commonly scoured bases, the improved sorting of the sands (in comparison with the other sandy facies), and the lack of grading, might suggest that Facies G sands were emplaced by a mechanism perhaps not due to direct fallout from sediment-gravity flows. Trough crossbedding occurs as single sets, averaging 30 mm thick, interpreted as representing bedload deposition from ripples. The average grain size of Facies G samples is 0.08 mm (3.61 Ø). Using bedform stability plots of mean size versus mean velocity (Blatt et al., 1980, p. 141), bottom current velocities would be in the range of 0.9 to 0.62 m• s^{-1}. This bottom velocity falls far above the normal background current velocities (<0.01 m• s^{-1}) near the seafloor (Fig. 16C) but within the range observed for turbidity currents (Fig. 15).

We suggest that these deposits may relate to the reworking of turbidity current deposited sands by reverse flow mechanisms (internal solitons, internal seiches: see Pantin and Leeder (1987) where it was noted reflection [of the turbidity current] occurred when the primary flow reached the [upward] sloping boundary at the far end of the basin). The lengths of the basins in Itirbilung Fiord before an upward slope is encountered due to intersection with an enclosing sill are small – from 6.0 km to 11 km in length. Considering that turbidite runout distances encountered in fiords can exceed 40 km (see Syvitski et al., 1987a), the effects of flow reversal as a viable mechanism for reworking initial turbidite sands seems likely. Events 6, 8, and 9 shown in Figure 15 are associated with currents that change flow direction.

Textural data summary

For facies with dispersed pebbles (i.e. facies A, E, and F) the coarse granule and pebble fraction was removed prior to analysis (see Clattenburg et al., 1983). As such, the mean

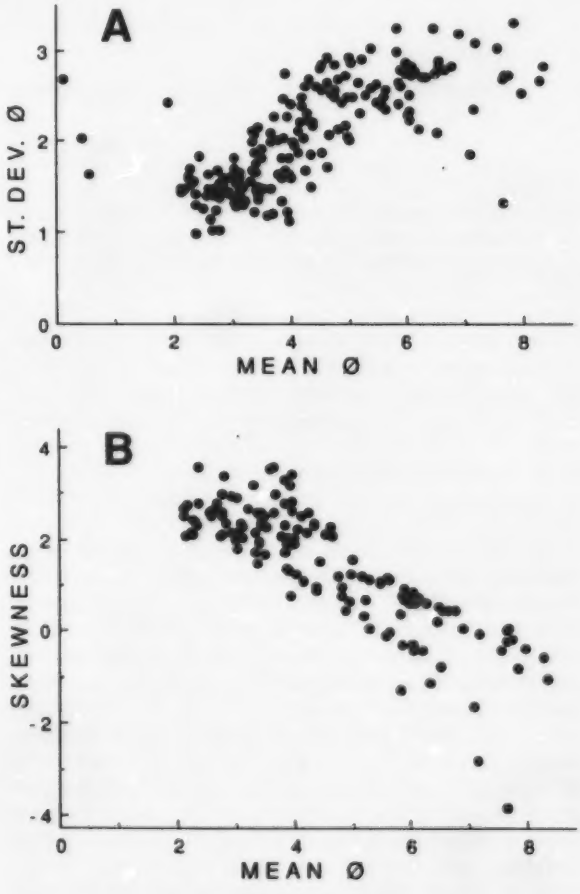

Figure 51. (A) Standard deviation (Ø) versus mean grain size (Ø) for all the samples analyzed in detail from Itirbilung cores. Standard deviation was calculated by the method of moments. **(B)** Skewness versus mean grain size (Ø) for all the samples analyzed in detail from Itirbilung cores. Skewness was calculated by the method of moments.

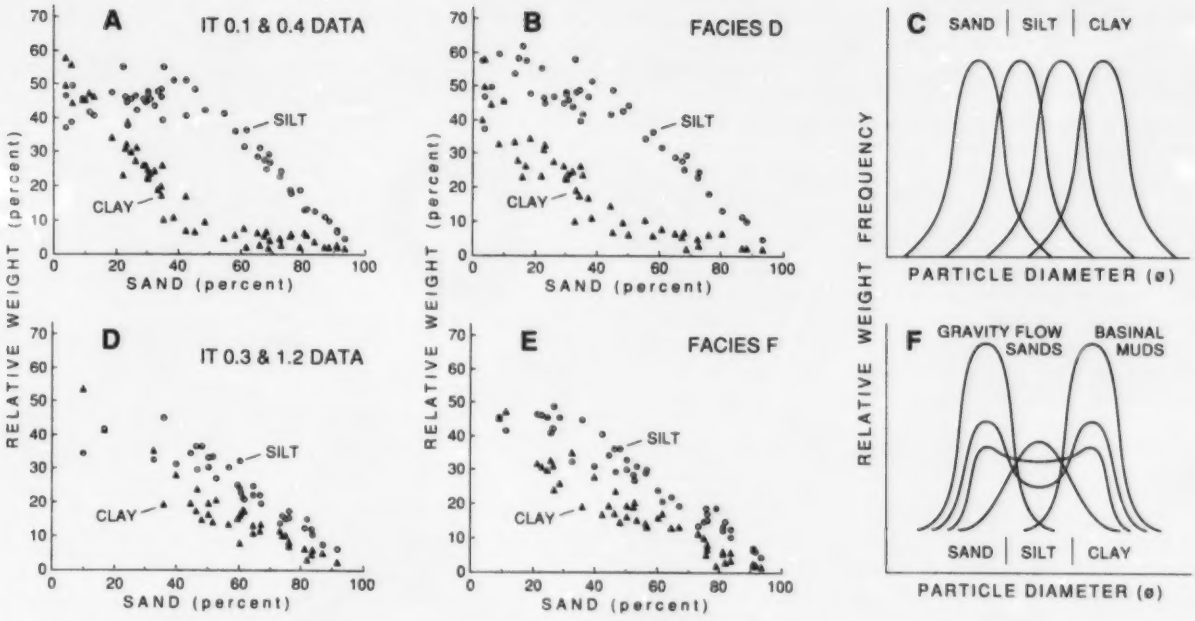

Figure 52. Per cent silt and per cent clay versus per cent sand for **(A)** cores dominated by Facies D, cores IT0.1P and IT0.4P; **(B)** for all facies D samples in all cores; **(C)** a hypothetical grain size model to explain the patterns seen in Facies D: a monotonically changing source function such as river discharge; **(D)** cores dominated by Facies F, cores IT0.3P and IT1.2P; and , **(E)** for all facies F samples in all cores; **(F)** a hypothetical grain size mixing model to explain the patterns seen in Facies F: the mixing of two source functions.

values for the coarser grained facies (A, E, and F) are biased in these coarser fractions. The average textural characterisitcs of the facies are given in Table 9. The average of the means for the different facies range from 1.53 Ø (medium sand) (Facies E), to 3.61 to 3.97 Ø (very fine sand) (Facies F and G), to 5.14 to 6.99 Ø (silt) (Facies A through D) (Table 9). The percentage of gravel is minor in most samples (0.1 to 1%), with the exception of Facies E, which has an average gravel composition of 9% (Table 9). The mud percentage ranges from 12 to 80%, with a concomitant range in sand percentage between 19 and 84%. Using the average mean and standard deviation values (Table 9), few of the facies can be distinguished from one another solely on the textural properties. Facies E is coarser grained and has a narrower standard deviation, compared with Facies A, which is finer grained, on average, and has a higher standard deviation. Using the textural properties from all the facies, there is an increase of standard deviation with decreasing mean grain size, with much higher standard deviations in the silt range (4 to 8 Ø), than in the fine sand and very fine sand range (2 to 4 Ø) (Fig. 51A). Skewness values decrease with decreasing grain size, with skewness between 0 and +4 (strongly fine-skewed) for the fine sand and very fine sand (2 to 4 Ø), and beween 0 and -4 (strongly coarse-skewed) for the silt (4 to 8 Ø) (Fig. 51B).

In examination of all of the textural data from the core samples, classified according to facies, two major types of textural populations can be recognized on plots of per cent silt or clay versus per cent sand (Fig. 52). The first consist of those samples belonging to Facies D (Fig. 52B) or proximal prodelta cores with a high proportion of Facies D (IT0.1 and 0.4, Fig. 52A). In these cases, clay content decreases linearly with increase in the sand content, whereas silt content is initially held constant at 50%. When the sand content exceeds approximately 40%, the contribution of silt decreases linearly as the clay fraction remains a constant at approximately 7%. A simple grain size model that can accommodate this textural trend is a series of similarly sorted size frequency distributions that vary only in the position of the mode (Fig. 52C). This model supports our interpretation that Facies D reflects a singular depositional mechanism, that of deposition from under a river plume; the shifting of the mode reflects changes in the level of discharge and thus the size of the suspended load.

The second type of textural population consists of those samples belonging to Facies F (Fig. 52E) or those cores with a high proportion of Facies F (IT0.3 and IT1.2, Fig. 52D). In this second type of textural class, both the silt and clay content decrease linearly with increases in sand content, and with a constant silt:clay ratio (about 1.4). For our interpretation of Facies F, we suggest a simple mixing model whereby nearshore sand (e.g. from delta foresets) is emplaced by sediment-gravity flows onto distal basinal muds that vary little in their textural character. In this scenario, we envisage the emplacement of sediment at a given location through two

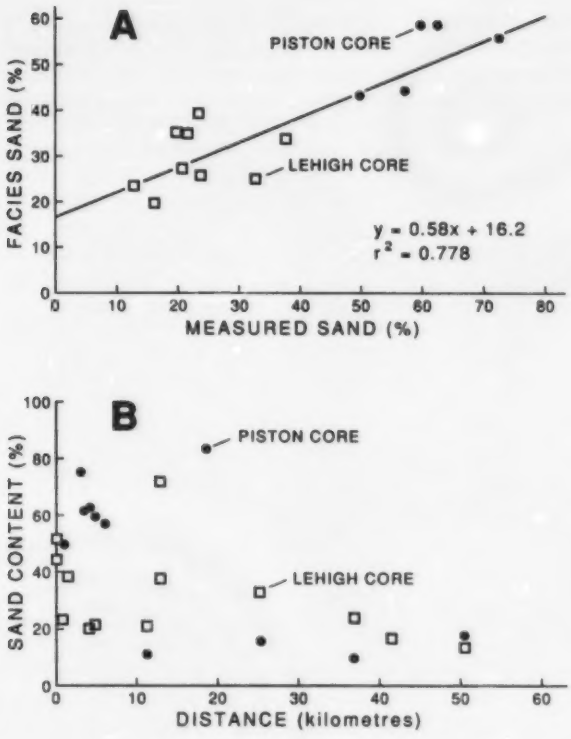

Figure 53. Comparison of measured sand content of piston and Lehigh cores with the sand content estimate from facies distribution (Tables 8 and 9).

independent sediment transport mechanisms, that of hemipelagic sedimentation of mud particles and the emplacement of sediment-gravity flow sands (Fig. 52F).

To test the reliability of assigning mean textural data to the various facies identified (Table 9) and at the same time test the reliability of the subjective identification of the various facies in a core (Table 8), we have calculated the per cent sand for a given core based on the crossproduct of tables 8 and 9, and then compared the result with the measured textural data for these same cores. For example, Lehigh core IT1.1 contains 5.4% Facies A (26.1% sand), 79.7% Facies B (19.1% sand) and 14.9% Facies F (69.0% sand). Based on these values the facies-predicted per cent sand for this core would be 27.1%. This can be compared with 21.0% sand based on the average of textural measurements from this core. Figure 53A presents this type of comparison for all Lehigh and piston cores where measured textural data is available. There is a significant correlation ($r = 0.9$) between the two, although the per cent sand estimated from the facies distribution under predicts in the sandy cores and over predicts in the muddy cores. Using the equation given on Figure 53, it is possible to predict the per cent sand from cores where no measured textural data are available, but where the facies distribution is known. Table 10 is a listing of measured or predicted sand content for all cores listed in Table 8.

Correlation between litho- and seismo-stratigraphy

It is impossible to specifically differentiate the individual facies on the high-resolution boomer deep-tow records. However, it is possible to correlate major reflectors with changes in lithology. Figure 54 provides three examples. For a complete presentation of core lithology and Huntec correlation see Syvitski et al. (1984d). Thin layers of Facies D (laminated sediments) or Facies F (sand lenses), of 0.05 to 0.1 m in thickness, that alternate within a dominant Facies B (bioturbated mud) provide enough of an impedance change to register as a reflector within an otherwise acoustically unstratified sequence. The approximately 1 m thick sand layer at the 3 m horizon in core 2.2 apparently has enough internal variation in texture and/or porosity to register as a series of tightly-spaced, albeit coherent, reflectors. It is not possible to assign a total thickness value of say turbidites, since the number of reflectors cannot be correlated with unit thickness. Slumps and blocky debris deposits are perhaps the easiest to acoustically define, with their marked surface roughness and abundant internal hyperbolics (cf. Fig. 37).

SUMMARY MODELS

Horizontal and vertical distribution of facies

The horizontal distribution of facies within the basin is quite variable and generally reflects the input of side-entry systems over the more dominant fiordhead sediment source, and the bathymetry (4 basins) of the fiord. As shown on the facies correlation charts (Fig. 32, 33), there is little correlation of facies between adjacent basins. In general, the laminated Facies D is common to prodelta regions, i.e. near the head of the fiord, and near side-entry fluvial input (Fig. 32, 33, 55B). This distribution reflects the exponential decrease in rates of sedimentation from under fluvial plumes and the seaward extent of the plumes. The erratic distribution of Facies F pebbly sand and sand (Fig. 55A) reflects the multiplicity of side-entry inputs and the different run-out distances of the different sediment gravity flows within the small basins. Facies F dominates cores from basins 2 and 3 (Fig. 18), in which there is sufficient entry of coarse clastic sediment through sediment-gravity flows or sandy debris flows. Much of this sediment is derived by mass-wasting of delta-front sands, submerged moraines, or side-entry prodelta fans. The wispy laminated Facies C (Fig. 55B) has a lateral distribution between that of Facies D and Facies F and may support the notion of being associated with hemipelagic deposition intermixed with early gravity flow deposition, possibly related to small failures or even meltout of sea ice covered in aeolian sediment. This suggests that Facies C may be an intermediate type flow, in terms of strength, duration and capacity, between the coarse grained fully turbulent sediment-gravity flows of Facies F and the fine grained river plumes of Facies D. Facies A and B have different lateral distributions downfiord (Fig. 55C) and may be an inverse proxy measure of the sedimentation rate. Facies A with its dropstone pebbles is relatively uncommon near the head of the fiord but increases sporadically down-fiord, with peak values at 25, 37, and 50 km. The bioturbated Facies B varies longitudinally in a dramatic but irregular fashion. These sites

appear to reflect positions within individual basins that are distal in terms of river plume sedimentation yet protected from the effects (both erosion and deposition) of sediment gravity flows, with a concomitant rise in the local biological mixing.

The vertical distribution of facies within cores is difficult to assess because of the short length and irrregular grain size sampling pattern in many of the cores. If one examines only the textural data, many of the cores show a finer grained upper portion (down to about 2 m depth) in which there is, in some cores (cf. IT0.1P), large variance in grain size on a small scale downcore (Fig. 56A). This is interpreted as reflecting the textural variation associated with Facies D (Fig. 57) . More irregular patterns reflect the interbedding of thin Facies F, with Facies B or D units (cf. IT0.4: Fig. 56B and Fig. 57). By contrast, where Facies F is thick, the sediment gradually coarsens then becomes finer grained upsection (cf. IT0.3, 300 to 112 cm depth, Fig. 56C). These may reflect upward coarsening and fining trends within individual layers of Facies F (Fig. 58). Many of the thick Facies F beds have dispersed fine grained intraclasts which may complicate the overall textural trends (compare IT1.2: Fig. 56E, 58). The cores containing thick layers of Facies F have textural patterns with a much more blocky appearance (Fig. 56C). In cores containing an alternation of facies patterns, the textural distribution tends to have a less organized appearance. For example, in core IT1.2 there are significant contributions of Facies A, D, E, and F. The corresponding textural pattern downcore has broad peaks (thick layers of Facies F), alternations of thin Facies F and D units (IT1.2, 150 to 250 cm, Fig. 56, Fig. 58). The coarsest bed, Facies E, is marked by a sharp peak toward the coarser end (about 112 to 150 cm, Fig. 56E, Fig. 58). The topmost narrow bands on the textural

Table 10. Measured or predicted (cf. Fig. 53) sand content of Itirbilung Cores. See Figures 1 and 18 for sample locations.

			Sand Content	
Core	Depth (m)	Distance (km)	Measured (per cent)	Predicted (cf. Fig. 53)
0.1L	55	0.8	23.4	
0.1P	55	0.8	49.8	
0.2L	88	1.6		38.5
62-20D L	85	0.16		52.0
62-20B L	91	0.18		44.5
LCF4	124	3.1		75.1
LCF5	139	3.45		61.2
0.4L	148	4.1	19.9	
0.4P	148	4.1	62.4	
0.3L	155	4.8	21.6	
0.3P	155	4.8	59.7	
1.0P	167	6.0	57.0	
1.1L	256	11.2	21.0	
1.1P	256	11.2		11.1
1.2L	293	12.9	37.7	
1.2P	293	12.9	72.1	
2.1P	310	18.4		83.4
2.2L	402	25.3	32.8	
2.2P	402	25.3		15.4
2.3L	424	37.0	23.9	
2.3P	424	37.0		9.7
3.0L	417	41.5	16.2	
3.1L	356	50.5	12.9	
3.1P	356	50.5		17.1

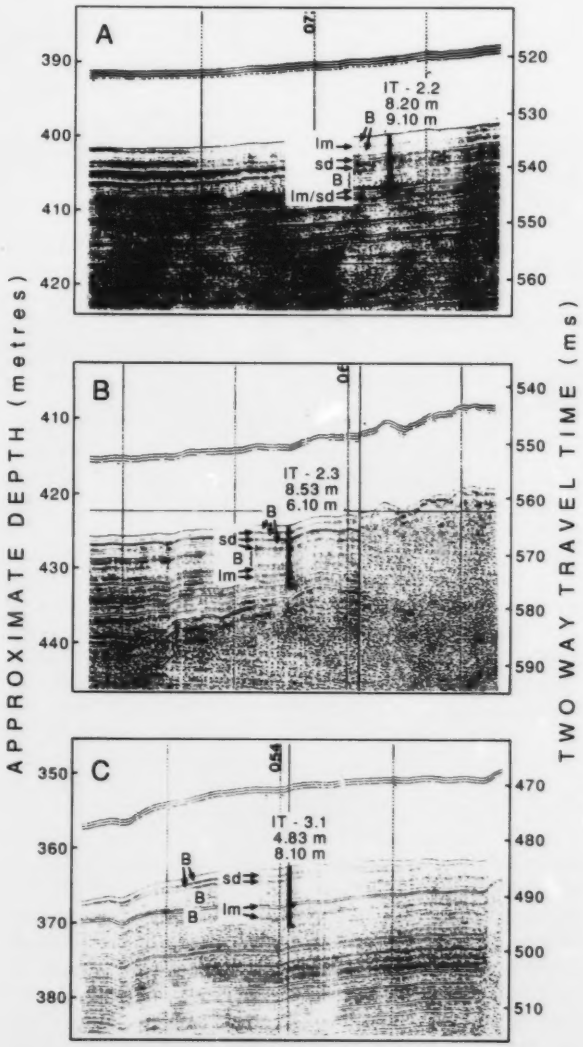

Figure 54. Identification of major seismic reflectors of Huntec deep-tow profiles over three core sites, based on facies description of cores (cf. Fig. 33). lm = laminated interval, sd = sand layer, B = bioturbated interval.

plot (Fig. 56) reflect the thin Facies F beds, with some of the fine peaks corresponding to thin interbedding of Facies D and B units (Fig. 56, 58, topmost 50 cm of core).

The texture of the most recent sediments within basins 1 and 2 (cf. Fig. 8), as sampled from Lehigh cores, are considerably finer grained than older sediments as sampled by piston core (Table 10). This observation may reflect the decrease in sedimentation rates following the initial phase of ablation following the Little Ice Age. Since the 1890(?) jøkolhlaup down the Itirbilung River, the pattern of sediment transport appears to have entered a waning phase, transporting lower sediment loads of finer material (see delta section). In addition, and possibly more apropos, the four paleo-tidewater glaciers that before 1950 discharged their sediment load directly into the fiord, have since ablated onto land and presently have a portion of their sediment load filtered through subaerial aggradation of their fan deltas.

This time-textural pattern reverses somewhat for cores collected in the outer portion of the fiord (basins 3 and 4: cf. Fig. 8) where the sand content of piston cores is lower than that found for Lehigh cores (Table 10). Cores from the more distal fiord basins reflect a considerably longer time history (Andrews, 1990; Andrews and Syvitski, in press; Syvitski et al., 1990). As such, the Lehigh cores may reflect the sedimentation regime of the paraglacial interval (acoustic unit 4) following the rapid ablation of the Late Foxe (Cockburn) ice advance. The piston cores from these basins would largely reflect ice distal sediments (i.e. acoustic unit 3) and therefore sedimentation of finer grained material (cf. Syvitski and Praeg, 1989).

Examination of Core 1.2 in detail (Fig. 58) clearly illustraties how complex the sedimentary history of the fiord system can be. Offshore of the side-entry Nuuksatsuguluk River there are a number of sediment inputs, corresponding to different periods of glaciofluvial discharge and mass-wasting events. Many moderate-size sediment gravity flows (Facies F) initiate the sedimentary fill that we have cored (4.80 to 6.25 m depth, Fig. 58). Most of the Facies F sands show some normal grading, and many have contorted and dispersed intraclasts, some with fluid escape dish structures. Then came a period of cessation of mass-wasting, with concomitant draping by hemipelagic deposition and bioturbation. This was renewed by another cycle of glaciofluvial and mass-wasting input, marked initially by Facies D laminated units (4.62 to 4.48 m depth, Fig. 58), which are abruptly overlain by ungraded to slight normally graded, predominantly structureless sands, some of which show fluid escape tubes, and less common bioturbation strucures. The period is generally acyclic, with no upward trends in grain size or bed thickness. The third cycle (2.45 to 1.50 m, Fig. 58) is dominated by Facies D, with thin layers of Facies F and B in which there are many subtle grain size trends, some coarsening-up, others fining-up, but no overall consistent pattern. This cycle is interpreted as reflecting predominantly glaciofluvial input to the basin. The topmost 1.5 m of the core consists of alternating periods dominantly by Facies F or E mass-wasting and more hemipelagic deposition as shown by Facies B and D units. Some of these cycles may be related to delta switching of lobes associated with fluvial processes of the Nuuksatsuguluk River. Alternatively, and concomitantly, these trends may reflect the interplay between the glaciofluvial runoff and the mass-wasting of the prodelta sands at this site.

In summary, the horizontal and vertical trends within the cores from Itirbilung Fiord reflect a complex interplay between sediment-gravity flow deposition, hemipelagic plume sedimentation, and reworking by bottom currents associated with sills, or by rebounding turbidity currents, and the biologic mixing by organisms. Because the fiord is divided into four essentially separate basins, the lack of distinctive markers and the lack of good dating control makes

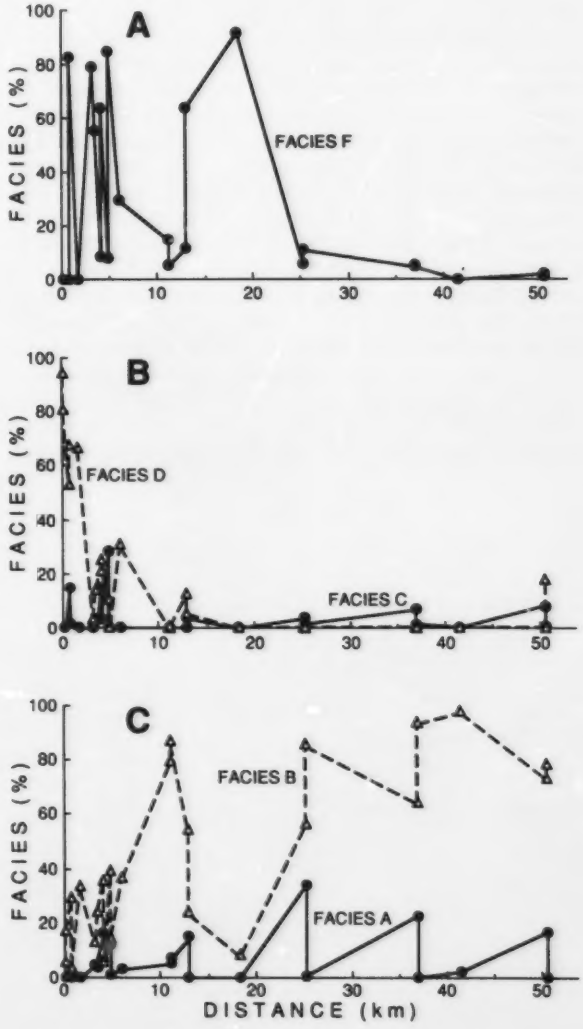

Figure 55. Down-fiord variation in facies percentages. **(A)** Facies F – pebbly sand and sand. **(B)** Facies C – wispy-laminated sand and mud, and Facies D – laminated sand and mud. **(C)** Facies A – pebbly sandy mud, and Facies B – bioturbated sand and mud.

it impossible to correlate events between basins. In general, Itirbilung Fiord is dominanted by mass-flow processes, because of the steep prodelta gradients both at the head of the fiord, and at positions of side-entry inputs, which fail continuously along major faults and small listric riders. The failures along the major faults produce the large sediment gravity flows (thick Facies F), whereas, failure along the smaller listric riders produce the smaller sediment gravity flows (Facies C and thin Facies F). The basin fill is very sandy, and for the most part is comprised of slumps, slides, debris flows and turbidites, with minor hemipelagic-bioturbated facies. The complex interdigitating of the facies in both space and time, within four basins, makes it difficult to draw an ideal facies model for such a basin.

One can construct a scenario of sedimentation of portions of the fiord during periods of either high (Fig. 59, 60) or low sedimentation. During periods of high sediment input into the basin (for example from 1860 to 1950, where glaciers extended to tidewater, there is direct input of coarse sand and gravel into the basins. Proportionately, most of this coarse debris is input into basin 1 (Fig. 59), because of the high sediment discharge from the main Itirbilung River and three tidewater glaciers, or into basin 2 (Fig. 60), because of high sediment discharge from the Nuuksatuguluk River, an un-named river, and a glacier on the north side of the fiord. Once sediment reaches the margins of the fiord, most of it is resedimented as coarse grained and fine grained sediment gravity-flows (Facies C, E, F), due to failure of delta-front sands, prodelta muds, subaqueous glacial outwash fans, and rock or talus cones along fiord walls. Reworking of turbidite sands by rebounding currents results in rare crossbedded sands (Facies G). Suspension fallout from fluvial plumes results in stratified sand and mud (Facies D), whereas suspension fallout from aeolian plumes results in disseminated sand throughout a finer-mud matrix (Facies B). Melting of debris-laden ice derived from calving ice fronts results in a pebbly sandy mud (Facies A). In areas of slower sedimentation rate, burrowing organisms rework the bottom sediment into burrowed sandy/silty mud (Facies B). Lateral facies patterns can be quite complex, reflecting the interaction between the fiordhead and side-entry systems, as well as the influence of the prominent bedrock sills on local sedimentation (Fig. 59, 60). During low sedimentation periods, rare sediment gravity flow events occur within a normal realm of mainly hemipelagic deposition, which serves to blanket most of the basin floor deposits.

Balancing sediment inputs and basin fill

Within the above sections we have provided information on both volumes of sediment (based on acoustic data) and sediment inputs (from empirical hindcasting techniques). It is appropriate to see if these data are in balance, because there is no direct information on whether the basin fill is a result of one or more glaciations. Acoustic units 1 and 2 (Fig. 34) account for 42% of the total submarine fill of about 3 km^3. If we assume a bulk density of 1.8 $t \cdot m^{-3}$, then the total mass of sediment in Itirbilung Fiord is 5.4 x 10^9 t. Unit 1 could represent ice-loaded sediments deposited from a previous glaciation (i.e. Early Foxe, see Gilbert, 1985). We assume, however, that the loading would have occurred from an ice advance during the Late Foxe (see regional acoustic facies discussion). As unit 2 is intimately interfingered with unit 1 we also assume that the timing of the ice loading and the deposition of unit 2 would be synchronous (i.e. Late Foxe).

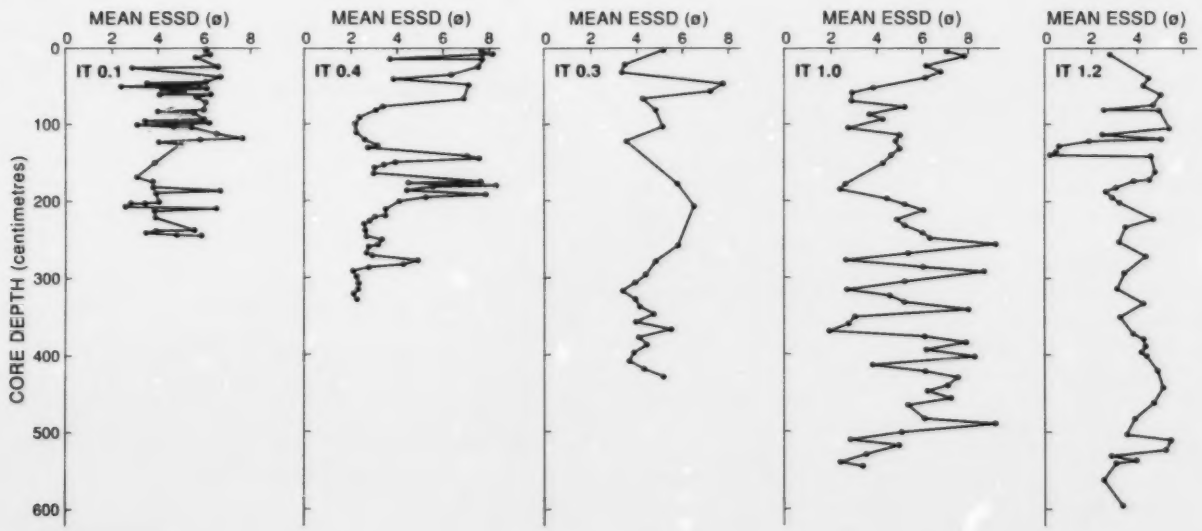

Figure 56. Downcore variation in mean grain size ESSD (equivalent spherical sedimentation diameter in phi units) for piston cores (A) IT0.1P, (B) IT0.4P, (C) IT0.3P, (D) IT1.0P, and (E) IT1.2P. Core depths in centimetres.

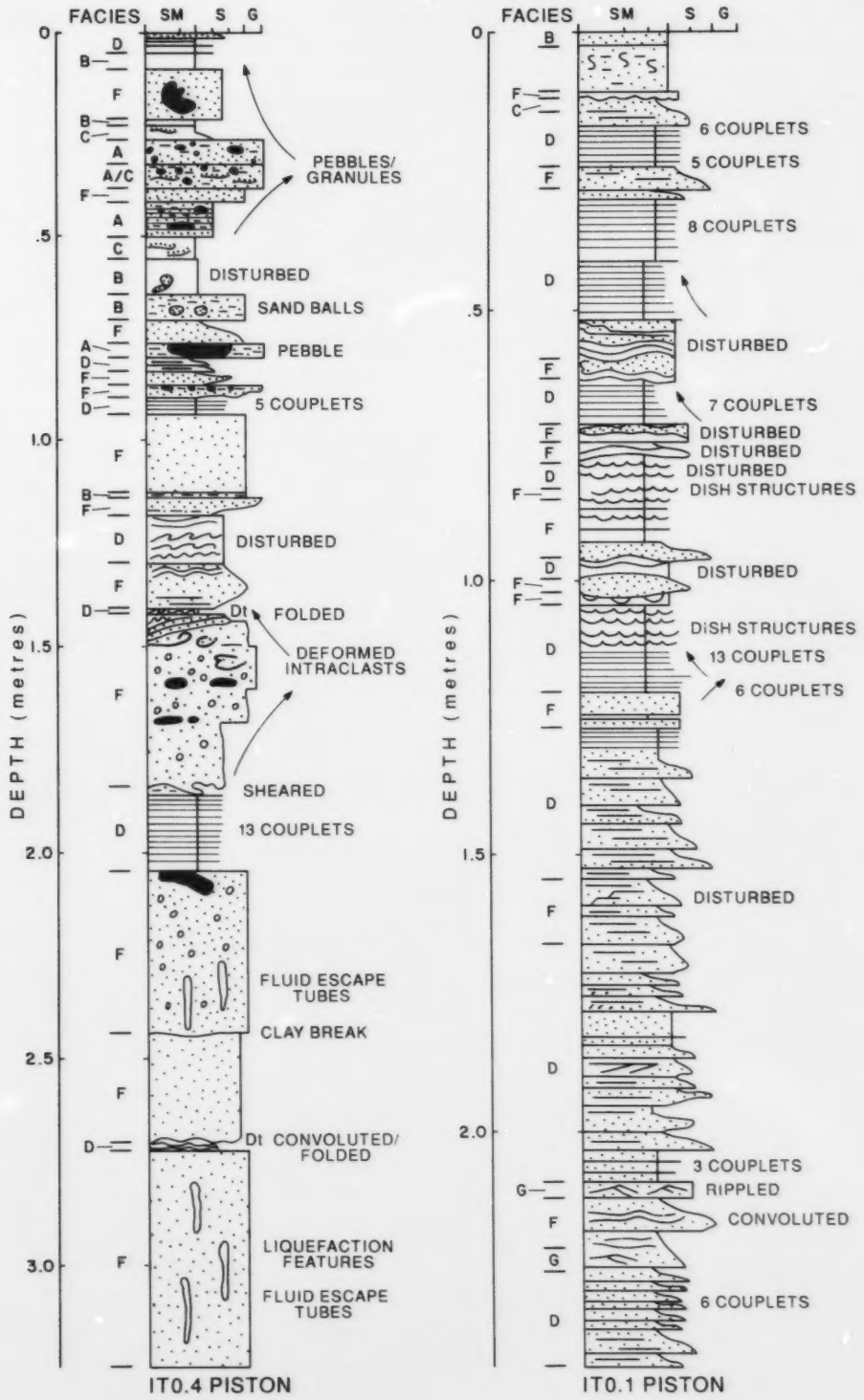

Figure 57. Representative Itirbilung Fiord piston core logs of cores with predominantly Facies D, laminated sands and muds with some interbeds of Facies F, pebbly sand and sand. Depths in metres. SM: silty mud, S: sand, G: granule/gravel, letters indicate Facies designation. See text for description and Figure 18 for core locations.

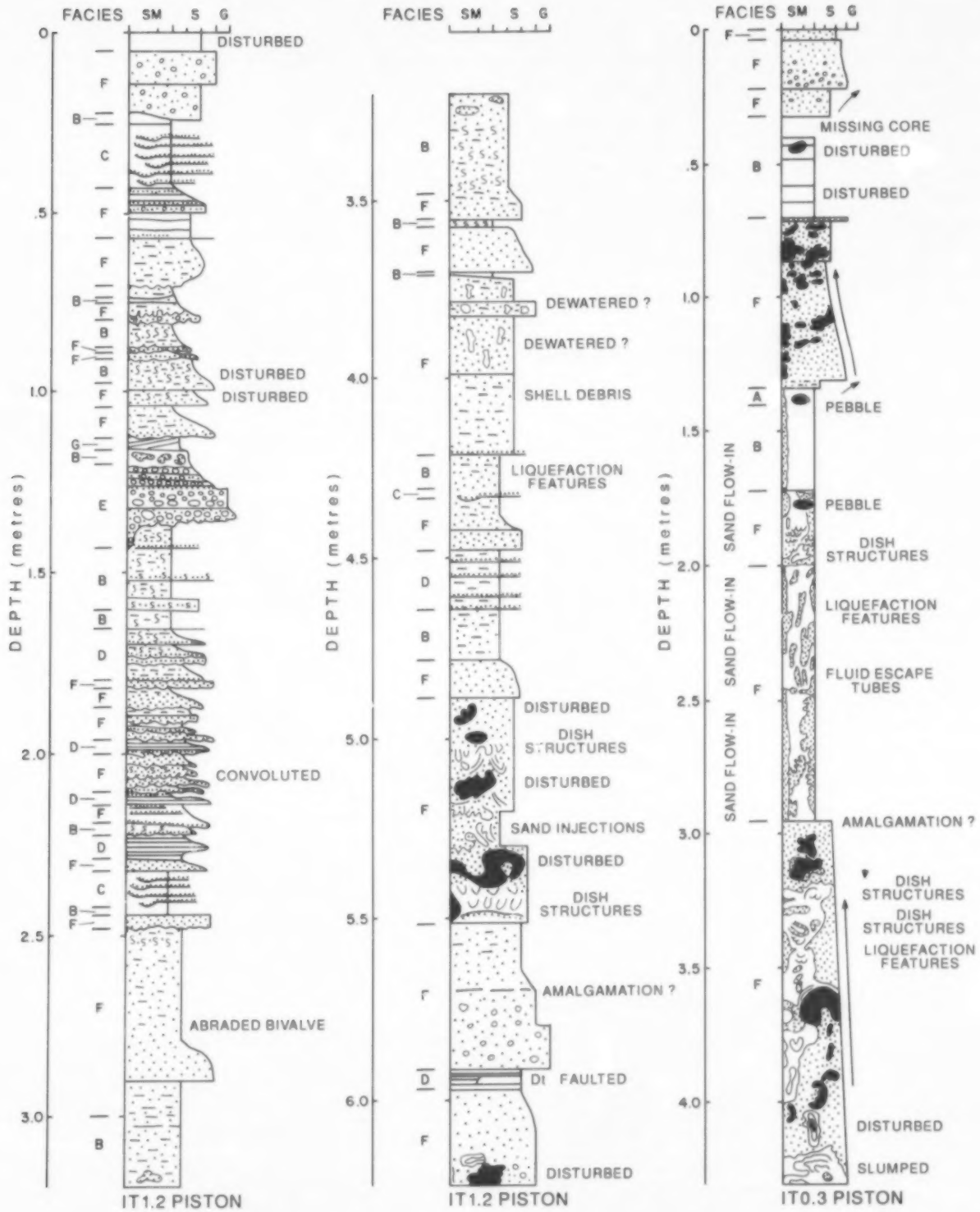

Figure 58. Representative Itirbilung Fiord piston core logs of IT1.2 with predominantly thin Facies F (sand), less common Facies E (gravel), Facies C (wispy-laminated sand and mud), and Facies B (bioturbated sand); IT0.3 with thick Facies F (pebbly sand) with dispersed intraclasts and fluid escape features. Depths in metres. SM: silty mud, S: sand, G: granule/gravel, letters indicate Facies designation. See text for description and Figure 18 for core locations.

Unit 3 is interpreted to represent ice distal deposition resulting from ablation of a marine ice terminus. It accounts for a sediment mass of 1.5 x 10^9 t. Based on partial exposures of unit 3 (up to 35 m) over a 15 km sandur that is about 1.5 km in width, then at least 1.4 x 10^9 t would have been deposited and subsequently exposed subaerially, for a grand total of 2.9 x 10^9 t of unit 3. Based on calculations given previously (glacial inputs section), we had surmised that the fiord head may have received from 5 to 7 times the present rate of sediment delivery, i.e. a larger drainage basin covered in an ablating ice sheet. Thus we calculate that the sediment flux to Itirbilung Fiord from 10 000 to 9000 years BP and 8600 years BP to 6000 years BP as 2.7 x 10^9 t. Thus the sediment yield for this period can account for 93% of the observed volume of unit 3, quite good considering the errors in estimation.

Units 4 and 5, representing the paraglacial and Neoglacial periods, account for 1.6 x 10^9 t of the Itirbilung basin fill. We assume that the sediment delivery from ice rafting can be included in our estimate of bedload delivery. We also assume that colluvium input largely stays on the margins of the fiord (submarine or subaerial) and is therefore not involved in our unit volume estimates of basin fill. If we assume that the sediment delivery rate from 6000 years BP to 100 years BP is 50% of the modern delivery rates of fluvial and aeolian sediment (a period of ice growth and reduced discharge), then 1.4 x 10^9 t would have been delivered to Itirbilung Fiord. This estimate would account for 88% of the measured volume of sediment associated with these units and, considering the associated errors in these calculations, can be considered in balance.

In summary, the bulk of the sediment volume in Itirbilung Fiord can be accounted for through sedimentation associated with the ablation of the Late Foxe ice advance into Itirbilung Fiord. As discussed earlier, this conclusion runs against those who suggest that the bulk of the sediment fill of Itirbilung Fiord and other Baffin fiords may relate to the Early Foxe glaciation (e.g. Gilbert, 1985). It is important to remember that we assumed that the Late Foxe glaciation was cold based and carried relatively clean meltwater during its period of ablation. However, when an order-of-magnitude more water is flushed through the fiord valley, even relatively clean water can transport an enormous load and many of the ice contact deltas that have been studied on Baffin Island show evidence of rapid sedimentation following the Late Foxe glaciation (Church and Ryder, 1972; Stravers and Syvitski, 1991). We therefore conclude that units 3 through 5 have been deposited over the last ten millennia, that unit 2 may have been deposited during the maximum tidewater phase of the Late Foxe glaciation (from 15 000 to 10 000 years BP), and that unit 1 remains of unknown origin and age.

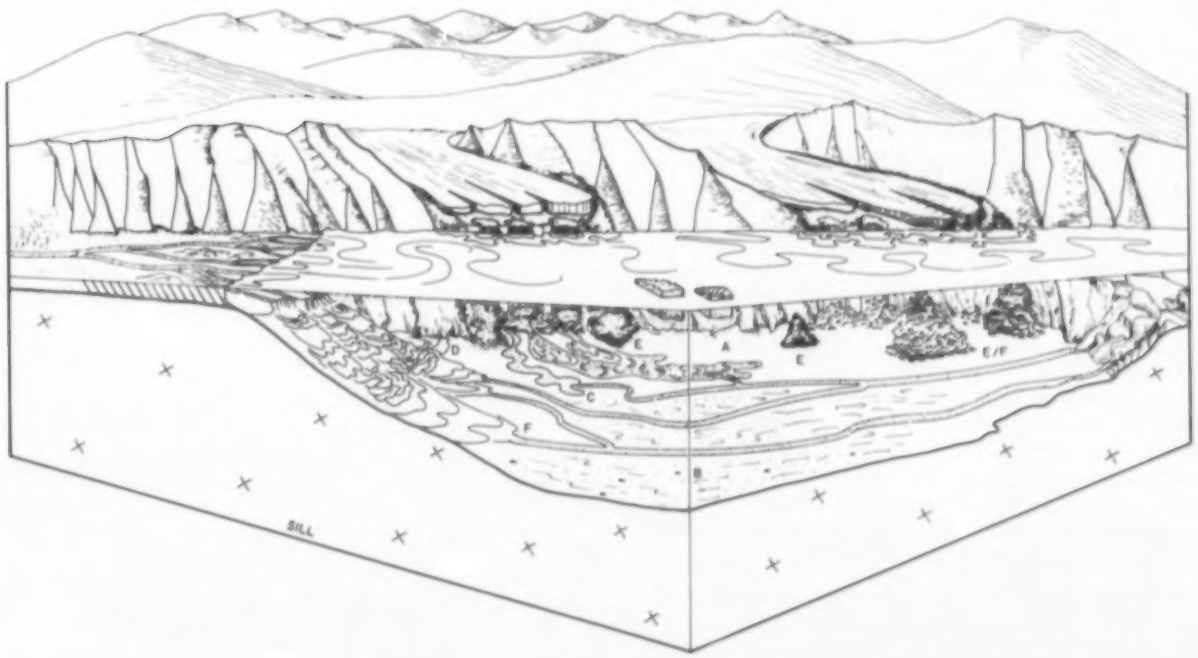

Figure 59. Paleogeographic reconstruction of basin 1 during a period of high sediment input, with tidewater glaciers, active fiordhead delta progradation and slumping of delta front sand and mud. Other sediment contributions are from side-entry talus cones and rock falls along the fiord walls, turbidity currents due to resedimentation of coarse grained nearshore sediment, deposition from fluvial plumes, fallout from aeolian sand and silt storms, and melting of debris-laden ice. Areas of low sedimentation are characterized by bioturbation. Letters refer to sedimentary facies as discussed in the text.

CONCLUSIONS

Itirbilung Fiord experiences episodic sedimentation events under arctic conditions; the annual discharge cycle is extremely short and half of the fluvial discharge is from nival melt in the early summer. Late summer flows occur as short duration events that relate equally to periods of rainfall and warm sunny days affecting the melt of hinterland ice sheets. A simple precipitation model is used to simulate the discharge of the large Itirbilung River. Sediment yield predictions for the hinterland drainage basins vary between 9 and 91 t• km^2 a^{-1}, of which 92% of the estimated annual flux of fluvial sediment (about 1.4 x 10^5 t• a^{-1}) enters near the head of the fiord.

Presently there are no tidewater glaciers along Itirbilung Fiord, although in the early 1950s four tidewater glaciers existed. These glaciers reached their maximum tidewater position during the Little Ice Age when the fiord received direct input of glacial sediment. These glaciers annually contributed up to one order-of-magnitude more sediment than is presently delivered to the fiord by river discharge. Paleohydraulic calculations suggest that for the period 8400 to 6000 years BP, Itirbilung fiord received 5 times the present rate of fluvial sediment delivery, reflecting the ablation of the Late Foxe Ice Sheet. For the period 6000 and 150 years BP, a time of Neoglacial ice storage, the sediment delivery rate is thought to have been reduced to half the present level of sediment delivery.

Winds are a constant feature of Itirbilung Fiord, blowing either up- or down-fiord. Events lasting a few days are a result of large weather systems over Baffin Island and Baffin Bay. Shorter duration events reflect a local katabatic influence. Critical winds for the movement of sediment in the down-fiord direction occur 20% of the time and affect 30% of the sandur surface. Threshold conditions for full sediment mobility occur only 1% of the year. The annual transport of aeolian sediment into the fiord basin is estimated to be 3.6 x 10^5 t• a^{-1}, approximately 3 times the estimate of fluvial sediment transport by the Itirbilung River.

Fiord currents are largely driven by meltwater discharge (from both rivers and melting sea ice) during the summer, wind-generated drift during the late summer and fall, deep-water exchanges during the fall, isohaline-generated circulation in winter, and tidal currents which operate over the entire year. There is some evidence that resuspension of sill sediment is associated with the influx of shelf water. Up-fiord winds initiate downwelling at the fiordhead. Particularly strong winds initiate an internal seiche the period of which is equal to the diurnal tide. Down-fiord winds cause a

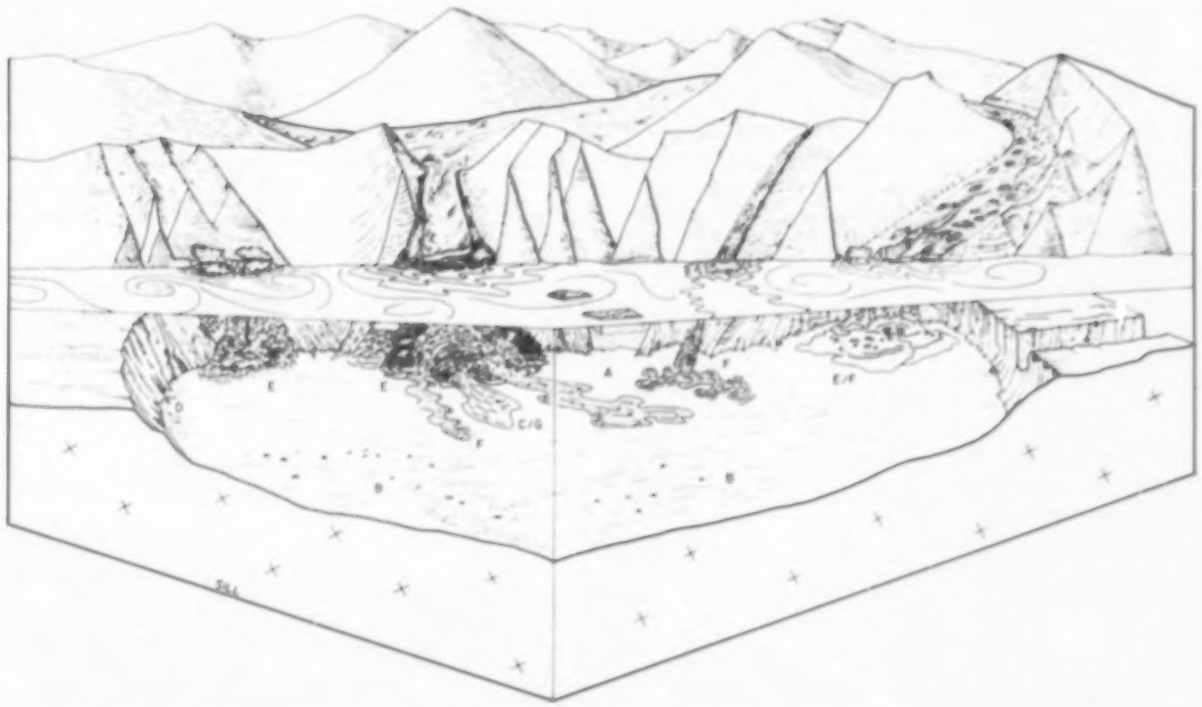

Figure 60. Paleogeographic reconstruction of basin 2 during a period of high sediment input, with tidewater glaciers, active side-entry delta progradation and slumping of delta front sand and mud. Other sediment contributions are from side-entry talus cones and rock falls along the fiord walls, turbidity currents due to resedimentation of coarse grained nearshore sediment, deposition from fluvial plumes, and melting of debris-laden ice. Areas of low sedimentation are characterized by bioturbation. Letters refer to sedimentary facies as discussed in the text.

dissipation of the internal tides. Although sea-bottom currents are usually weak, 9 gravity flow events (up to 0.36 $m \cdot s^{-1}$) were measured in a submarine channel over a 5 week period. Each event lasted 1 to 5 hours. Two types of sediment gravity flows were observed: (1) powerful single events which appear to represent coarse grained delta front chute failures, and (2) weaker multi-event flows which may result from retrogressive slide failures of the prodelta muds.

Itirbilung delta is one of the largest sandurs on Baffin Island, and has been largely conditioned by Little Ice Age events. For example, the advance into the river valley of three prominent side-entry glaciers has contributed large volumes of push moraines and stagnation deposits which presently supply fluvial and aeolian sediment. Although the sandur deposits principally reflect the aggradation and progradation of a bedload-dominated braided river system, the effects of aeolian transport are ubiquitous. The action of waves, a consequence of autumn winds, is confined to a limited area of tidal flats. A catastrophic jøkolhlaup, about 100 years ago, removed much of the raised marine deposits that once covered the Itirbilung River sandur. The sandur surface was left armoured with gravel waves and large boulders. We suspect a 10 m thick ponded slide mass (20 million m^3), located between 7 and 9 km offshore, relates to the jøkolhlaup event and its massive transport of sediment offshore.

The Itirbilung River prodelta annually receives approximately 0.5×10^6 t of sediment: 75% through aeolian transport and 25% as stream load. Sixty-one per cent of the fluvial bedload is used in the annual delta front progradation rate of 2.6 $m \cdot a^{-1}$. The remaining sediment is moved offshore in the form of slumping and turbidity currents along chutes and channels that cover the seafloor. The channels are of low sinuosity, their floors covered in sand. Other features related to semi-continuous slope failure include listric fault scarps often broken by crevasses and conjugate fractures. A deep-seated growth fault may control these retrogressive slide scarps.

Bedrock-controlled sills separate Itirbilung Fiord into four basins, of which two contain ≥150 m of Quaternary fill. Sediments are largely ponded between the fiord walls, although two of the sills are mantled by hemipelagic deposits. Using various lines of evidence, the rate of sedimentation decreases down the fiord. This pattern is punctuated by side-entry fan deltas that have often failed prograding onto the steep margins of the fiord, further contributing large volumes of sediment to the basin floors. The total autochthonous component within Itirbilung Fiord sediments is about 3.5% by weight, dominated by the siliceous tests of pelagic diatoms that accumulate in basinal muds.

Five seismo-stratigraphic units may represent a single phase of ice sheet advance and retreat. Units include: (1) ice-contact sediment subdivided into a depositional facies and an ice loaded facies, (2) rapidly deposited ice-proximal sediment under the influence of submarine glaciofluvial discharge partly syndepositional with unit 1, (3) ice-distal accumulation of glaciomarine sediment from hemipelagic deposition under turbid surface plumes, (4) paraglacial deposits associated with the rapid growth of deltas from the terrestrially-based ice cap and during a period of rapidly falling sea level, and (5) Neoglacial deposits when sea level was more or less stable and sedimentation considerably reduced. Little Ice Age deposits are very thin over most of the fiord and are only of significance in the inner of the four basins. The most recent sediments within basins 1 and 2 are considerably finer grained than older sediments and may reflect the decrease in sedimentation following the initial phase of ablation of the Little Ice Age. In basins 3 and 4, where sedimentation rates are much lower, the coarser and more surficial sediments may reflect the sedimentation regime of unit 4. The older and more deeply buried sediments which are finer grained may reflect the ice-distal sediments of unit 3. Through mass balance calculations we surmise that units 2 through 5 have deposited since the advance and ablation of the Late Foxe ice dome. Unit 1 may or may not represent sediment deposits that predate this event.

Seven sedimentary facies have been identified within cores collected from deposits of units 4 and 5 and possibly unit 3. Facies A, pebbly-sandy-mud, comprises less than 7% of the sediment volume and relates to the meltout of material from debris-laden ice of local origin. Its contribution increases dramatically down-fiord, probably a reflection of decreasing rates of sedimentation. Facies B, burrowed/mottled mud, dominates the sediment column accounting for just under half of the sampled volume, and implies that locally the rate of biological mixing exceeds the rate of sedimentation. The distribution of Facies B reflect locations under the distal influence of river plumes. Facies C, wispy laminated/mottled mud, accounts for less than 4% of the sampled volume and may relate to suspension fallout punctuated by small volume, low velocity turbidity currents. An alternate explanation may have the thin sand lenses related to the meltout of aeolian sand initially transported onto the sea ice cover of winter. Facies D, laminated sand and mud, accounts for 21% of the sediment volume and relates to the high sedimentation fallout of sand and mud from hypopycnal discharge of river plumes. The shifting of the modal grain size reflects the changes in the level of discharge and thus the particle size of the suspended load. Facies E, coarse sand/gravel, is an extremely rare facies possibly an end-member of Facies F. Facies F, pebbly sand and sand, accounts for 24% of the cored sediment volume and represents very rapid deposition from high concentration, viscous sediment-gravity flows, either as turbidity currents or as sandy debris flows. Facies F sands are typically interlayered with Facies B basinal muds. Facies G, crossbedded sands, is also an extremely rare facies (<1% by volume) that may relate to the reworking of turbidity current deposited sands by reverse flow mechanisms.

In conclusion, Itirbilung Fiord contains a very sandy basin fill dominated by episodic and high-energy sedimentation events. The fill sediments contain a wide variety of sedimentary and acoustic facies, with the former showing little correlation between basins. The fill is believed to largely relate to the sedimentation period encompassing the advance and ablation of the Late Foxe glaciation.

REFERENCES

Andrews, J.T.
1990: Fiord to deep sea sediment transfers along the northeastern Canadian continental margin: models and data; Géographie physique et Quaternaire, v. 44, p. 55-70.

Andrews, J.T. and Jennings, A.E.
1987: Influence of sediment source and type on the magnetic susceptibility of fiord and shelf deposits, Baffin Island and Baffin Bay, N.W.T.; Canadian Journal of Earth Sciences, v. 24, p. 1386-1401.

Andrews, J.T. and Miller, G.H.
1972: Quaternary history of northern Cumberland Peninsula, Baffin Island, N.W.T., Canada. Part IV: maps of the present glaciation limits and lowest equilibrium line altitude for north and south Baffin Island; Arctic and Alpine Research, v. 4, p. 45-59.
1984: Quaternary glacial and nonglacial correlations for the Eastern Canadian Arctic; in Quaternary Stratigraphy of Canada – A Canadian Contribution to IGCP Project 24 R.J. Fulton (ed.); Geological Survey of Canada, Paper 84-10, p. 101-116.

Andrews, J.T. and Syvitski, J.P.M.
in press: Sediment fluxes along high latitude glaciated continental margins: Northeast Canada and Eastern Greenland; in Global Sedimentary Geofluxes, M. Maybeck and W. Hay (ed.); National Academy of Sciences Press, Washington.

Andrews, J.T., Barry, R.G., and Drapier, L.
1970a: An inventory of the present and past glacierization of Home Bay and Okoa Bay, East Baffin Island, N.W.T., Canada and some climatic and paleoclimatic considerations; Journal of Glaciology, v. 9, p. 337-362.

Andrews, J.T., Buckley, J.T., and England, J.H.
1970b: Late-Glacial Chronology and Glacio-Isostatic Recovery, Home Bay, East Baffin Island, Canada; Geological Society of America Bulletin, v. 81, p. 1123-1148.

Andrews, J.T., Jull, A.J.T., Donahue, D.J., Short, S.K., and Osterman, L.E.
1985: Sedimentation rates in Baffin Island fiord cores from comparative radiocarbon dates; Canadian Journal of Earth Sciences, v. 22, p. 1827-1834.

Andrews, J.T., Laymon, C.A., and Briggs, W.M.
1989: Radiocarbon date list VI: Baffin Island, N.W.T., Canada; Institute of Arctic and Alpine Research, University of Colorado, Occasional Paper, no. 46, Chap. 5, Home Bay and East Central Fiords, p. 41-46.

Asprey, K.W. and Johnston, L.
198 Report on CSS HUDSON cruise 83-028, Baffin Island fjords; Geological Survey of Canada, Open File 1004, 189 p.

Asprey, K.W., Bishop, P., Blakeney, C., LeBlanc, W., Syvitski, J.P.M., and Winters, G.
1983: SAFE 1982 suspended particulate matter data; in Sedimentology of Arctic Fjords Experiment: HU 82-031 Data Report, Volume 1, J.P.M. Syvitski and C.P. Blakeney (comp.); Canadian Data Report of Hydrography and Ocean Sciences, no. 12, p. 5-1 to 8-30.

Bagnold, R.A.
1954: The Physics of Wind Blown Sand and Desert Dunes; Methuen & Co. Ltd., London, 265 p.
1956: The flow of cohesionless grains in fluids; Proceedings of the Royal Society of London, Series A, v. 249, p. 235-297.
1973: The nature of saltation and of "bed-load" transport in water; Proceedings of the Royal Society of London, Series A, v. 332, p. 473-504.

Basham, P.W., Forsyth, D.A., and Wetmiller, R.J.
1977: The seismicity of northern Canada; Canadian Journal of Earth Sciences, v. 14, p. 1646-1667.

Blatt, H., Middleton, G., and Murray, R.
1980: Origin of Sedimentary Rocks; Prentice-Hall, Englewood Cliffs, New Jersey, 782 p.

Boulton, G.S.
1986: Push-moraines and glacier-contact fans in marine and terrestrial environments; Sedimentology, v. 33, p. 677-698.

Boulton, G.S., Van der Mewer, J.J., and Cameraac, G.
1984: Chapter 12. Appendix 1. Side-entry systems, Inputs to the fjords from their margins. (3 maps, Itirbilung, McBeth and Cambridge fiords); in Sedimentology of Arctic fjords experiment: HU 83-028 data report, Volume 2, J.P.M. Syvitski (comp.); Canadian Data Report of Hydrography and Ocean Sciences, no. 28, 1130 p. (3 maps).

Carey, D.L. and Roy, D.C.
1985: Depositon of laminated shale: A field and experimental study; Geo-Marine Letters, v. 5, p. 3-9.

Church, M.
1972: Baffin Island sandurs: A study of arctic fluvial processes; Geological Survey of Canada, Bulletin 216, 208 p.

Church, M. and Ryder, R.M.
1972: Paraglacial sedimentation: A consideration of fluvial processes conditioned by glaciation; Geological Society of America, v. 83, p. 3059-3072.

Clattenburg, D., Cole, F., Kelly, B., LeBlanc, W., Bishop, P., Rashid, M., Schafer, C.T., and Syvitski, J.P.M.
1983: SAFE: 1982 Bottom grab samples; in Sedimentology of Arctic Fjords Experiment: HU 82-031 Data Report, Volume 1, J.P.M. Syvitski and C.P. Blakeney (comp.); Canadian Data Report of Hydrography and Ocean Sciences, no. 12, p. 8-1 to 8-94.

Cole, F. and Blakeney, C.P.
1983: Description and X-radiographs of Baffin Island cores; in Sedimentology of Arctic Fjords Experiment: HU 82-031 Data Report, Volume 1, J.P.M. Syvitski, and C.P. Blakeney, (comp.), Canadian Data Report of Hydrography and Ocean Sciences, no. 12, p. 12-1 to 12-96.

DeRaaf, J.F.M., Reading, H.G., and Walker, R.G.
1965: Cyclic sedimentation in the Lower Westphalian of North Devon; Sedimentology, v. 4, p. 1-52.

Dowdeswell, E.K. and Andrews, J.T.
1985: The fiords of Baffin Island: description and classification; in Quaternary Environments: Eastern Canadian Arctic, Baffin Bay and Western Greenland, J.T. Andrews (ed.); George Allen & Unwin Publishers, London, p. 93-123.

Dyke, A.S. and Prest, V.K.
1987: Paleogeography of northern North America, 18 000 - 5000 years ago; Geological Survey of Canada, Map 1703A, scale 1:12 500 000.

Ekdale, A.A., Bromley, R.G., and Pemberton, S.G.
1984: Ichnology: Trace fossils in sedimentology and stratigraphy; Society of Economic Paleontologists and Mineralogists, Short Course Notes, v. 15, 317 p.

Fitzgerald, R.A.
1984: Geochemical data for marine sediments from eastern Baffin Island including Cambridge Fjord, Itirbilung Fjord, and McBeth Fjord (Lehigh cores); in Sedimentology of Arctic Fjords Experiment: HU83-028 data report, Volume 2, J.P.M. Syvitski (comp.); Canadian Data Report of Hydrography and Ocean Sciences, no. 28, p. 10-1 to 10-128.

Frey, R.W. and Seilacher, A.
1980: Uniformity in marine invertebrate ichnology; Lethaia, v. 13, p. 183-207.

Gilbert, R.
1983: Sedimentary processes of Canadian arctic fjords; Sedimentary Geology, v. 36, p. 147-175.
1984: Coarse particles in the sediments of Cambridge, McBeth and Itirbilung Fiords; in Sedimentology of Arctic Fjords Experiment: HU 83-028 data report, Volume 2, J.P.M. Syvitski (comp.) Canadian Data Report of Hydrography and Ocean Sciences, no. 28, p. 9-1 to 9-25.
1985: Quaternary glaciomarine sedimentation interpreted from seismic surveys of fiords on Baffin Island, N.W.T.; Arctic, v. 38, p. 271-280.

Gilbert, R. and Horvath, V.
1984: Preliminary observations on cores from Cambridge and Itirbilung Fiords; in Sedimentology of Arctic fjords experiment: HU 83-028 data report, Volume 2, J.P.M. Syvitski (comp.) Canadian Data Report of Hydrography and Ocean Sciences, no. 28, p. 14-1 to 14-21.

Gilbert, R. and MacLean, B.
1983: Geophysical studies based on conventional shallow and Huntec high resolution seismic surveys of fiords on Baffin Island; in Sedimentology of Arctic Fjords Experiment: HU 82-031 data report, Volume 1, J.P.M. Syvitski and C.P. Blakeney (comp.); Canadian Data Report of Hydrography and Ocean Sciences, no. 12, chap. 15, 90 p.

Hein, F.J.
1982: Depositional mechanisms of deep-sea coarse clastic sediments, Cap Enrage Formation, Quebec; Canadian Journal of Earth Sciences, v. 19, p. 267-287.
1987: Core logs for HU 83-028 piston cores and PA 85-062 Lehigh cores from Itirbilung Fiord; in Sedimentology of Arctic Fjords Experiment: data report, Volume 3, J.P.M. Syvitski and D.B. Praeg (comp.); Canadian Data Report of Hydrography and Ocean Sciences, no. 54, p. 9-1 to 9-44.

Hein, F.J. and Longstaffe, F.J.
1983: Geotechnical, sedimentological and mineralogical investigations of Arctic fjords; in Sedimentology of Arctic Fjords Experiment: HU82-031 Data Report, Volume 1, J.P.M. Syvitski and C.P. Blakeney (comp.); Canadian Data Report of Hydrography and Ocean Sciences, no. 12, p. 11-1 to 111-158.
1985: Sedimentologic, mineralogic, and geotechnical descriptions of fine-grained slope and basin deposits, Baffin Island Fiords; Geo-Marine Letters, v. 5, p. 11-16.

Hein, F.J. and Syvitski, J.P.M.
1987: Sedimentology of Itirbilung Fiord, Baffin Island Canada; Proceedings 16th Arctic Workshop, Boreal Institute for Northern Studies, University of Alberta, Edmonton, p. 53-55.
1989: Sea floor gouges and pits in deep fjords, Baffin Island: Possible mammalian feeding traces; Geo-marine Letters, v. 9, p. 91-94.

Hein, F.J. and Walker, R.G.
1982: The Cambro-Ordovician Cap Enrage Formation, Quebec, Canada: conglomeratic deposits of a braided submarine channel with terraces; Sedimentology, v. 29, p. 309-329.

Henderson, J.R.
1980: Geologic Map: McBeth Fiord (27C), District of Franklin, Northwest Territories; Geological Survey of Canada, Open File 705.
1985: Geology, McBeth Fiord-Cape Henry Kater, District of Franklin, Northwest Territories; Geological Survey of Canada, Map 1605A, scale 1:250 000.

Howard, J.D.
1978: Sedimentology and trace fossils; in The Study of Trace Fossils, R.W. Frey (ed.); Springer-Verlag, New York, p. 131-146.

Hsu, S.A.
1974: Computing eolian sand transport from routine weather data; Chapter 94 of the Fourteenth Coastal Engineering Conference, Copenhagen, Denmark, p. 1619-1626.

Jackson, G.D. and Taylor, F.C.
1972: Correlation of major Aphebian rock units in the northeastern Canadian Shield; Canadian Journal of Earth Sciences, v. 9, p. 1650-1669.

King, C.A.M.
1969: Glacial geomorphology and chronology of Henry Kater Peninsula, east Baffin Island, N.W.T.; Arctic and Alpine Research, v. 1, p. 195-212.

Laine, E.P.
1980: New evidence from beneath the western North Atlantic for the depth of glacial erosion in Greenland and North America; Quaternary Research, v. 14, p. 188-198.

LeBlanc, K.W.G., Syvitski, J.P.M., and Maillet, L.
1988: Examination of the suspended particulate matter within Arctic fjords; Geological Survey of Canada, Open File 1733, 302 p.

Løken, O.H.
1965: Postglacial emergence at the south end of Inugsuin Fiord, Baffin Island, N.W.T.; Geographical Bulletin, v. 7, p. 243-258.
1966: Baffin Island refugia older than 54 000 years; Science, v. 153, p. 1378-1380.

Løken, O.H. and Hodgson, D.A.
1971: On the submarine geomorphology along the east coast of Baffin Island; Canadian Journal of Earth Sciences, v. 8, p. 187-195.

MacLean, B.
1985: Geology of the Baffin Island shelf; in Quaternary Environments: Eastern Canadian Arctic, Baffin Bay and Western Greenland, J.T. Andrews (ed); George Allen & Unwin Publishers, London. p. 154-177.

Masson, A. and Locat, J.
1987: Descriptions et Essais Cambridge, Terre de Baffin, Canada; in Sedimentology of Arctic Fjords Experiment: data report, Volume 3, J.P.M. Syvitski and D.B. Praeg (comp.); 1987,Canadian Data Report of Hydrography and Ocean Sciences, no. 54, p. 10-1 to 10-20.

McKenna-Neuman, C. and Gilbert, R.
1986: Aeolian processes and landforms in glaciofluvial environments of southeastern Baffin Island, N.W.T., Canada; in Aeolian Geomorphology, W.G. Nickling (ed); Proceedings of the Seventeenth Annual Binghamton Geomorphology Symposia, Geo Books, Norwich, chap. 12, p. 213-235.

Middleton, G.V.
1966a: Experiments on density and turbidity currents, I; Canadian Journal of Earth Sciences, v. 3, p. 523-546.
1966b: Experiments on density and turbidity currents, II; Canadian Journal of Earth Sciences, v. 3, p. 627-637.
1967: Experiments on density and turbidity currents, III; Canadian Journal of Earth Sciences, v. 4, p. 475-505.

Miller, G.H.
1985: Aminostratigraphy of Baffin Island shell-bearing deposits; in Quaternary Environments: Eastern Canadian Arctic, Baffin Bay and Western Greenland, J.T. Andrews (ed); George Allen & Unwin Publishers, London. p. 394-427.

Miller, G.H., Bradley, R.S., and Andrews, J.T.
1975: The glaciation level and lowest equilibrium line altitude in the high Canadian Arctic: Maps and climatic interpretation; Arctic and Alpine Research, v. 7, p. 155-168.

Mothersill, J.S. and Tabrez, A.R.
1987: Sedimentologic data from 82-031 SAFE cores MC-1, MC-7, IT-1 and TI-1A; in Sedimentology of Arctic Fjords Experiment: data report, Volume 3, J.P.M. Syvitski and D.B. Praeg (comp.); Canadian Data Report of Hydrography and Ocean Sciences, no. 54, p. 11-1 to 11-8.

Nielsen, T.K. and Ottesen-Hansen, N.E.
1980: Mixing and exchange processes in a small Greenland sill fjord; in Fjord Oceanography, H.J. Freeland, D.M. Farmer, and C.D. Levings (ed); Plenum Press, New York, N.Y., p. 219-225.

Østrem, G., Bridge, C.W., and Rannie, W.F.
1967: Glacio-hydrology, discharge and sediment transport in the Decade Glacier Area, Baffin Island, N.W.T.; Geographiska Annaler, v. 49A, p. 268-282.

Pantin, H.M. and Leeder, M.R.
1987: Reverse flow in turbidity currents: the role of internal solitons; Sedimentology, v. 34, p. 1143-1155.

Petrie, W.M. and Trites, R.W.
1984: Synoptic oceanography, Baffin Island fjords, cruise 83-028; in Sedimentology of Arctic Fjords Experiment: HU 83-028 data report, Volume 2, J.P.M. Syvitski (comp.); Canadian Data Report of Hydrography and Ocean Sciences, no. 28, chap. 2, 133 p.

Praeg, D.B. and Prime, W.
1987: Amendments to grain size data from SAFE data reports volume 1 & 2; in Sedimentology of Arctic Fjords Experiment: data report, Volume 3, J.P.M. Syvitski and D.B. Praeg (comp.); Canadian Data Report of Hydrography and Ocean Sciences, no. 54, p. 15-1 to 15-14.

Praeg, D.B., Syvitski, J.P.M., and Clattenburg, D.C.
1987: Sedimentologic studies of HU 82-031 and 83-028 piston cores; in Sedimentology of Arctic Fjords Experiment: data report, Volume 3, J.P.M. Syvitski and D.B. Praeg (comp.); Canadian Data Report of Hydrography and Ocean Sciences, no. 54, p. 8-1 to 8-129.

Quinlan, G.
1985: A numerical model of postglacial relative sea level change near Baffin Island; in Quaternary Environments: Eastern Canadian Arctic, Baffin Bay and Western Greenland, J.T. Andrews (ed); George Allen & Unwin Publishers, London, p. 560-584.

Reasoner, M.A. and Hein, F.J.
1984: Sedimentology and geotechnical properties of surficial bottom sediment, Baffin Island fjords; in Sedimentology of Arctic fjords experiment: HU 83-028 data report, Volume 2, J.P.M. Syvitski (comp.); Canadian Data Report of Hydrography and Ocean Sciences, no. 28, p. 11-1 to 11-111.

Schafer, C., Clattenburg, D., Cole, F.E., LeBlanc, W., and Syvitski, J.P.M.
1984: SAFE: 1983 Hudson bottom grab samples; in Sedimentology of Arctic fjords experiment: HU 83-028 data report, Volume 2, J.P.M. Syvitski (comp.); Canadian Data Report of Hydrography and Ocean Sciences, no. 28, p. 7-1 to 7-73.

Schafer, C.T., Smith, J.N., and Seibert, G.
1983: Significance of natural and anthropogenic sediment inputs to the Saguenay Fjord, Quebec; Sedimentary Geology, v. 36, p. 177-194.

Stanely, A.D. and Land, J.
1968: Discharge measurements of the Decade and Inugsuin Rivers - 1967; in North-Central Baffin Island Field Report 1967, Inland Waters Branch D.E.M.R., Ottawa, 22 p.

Stravers, J., and Syvitski, J.P.M.
1991: Land-sea correlations and evolution of the Cambridge Fiord marine basin during the last deglaciation of Northern Baffin Island; Quaternary Research, v. 35, p. 72-90.

Syvitski, J.P.M.
1982: Cruise report: C.S.S. Hudson 82-031; Geological Survey of Canada, Open File no. 897, 77 p.

1984a: Sedimentology of Arctic Fjords Experiment: HU 83-028 data report, Volume 2; Canadian Data Report of Hydrography and Ocean Sciences, no. 28, 1130 p., 3 maps.
1984b: SAFE 1983 geophysical investigations; in Sedimentology of Arctic Fjords Experiment: HU 83-028 data report, Volume 2, J.P.M. Syvitski (comp.) Canadian Data Report of Hydrography and Ocean Sciences, no. 28, chap. 16, 26 p.
1985: Subaqueous slope failures within seismically active arctic fjords; in Arctic Land-Sea Interaction, G. Vilks and J.P.M. Syvitski (ed.) Geological Survey of Canada, Open File no. 1223, p. 60-63.
1986: Estuaries, deltas and fjords of eastern Canada; Geoscience Canada, v. 13, p. 91-100.
1987a: Airphoto interpretation of changes to the tidewater position of glaciers and deltas along the NE Baffin coast; in Sedimentology of Arctic Fjords Experiment: data report, Volume 3, J.P.M. Syvitski and D.B. Praeg (ed.); Canadian Data Report of Hydrography and Ocean Sciences, no. 54, chap. 14, 11 p.
1987b: Proximal prodelta investigations at two arctic deltas: Itirbilung and Cambridge Fiords, Baffin Island; in Sedimentology of Arctic Fjords Experiment: data report, Volume 3, J.P.M. Syvitski and D.B. Praeg (ed.); Canadian Data Report of Hydrography and Ocean Sciences, no. 54, chap. 6, 16 p.
1989: On the deposition of sediment within glacier-influenced fjords: Oceanographic controls; Marine Geology, v. 85, p. 301-329.
in press: Towards an understanding of sediment deposition on glaciated continental shelves: Sequence stratigraphy; Continental Shelf Research.

Syvitski, J.P.M., Asprey, K.W., Blakeney, C.P., and Clattenburg, D.
1983a: SAFE: 1982 delta report; in Sedimentology of Arctic Fjords Experiment: HU 82-031 data report, Volume 1, J.P.M. Syvitski and C.P. Blakeney (comp.); Canadian Data Report of Hydrography and Ocean Sciences, no. 12, chap. 18, 41 p.

Syvitski, J.P.M. and Blakeney, C.P.
1983a: Sedimentology of Arctic Fjords Experiment: HU 82-031 data report, Volume 1; Canadian Data Report of Hydrography and Ocean Sciences, no. 12, 935 p.
1983b: SAFE HU82-031 sidescan sonar and sounder profiles; in Sedimentology of Arctic Fjords Experiment: HU 82-031 data report, Volume 1, J.P.M. Syvitski and C.P. Blakeney (comp.) Canadian Data Report of Hydrography and Ocean Sciences, no. 12, chap. 16, 49 p.

Syvitski, J.P.M., Blakeney, C.P., and Hay, A.E.
1983b: SAFE: HU82-031 Sidescan sonar and sounder profiles; in Sedimentology of Arctic Fjords Experiment: HU 82-031 Data Report, Volume 1, J.P.M. Syvitski and C.P. Blakeney (comp.); Canadian Data Report of Hydrography and Ocean Sciences, no. 12, p. 16-1 to 16-49.

Syvitski, J.P.M., Burrell, D.C., and Skei, J.M.
1987a: Fjords: Processes and Products; Springer-Verlag, New York, 379 p.

Syvitski, J.P.M., Cole, F.E., and Hoskin, S.
1984d: Observations on some piston and Lehigh cores from Itirbilung, McBeth and Cambridge Fiords; in Sedimentology of Arctic fjords experiment: HU 83-028 data report, Volume 2, J.P.M. Syvitski (comp.); Canadian Data Report of Hydrography and Ocean Sciences, no. 28, p. 13-1 to 13-55.

Syvitski, J.P.M., Fader, G., Josenhans, H., and Piper, D.J.W.
1983c: Seabed investigations of the Canadian east coast and Arctic using PISCES IV; Geoscience Canada, v. 10, p. 59-68.

Syvitski, J.P.M. and Farrow, G.E.
1989: Fjord sedimentation as an analogue for small hydrocarbon-bearing fan deltas; in Deltas: Sites and Traps for Fossil Fuels, M.K.G. Whateley and K.T.Pickering (ed.); Geological Society (London) Special Publication 41, p. 21-43.

Syvitski, J.P.M., Farrow, G.E., Atkinson, R.J.A., Moore, P.G., and Andrews, J.T.
1989: Baffin island fjord macrobenthos: bottom communities and environmental significance; Arctic, v. 42, p. 232-247.

Syvitski, J.P.M., Farrow, G.E., Taylor, R.B., Gilbert, R., and Emory-Moore, M.
1984a: SAFE: 1983 delta survey report; in Sedimentology of Arctic Fjords Experiment: HU 83-028 data report, Volume 2, J.P.M. Syvitski (comp.); Canadian Data Report of Hydrography and Ocean Sciences, no. 28, chap. 18, 91 p.

Syvitski, J.P.M., Hay, A.E., Schafer, C.T., and Asprey, K.W.
1984b: SAFE: 1984 bayhead prodelta investigations; in Sedimentology of Arctic Fjords Experiment: HU 83-028 data report, Volume 2, J.P.M. Syvitski (comp.); Canadian Data Report of Hydrography and Ocean Sciences, no. 28, chap. 17, 62 p.

Syvitski, J.P.M., Lamplugh, M., and Kelly, B.
1984c: Fjord morphology; in Sedimentology of Arctic Fjords Experiment: HU 83-028 data report, Volume 2, J.P.M. Syvitski (comp.); Canadian Data Report of Hydrography and Ocean Sciences, no. 28, chap. 20, 27 p.

Syvitski, J.P.M., LeBlanc, K.W., and Cranston, R.
1990: The flux and preservation of organic carbon in Baffin Island fjords; in Glaciomarine processes and products, J.D. Scorse and J. Dowdeswell (ed.); Geological Society of London Special Publication, no. 53, p. 217-239.

Syvitski, J.P.M. and Piper, D.J.W.
1990: Baffin Island Fiords; in Chapter 10 of Geology of the Continental Margin of Eastern Canada, M.J. Keen and G.L. Williams (ed.); Geological Survey of Canada, Geology of Canada, no. 2, p. 563-566.

Syvitski, J.P.M. and Praeg, D.B.
1987: Sedimentology of Arctic Fjords Experiment: data report, Volume 3; Canadian Data Report of Hydrography and Ocean Sciences, no. 54, 468 p.
1989: Quaternary sedimentation in the St. Lawrence Estuary and adjoining areas, Eastern Canada: An overview based on high resolution seismo-stratigraphy; Géographie physique et Quaternaire, v. 43, p. 291-310.

Syvitski, J.P.M. and Schafer, C.T.
1985: Sedimentology of Arctic Fjords Experiment (SAFE): Project introduction; Arctic, v. 38, p. 264-270.

Syvitski, J.P.M., Schafer, C.T., Asprey, K.W., Hein, F.J., Hodge, G.D., and Gilbert, R.
1985: Sedimentology of Arctic Fjords Experiment: 85-062 expedition report; Geological Survey of Canada Open File no. 1234, 80 p.

Syvitski, J.P.M., Taylor, R.B., and Stravers, J.
1987b: Suspended sediment loads along the coast of N.E. Baffin and Bylot Islands, N.W.T.; in Sedimentology of Arctic Fjords Experiment: data report, Volume 3, J.P.M. Syvitski and D.B. Praeg (ed.); Canadian Data Report of Hydrography and Ocean Sciences, no. 54, chap. 4, 20 p.

Trites, R.W.
1985: Oceanographic reconnaissance of selected Baffin Island fjords; in Arctic Land-Sea Interactions, G. Vilks and J.P.M. Syvitski (ed.); Geological Survey of Canada, Open File no. 1223, p. 54-57.

Trites, R.W., Petrie, W.M., Hay, A.E., and DeYoung, B.
1983: Synoptic Oceanography; in Sedimentology of Arctic Fjords Experiment: HU 82-031 data report, Volume 1, J.P.M. Syvitski and C.P. Blakeney (comp.); Canadian Data Report of Hydrography and Ocean Sciences, no. 12, chap. 2, 129 p.

Vilks, G. and Powell, C.
1987: Cruise report and preliminary results C.S.S. Hudson 87-033, 65 p.

Walker, R.G.
1975: Generalized facies models for resedimented conglomerates of turbidite association; Geological Society of America Bulletin, v. 86, p. 737-748.

Winters, G.V., Syvitski, J.P.M., and Maillet, L.
1985: Distribution and dynamics of suspended particulate matter in Baffin Island fjords; in Arctic Land-Sea Interaction, G.Vilks and J.P.M. Syvitski (ed.); Geological Survey of Canada, Open File no. 1223, p. 73-77.